Nuclear Instruments and Methods in Physics Research B 129 (1997) 153–193

ELSEVIER

NIM B
Beam Interactions with Materials & Atoms

Cross sections for the production of residual nuclides by low- and medium-energy protons from the target elements C, N, O, Mg, Al, Si, Ca, Ti, V, Mn, Fe, Co, Ni, Cu, Sr, Y, Zr, Nb, Ba and Au

R. Michel [a,*], R. Bodemann [a], H. Busemann [a], R. Daunke [a], M. Gloris [a], H.-J. Lange [a], B. Klug [a], A. Krins [a], I. Leya [a], M. Lüpke [a], S. Neumann [a], H. Reinhardt [a], M. Schnatz-Büttgen [a], U. Herpers [b], Th. Schiekel [b], F. Sudbrock [b], B. Holmqvist [c], H. Condé [d], P. Malmborg [e], M. Suter [f], B. Dittrich-Hannen [f], P.-W. Kubik [g], H.-A. Synal [g], D. Filges [h]

[a] *Center for Radiation Protection and Radioecology, University of Hannover, Am Kleinen Felde 30, D-30 167 Hannover, Germany*
[b] *Department of Nuclear Chemistry, University of Cologne, Cologne, Germany*
[c] *Department of Neutron Research at Studsvik, University of Uppsala, Uppsala, Sweden*
[d] *Department of Neutron Research, University of Uppsala, Uppsala, Sweden*
[e] *The Svedberg Laboratory, University of Uppsala, Uppsala, Sweden*
[f] *Institute for Particle Physics, ETH Hönggerberg, Zürich, Switzerland*
[g] *Paul Scherrer Institute c/o Institute for Particle Physics, ETH Hönggerberg, Zürich, Switzerland*
[h] *Institute for Nuclear Physics, KFA Jülich, Jülich, Germany*

Received 3 January 1997; revised form received 14 March 1997

Abstract

Cross sections for residual nuclide production by p-induced reactions were measured from thresholds up to 2.6 GeV using accelerators at CERN/Geneve, IPN/Orsay, KFA/Jülich, LANL/Los Alamos, LNS/Saclay, PSI/Villigen, TSL/Uppsala, LUC/Louvain La Neuve. The target elements C, N, O, Mg, Al, Si, Ca, Ti, V, Mn, Fe, Co, Ni, Cu, Sr, Y, Zr, Nb, Ba and Au were investigated. Residual nuclides were measured by X- and γ-spectrometry and by Accelerator Mass Spectrometry (AMS). The measured cross sections were corrected for interfering secondary particles in experiments with primary proton energies above 200 MeV. Our consistent database covers presently ca 550 nuclear reactions and contains nearly 15000 individual cross sections of which about 10000 are reported here for the first time. They provide a basis for model calculations of the production of cosmogenic nuclides in extraterrestrial matter by solar and galactic cosmic ray protons. They are of importance for many other applications in which medium energy nuclear reactions have to be considered ranging from astrophysics over space and environmental sciences to accelerator technology and accelerator-based nuclear waste transmutation and energy amplification. The experimental data are compared with theoretical ones based on calculations using an INC/E model in form of the HETC/KFA2 code and on the hybrid model of preequilibrium reactions in form of the AREL code.

1. Introduction

During recent years we investigated systematically the production of residual nuclides induced by low- and medium-energy protons. The main goal of these studies was to provide a database for model calculations of the production of cosmogenic nuclides in extraterrestrial matter by solar and galactic cosmic ray protons [1–8]. Consequently, the target elements were chosen according to their relevance in cosmo-chemistry and -physics. For a survey on this field of science see e.g. [8].

At the same time, such data are of importance for other applications in which medium energy nuclear reactions have to be considered. These applications range from astrophysics over space and environmental sciences, medicine (radionuclide production, dosimetry in mixed nucleon fields, radiation therapy), accelerator technology (activation of detectors, radiation protection, on-line mass separation), space and aviation technology to accelerator-based nuclear waste transmutation and energy amplification.

* Corresponding author. Fax: +49-511-762-3319; email: michel@mbox.zsr.uni-hannover.de

PII S0168-583X(97)00213-9

In an early phase of these investigations experiments were performed using accelerators at KFA Jülich ($E \leq 45$ MeV), LUC/Louvain La Neuve ($E \leq 70$ MeV), IPN/Orsay ($E \leq 180$ MeV) and at CERN ($E = 600$ MeV). These experiments covered mainly the target elements Ti, V, Fe, Co, Ni and Ba [3,9–16].

Later on, these investigations were intensified and enlarged with respect to the energy range as well as the target element and product nuclide coverage. Experiments were performed at PSI/Villigen ($E \leq 72$ MeV), LNS/Saclay ($E = 200$–400 MeV and 1.2–2.6 GeV) and at LANL/Los Alamos ($E = 800$ MeV). The target elements investigated at this time covered nearly all cosmochemically relevant elements, i.e. C, N, O, Mg, Al, Si, Ca, Ti, Mn, Fe, Co, Ni, Sr, Y, Zr, Nb, Ba. In addition, the elements V, Cu, Nb and Au were investigated for the sake of nuclear systematics. The mono-isotopic elements among them are particularly well suited for tests of nuclear reaction theories.

Detailed reports of the latter experiments at the Laboratoire National Saturne (LNS)/Saclay and at the The Svedberg Laboratory (TSL)/Uppsala were recently published [17–19] containing results for the target elements up to copper and barium. Residual radionuclides with half-lives above a few hours were measured by γ-spectrometry. Long-lived radionuclides such as ^{10}Be, ^{26}Al, ^{36}Cl and ^{41}Ca were investigated by accelerator mass spectrometry (AMS) [15,19–26] and stable rare gas isotopes by conventional mass spectrometry [14,16,18,19,27,28]. Further extensions of such investigations, e.g. measurements of cross sections for the production of ^{14}C, ^{53}Mn, ^{59}Ni, ^{129}I are still underway [30–32]. Preliminary reports of the new measurements have been made regularly to NEA/OECD [4,12,33–44]. Many of the cross sections were reported as parts of Ph.D. theses [45–53].

In this work, we report new results of our measurements on the target elements C, N, O, Mg, Al, Si, Ca, Ti, V, Mn, Fe, Co, Ni, Cu, Sr, Y, Zr, Nb, Ba and Au obtained by experiments at PSI, TSL, CERN, LANL and LNS. The entire data set now covers ca 550 target/product combinations with a total of nearly 15000 cross sections, from which about 10000 cross sections for more than 400 reactions are published here for the first time. For many reactions we now have detailed and consistent excitation functions from thresholds up to 2.6 GeV. We present the experimental details, representative results and some theoretical analyses of the new data.

During the last three years we have further increased the number of target elements of our investigations and started a systematic study of radionuclide production by medium-energy protons (70 MeV $\leq E \leq$ 2.6 GeV) for medium- and heavy-mass target elements. This was done to satisfy some of the data needs of feasibility studies for accelerator based nuclear waste transmutation [54,55] and energy amplification [56]. See in this context Refs. [57,58]. These still ongoing experiments are performed at TSL/Uppsala (70 MeV $\leq E \leq$ 180 MeV) and LNS/Saclay (200 MeV $\leq E \leq$ 2.6 GeV). The excitation functions will be completed by experiments at PSI/Villigen ($E \leq 72$ MeV). Only some preliminary data have been published so far [59–63].

In the investigations reported in this work the experimental data were analyzed by our group with various models and codes. Theoretical data were obtained from several versions of the ALICE code [64–67], from HETC/KFA2 [68], GNASH [69], ISABEL [70] in combination with SMM [71] and from the systematics of spallation reactions using Rudstam's formula [72] as well as various versions of the Tsao and Silberberg formulas [73]. Moreover, the experimental cross sections for the target elements O, Al, Fe, Co, Zr and Au were used as the experimental database for an International Model and Code Intercomparison of Intermediate Energy Activation Yields [74].

It was a general experience that all these models and codes did not satisfy the accuracy needs of model calculations neither for the production of cosmogenic nuclides in extraterrestrial matter, e.g. [4,5,7,8], nor for thick-target experiments by which the interactions of galactic protons with meteoroids were simulated [6,8,14,75–78]. Therefore, the experimental determination of cross sections remains indispensable if high quality data are needed for applications. This statement is supported by the results of a recent International Model and Code Intercomparison of Medium Energy Activation Yields [74] in which 22 different models and codes were tested for a wide range of target/product combinations and energies.

However, detailed analyses of experimental data with nuclear reaction codes and models can provide the basis for the necessary improvements of nuclear reaction models. Only then it may be possible to predict reliably those cross sections which are not accessible by present days experimental techniques and, moreover, to use such models for evaluation purposes. We shall perform such analyses here for two models: for the hybrid model of preequilibrium reactions [79] in form of the AREL code [67] and for an Intra-Nuclear-Cascade/Evaporation (INC/E) model in form of the HETC/KFA2 [68] code.

2. Experimental

The new cross sections were obtained from experiments at PSI/Villigen ($E < 72$ MeV), TSL/Uppsala (70 MeV $< E <$ 180 MeV) and LANL/Los Alamos (800 MeV) and LNS/Saclay ($E > 200$ MeV). Up to 180 MeV, cross sections were obtained using the stacked foil technique. Above 200 MeV single energy points were investigated as described elsewhere in detail; see Ref. [19] for energies between 200 MeV and 400 MeV and Ref. [18] for energies above 600 MeV. Below 200 MeV the experiments of this work were performed at PSI/Villigen/Ch and TSL/Up-

psala/S. The experiments at TSL were done as described by Bodemann et al. [17] for initial proton energies up to 100 MeV. The new irradiation experiments at TSL with proton energies of 160 MeV and 180 MeV used the same set-up as described there.

At PSI, stacks were irradiated with 45 MeV and 72 MeV protons. The stacks were of the same type as used at TSL [17] with the exception that the individual targets in the stacks and the total thicknesses of the stacks were much smaller. The targets in the stacks consisted of foils of pure element C, Mg, Al, Si, Ti, Fe, Co, Ni, Cu, Y, Zr, Nb, Au and of some composite materials for the target elements N (Si_3N_4), O (SiO_2), Ca ($Ca(HCOO)_2$), Mn (84.5% Mn/15.5% Ni alloy), Sr (SrF_2) and Ba (Ba containing glass). The targets were made of high purity materials with diameters of either 15.7 mm or 15.0 mm. Their thicknesses ranged from 0.036 mm up to 3.25 mm. They were chosen to be optimal for the respective primary proton energy and the energy range investigated.

Mostly, at least three foils of each element were irradiated together. In order to compensate for recoil losses and to avoid cross contaminations only the inner ones were used for measurements. Exceptions were the elements Ca, Sr and Ba, for which only one foil, each, was used with thicknesses between 1 mm and 3.25 mm. The $Ca(HCOO)_2$ targets were wrapped in 0.036 mm Al-foil in order to prevent cross contaminations of other targets in case of a target destruction by radiation damages or heating during the irradiation. All elemental target sets were separated by sets of three thin Al-foils (0.036 mm or 0.125 mm) and Cu-foils (0.050 mm) in order to minimize cross contamination. In addition, the inner ones of the three thin Al and Cu foils between the different target elements were used for flux monitoring.

The proton energies for the individual targets were calculated by a computer program based on the work of Andersen and Ziegler [80]. According to these authors, the applicability of their work is restricted to energies between 1 MeV and 100 MeV. Therefore, respective calculations were also performed using the work of Williamson et al. [81] and of Janni [82]. It was found that the deviations between the different calculations were about 3% on average. Also calculations according to formulae and data given in the recent Table of Isotopes [83] which are valid for energies between 10 MeV and 2 GeV confirm our energies within the above mentioned uncertainties. The latter reference [83] is based on actual updates of the work by Ziegler and Biersack [84]. The energy degradation in each stack was about 40–50 MeV at PSI and up to 80 MeV at TSL where the stacked-foil technique was used. For the irradiations above 600 MeV at LANL and LNS the stacks were chosen to degrade the energy less than 25 MeV. We demonstrate these uncertainties due to the energy loss calculations by an experiment at Uppsala. The initial p-energy was determined to be 136 ± 0.5 MeV by time-of-flight techniques. The calculated p-energy in the last target foil of the stack was 58.48 MeV according to Andersen and Ziegler [80] and 58.93 MeV using the more recent Ref. [83]. The estimated uncertainty of the p-energy in this target was 1.85 MeV taking into account that of the initial p-energy, the uncertainty due to the finite thickness of the target, itself, and a Gaussian energy straggling [85] with an energy straggling parameter according to Marmier and Sheldon [86]. The small uncertainties between the different stopping calculations were neglected.

All the new data were measured relatively to the monitoring reaction $^{27}Al(p,3p3n)^{22}Na$. For energies up to 200 MeV the results by Steyn et al. [87] were adopted as monitor cross sections, while for energies above 200 MeV the recommended cross sections (*valeurs adoptées*) by Tobailem and de Lassus St. Genies [88,89] were used (Table 1). For energies below 200 MeV this procedure differs from that of our earlier work [3,13,17] where also the recommended cross sections by Tobailem and de Lassus St. Genies [88,89] were adopted for monitoring below 200 MeV. Therefore, the problem of monitoring and consistency of our data is discussed in some detail in Section 4.3.

At PSI, the stacks were irradiated in air with mean proton currents of 30–40 nA three to seven hours, each. The beam was positioned by measuring the proton current on an empty stackholder and on an uncalibrated Faraday cup and by minimizing the current on the first one and maximizing it on the latter one. Beam currents were continuously recorded during irradiation by the uncalibrated Faraday cup connected to digitizing current meter coupled to a PC. The fluctuation of the beam intensity usually was small. However, intensity variation exceeding 10% and interruptions longer than 15 min were considered in the calculations of cross sections and flux densities using the logged data from the uncalibrated Faraday cup.

After a completed irradiation at PSI, first measurements of short-lived radionuclides (e.g. ^{61}Cu) were performed (by courtesy of A. Wyttenbach and L. Tobler). Then the irradiated targets were transported to Cologne and Hannover within 12 h and 24 h, respectively. A set of typically five stacks was involved in this procedure. Subsequently, non-destructive measurements were made several times by X- and γ-spectrometry using various Ge(Li)- and high purity Ge-detectors and a total of three automatic sample changers. Repeated measurements during one year allowed us to get a minimum of three spectra for all isotopes investigated. Often up to fifteen spectra were available for the evaluation of one product nuclide in a particular target. A detailed description of the measurement and evaluation procedure has been given earlier by Michel et al. [3,9–11,13,90].

The efficiencies of the γ-spectrometers at Cologne and Hannover were measured with different sets of calibration sources each having a certified uncertainty of their activities of less than 2%. Frequently, measurements of the same targets were performed at Hannover and Cologne for

Table 1
Monitor cross sections of the reaction $^{27}Al(p,3p3n)^{22}Na$ from the evaluation of [89] and from the measurements by [87]. In contrast to our earlier work, [3,13,17] and references therein, we used the Steyn et al. [87] data for monitoring of primary protons with energies above 90 MeV

Energy [MeV]	Cross section [mb]	Ref.
25.2	0.035 ± 0.015	[87]
26.8	0.181 ± 0.028	[87]
28.4	0.671 ± 0.060	[87]
29.9	2.09 ± 0.15	[87]
30.0	1.00	[89]
31.4	5.26 ± 0.34	[87]
32.8	9.87 ± 0.61	[87]
34.1	16.0 ± 0.98	[87]
35.0	20.0	[89]
35.4	22.0 ± 1.3	[87]
36.7	27.7 ± 1.7	[87]
38.0	32.7 ± 2.0	[87]
39.2	36.6 ± 2.2	[87]
40.0	40.0	[89]
40.9	41.4 ± 2.5	[87]
43.2	43.5 ± 2.6	[87]
45.0	45.0	[89]
45.4	43.1 ± 2.6	[87]
47.5	40.7 ± 2.4	[87]
49.6	38.3 ± 2.3	[87]
50.0	38.4	[89]
51.5	35.1 ± 2.1	[87]
53.5	33.1 ± 2.0	[87]
55.4	30.6 ± 1.9	[87]
57.2	28.3 ± 1.7	[87]
59.0	27.0 ± 1.6	[87]
60.0	27.1	[89]
60.7	25.9 ± 1.6	[87]
62.4	24.9 ± 1.51	[87]
64.1	23.8 ± 1.4	[87]
65.7	23.0 ± 1.4	[87]
67.0	22.7 ± 1.4	[87]
69.7	21.9 ± 1.4	[87]
70.0	23.4	[89]
72.3	21.7 ± 1.3	[87]
74.8	20.3 ± 1.3	[87]
77.3	20.3 ± 1.3	[87]
79.7	20.2 ± 1.2	[87]
80.0	21.2	[89]
82.1	20.0 ± 1.2	[87]
84.4	20.7 ± 1.3	[87]
86.6	19.9 ± 1.2	[87]
88.8	20.0 ± 1.2	[87]
90.0	19.8	[89]
91.0	19.9 ± 1.2	[87]
93.2	19.8 ± 1.2	[87]
95.6	19.8 ± 1.3	[87]
100	18.8	[89]
101	19.7 ± 1.2	[87]
107	19.1 ± 1.2	[87]
114	18.8 ± 1.2	[87]
119	18.1 ± 1.1	[87]
120	17.3	[89]
122	18.2 ± 1.3	[87]
126	18.0 ± 1.3	[87]
131	17.7 ± 1.3	[87]
136	17.7 ± 1.2	[87]
141	17.2 ± 1.2	[87]
146	17.3 ± 1.2	[87]
150	16.0	[89]
152	17.0 ± 1.1	[87]
157	16.9 ± 1.1	[87]
163	16.9 ± 1.1	[87]
169	16.7 ± 1.1	[87]
174	16.3 ± 1.0	[87]
180	15.3	[89]
181	16.1 ± 1.0	[87]
188	15.8 ± 1.0	[87]
193	15.2 ± 0.9	[87]
200	15.0	[89]
200	15.0 ± 0.9	[87]
220	14.9	[89]
250	15.0	[89]
300	15.4	[89]
350	15.6	[89]
400	15.8	[89]
450	15.9	[89]
500	16.0	[89]
600	16.0	[89]
700	15.8	[89]
800	15.5	[89]
900	15.3	[89]
1000	15.0	[89]
1500	13.5	[89]
2000	12.3	[89]
3000	11.1	[89]
5000	10.7	[89]
10000	10.4	[89]

quality control of the efficiency calibration. The results agreed always within the calculated errors (see Section 3.5) so that there is no indication of interlaboratory inconsistencies. Moreover, each target was measured on a number of different detectors in order to decrease the effects of systematic errors due to an accidental miscalibration of a particular detector.

The evaluation of the γ-spectra was done by two different codes: the already previously used, unpublished code GAMMA for a fast evaluation of spectra by a trapezoidal background subtraction method without unfolding of multipletts and the code GAMMA-W [91] for unfolding of complex spectra [92,93] in particular for the heavy target elements.

The use of unfolding techniques was essential for the

analysis of the gold targets which were extremely complex. See, for example, a spectrum of a gold target irradiated with 367 MeV protons after a decay time of 11 months (Fig. 1). The results of both codes agreed within statistical errors for those spectra for which both methods were applicable. The unfolding of very complex spectra could not be performed in an automatic mode, but had to be done interactively to have permanent control of the quality of the fit. Since this might introduce systematic human errors when analyzing the spectra, a large series of spectra was analyzed twice by different experimentalists as a blind intercomparison and it was gratifying to see that again the results agreed within the quoted errors of the unfolding procedures.

For the determination of the long-lived radionuclides ^{10}Be, ^{26}Al and ^{36}Cl accelerator mass spectrometry at the PSI/ETH AMS facility Zürich/CH was used. For the separation of ^{10}Be and ^{26}Al from C, Si_3N_4, SiO_2, Mg, Al and Si and for the preparation of samples for AMS, we used the same procedures as described earlier [17,19,21–23]. See Ref. [19] for references and reports of the — partially newly developed — chemical procedures.

A description of the AMS technique for the individual radionuclides is given elsewhere [94–98]. The measured isotope ratios have been normalized to the standards S555 with $^{10}Be/^{9}Be = (9.55 \pm 0.23) \times 10^{-11}$ [95], Al1092 with $^{26}Al/^{27}Al = (1.13 \pm 0.23) \times 10^{-10}$, and K380/4 with $^{36}Cl/^{nat}Cl = (1.53 \pm 0.05) \times 10^{-11}$. The ^{36}Cl standard is a secondary standard which was calibrated using the ^{36}Cl standard reference material NIST SRM 4943. It is in good (2%) agreement also with the UCSD standard ($^{36}Cl/^{nat}Cl = 9.944 \times 10^{-12}$) [99].

Typical isotope ratios (radioactive isotope/stable isotope) of the measured samples were between 10^{-12} to 10^{-10}. For each target element also non-irradiated material was analyzed for blank control of the material as well as for monitoring of cross contaminations during the chemical treatment. Since isotope ratios of the blanks were about 10^{-14}, the corrections were only a few percent if the isotope ratios measured for an irradiated target were near to 10^{-12}. In most cases they were negligible.

3. Data evaluation and error analysis

For quality assurance, we shortly document the data evaluation procedures used. Then, we discuss in detail the problem of absolute calibration of cross sections and the sources of experimental errors considered in this work.

3.1. Calculation of cross sections

Given a target with a number of target atoms N_T which is irradiated by protons of a flux density Φ (cm^{-2} s^{-1}) starting at the time at Begin Of Irradiation, t_{BOI}, to the time at End Of Irradiation, t_{EOI}. The irradiation lasted for

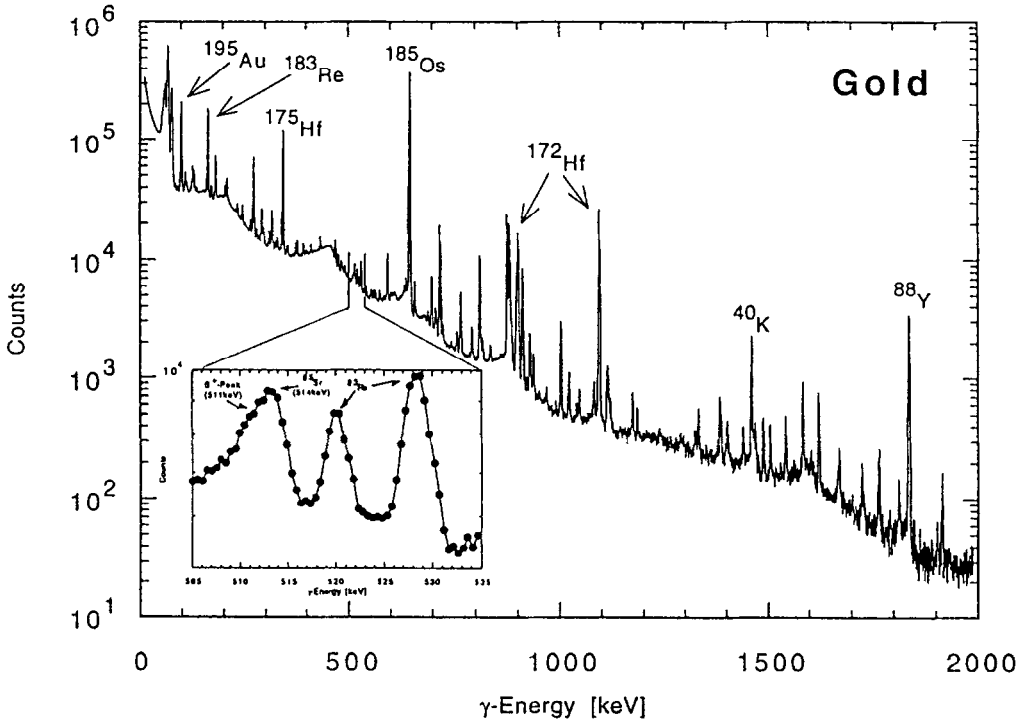

Fig. 1. Observed γ-spectrum of a gold target irradiated with 367 MeV protons after a decay time of 11 months.

Table 2
Survey on target elements and product nuclides covered by our experiments on medium and heavy mass target elements

Target element	Product nuclides							
C	Be-7	Be-10						
N	Be-7	Be-10						
O	Be-7	Be-10						
F	Be-7							
Mg	He-3c	He-3d	He-4	Be-7	Be-10	Ne-20	Ne-21	Ne-22c
	Ne-22d	Na-22	Na-24	Al-26				
Al	He-3c	He-3d	He-4	Be-7	Be-10	Ne-20	Ne-21	Ne-22c
	Ne-22d	Na-22	Na-24	Al-26				
Si	He-3c	He-3d	He-4	Be-7	Be-10	Ne-20	Ne-21	Ne-22c
	Ne-22d	Na-22	Na-24	Mg-28	Al-26			
Ca	Na-22	Na-24	Mg-28	Al-26	Cl-36	K-42	K-43	
	Ca-47	Sc-44m	Sc-46	Sc-48				
Ti	Be-7	Be-10	Na-22	Na-24	Al-26	Cl-36	K-42	K-43
	Ca-47	Sc-43	Sc-44	Sc-44m	Sc-46	Sc-47	Sc-48	Ti-44
	V-48							
V	Be-7	Na-22	K-43	Ca-47	Sc-44m	Sc-46	Sc-47	Sc-48
	V-48	Cr-48	Cr-49	Cr-51				
Mn	Be-7	Be-10	Na-22	Na-24	Mg-28	Al-26	Cl-36	K-42
	K-43	Ca-47	Sc-44m	Sc-46	Sc-47	Sc-48	V-48	Cr-51
	Mn-52	Mn-54						
Fe	He-3c	He-3d	He-4	Be-7	Be-10	Ne-21	Na-22	Na-24
	Mg-28	Al-26	Cl-36	Ar-38	K-42	K-43	Sc-44m	Sc-46
	Sc-47	Sc-48	Ti-44	V-48	Cr-48	Cr-51	Mn-52	Mn-54
	Fe-52	Co-55	Co-56	Co-57	Co-58			
Co	Be-7	Be-10	Na-22	Na-24	Al-26	Cl-36	K-42	K-43
	Sc-44m	Sc-46	Sc-47	V-48	Cr-48	Cr-51	Mn-52	Mn-52m
	Mn-54	Mn-56	Co-55	Co-56	Co-57	Co-58	Ni-56	Ni-57
Ni	He-3c	He-3d	He-4	Be-7	Be-10	Ne-20	Ne-21	Ne-22c
	Ne-22d	Na-22	Na-24	Al-26	Cl-36	Ar-36d	Ar-38	K-42
	K-43	Sc-44m	Sc-46	Ti-44	V-48	Cr-48	Cr-51	Mn-52
	Mn-54	Fe-59	Co-55	Co-56	Co-57c	Co-57	Co-58	Co-60
	Ni-56	Ni-57	Cu-61					
Cu	Be-7	Na-22	Na-24	K-42	K-43	Sc-44	Sc-44m	Sc-46
	Sc-47	V-48	Cr-48	Cr-51	Mn-52	Mn-54	Fe-59	Co-55
	Co-56	Co-57	Co-58	Co-60	Ni-56	Ni-57	Cu-61	Cu-64
	Zn-62	Zn-65						
Sr	Na-22	Sc-44m	Sc-46	V-48	Cr-51	Mn-52	Mn-54	Fe-59
	Co-56	Co-57	Co-58	Co-60	Zn-65	Ga-67	Ge-68	Ge-69
	As-71	As-73	As-74	Se-72	Se-75	Br-77	Br-82	Kr-76
	Kr-79	Rb-83c	Rb-83	Rb-84	Rb-86	Sr-82	Sr-83	Sr-85
	Y-86	Y-87	Y-87m	Y-88				
Y	Be-7	Na-22	Sc-44m	Sc-46	V-48	Cr-51	Mn-52	Mn-54
	Fe-59	Co-56	Co-58	Co-60	Zn-65	Ge-68	Ge-69	As-71
	As-73	As-74	Se-72	Se-75	Br-76	Br-77	Kr-79	Rb-83c
	Rb-83	Rb-84	Rb-86	Sr-82	Sr-83	Sr-85	Y-85m	Y-86
	Y-87	Y-87m	Y-88	Zr-86	Zr-87	Zr-88	Zr-89	
Zr	Be-7	Na-22	Na-24	Sc-44m	Sc-46	Sc-47	V-48	Cr-51
	Mn-52	Mn-54	Fe-59	Co-56	Co-57	Co-58	Co-60	Ni-57
	Zn-65	Ga-67	Ge-68	Ge-69	As-71	As-73	As-74	Se-72
	Se-75	Br-76	Br-77	Kr-79	Rb-83c	Rb-83	Rb-84	Rb-86
	Sr-82	Sr-83	Sr-85	Y-86	Y-87	Y-87m	Y-88	Zr-86
	Zr-88	Zr-89	Zr-95	Nb-90	Nb-91m	Nb-92m	Nb-95	Nb-95m
	Nb-96							
Nb	Be-7	Na-22	Sc-46	V-48	Cr-51	Mn-52	Mn-54	Fe-59
	Co-56	Co-58	Co-60	Zn-65	Ga-67	Ge-68	Ge-69	As-71

Table 2 (continued)

Target element	Product nuclides							
	As-73	As-74	Se-72	Se-75	Br-77	Kr-79	Rb-83c	Rb-83
	Rb-84	Sr-82	Sr-83	Sr-85	Y-86	Y-87	Y-87m	Y-88
	Zr-86	Zr-88	Zr-89	Nb-90	Nb-91m	Nb-92m		
Ba	Sc-46	V-48	Mn-52	Mn-54	Fe-59	Co-56	Co-58	Co-60
	Zn-65	Ge-69	As-74	Se-75	Rb-83	Rb-84	Rb-86	Sr-82
	Sr-83	Sr-85	Y-87	Y-88	Zr-89	Nb-90	Nb-92m	Nb-95
	Tc-95m	Tc-96	Rh-99	Rh-101	Rh-101m	Rh-102	Pd-100	Ag-105
	Ag-106m	Ag-110m	In-111	In-114m	Sn-113	Sb-120m	Sb-122	Sb-124
	Te-119	Te-119m	Te-121	Te-121m	I-124	I-126	I-130	I-131
	Xe-124	Xe-125	Xe-126	Xe-127	Xe-128	Xe-129	Xe-130	Xe-131
	Xe-132	Xe-134	Cs-129	Cs-132	Cs-134	Cs-136	Cs-137	Ba-128
	Ba-131	Ba-133	Ba-133m	Ba-135m	La-132	La-133	La-135	
Au	Be-7	Na-22	Na-24	Sc-46	V-48	Cr-51	Mn-54	Fe-59
	Co-56	Co-58	Co-60	Ni-56	Zn-65	As-74	Se-75	Br-82
	Rb-83c	Rb-83	Rb-84	Rb-86	Sr-85	Y-87	Y-88	Zr-88
	Zr-89	Zr-95	Nb-95	Tc-96	Ru-103	Ru-106	Rh-101	Rh-101m
	Rh-102	Rh-102m	Ag-105	Ag-110m	Sn-113	Te-121	Te-121m	Xe-127
	Ba-131	Ba-133	Ce-139	Pm-143	Eu-145	Eu-147	Eu-148	Eu-149
	Gd-146	Gd-147	Gd-149	Gd-151	Gd-153	Tb-151	Tb-153	Tb-155
	Dy-155	Dy-157	Er-160	Tm-165	Tm-167	Tm-168	Yb-166	Yb-169
	Lu-169	Lu-170	Lu-171	Lu-173	Hf-170	Hf-172	Hf-173	Hf-175
	Ta-182	W-178	Re-181	Re-182	Re-183	Os-182	Os-183m	Os-185
	Os-191	Ir-185	Ir-186	Ir-187	Ir-188	Ir-189	Ir-190	Ir-192
	Ir-194m	Pt-188	Pt-189	Pt-191	Au-193	Au-194	Au-195	Au-196
	Hg-193m	Hg-194	Hg-195m	Hg-197m				

the time t_{irr}. Then for any time t after t_{EOI} the activity $A_p(t)$ of a product nuclide p with a decay constant λ_p is given by

$$A_p(t) = N_T \sigma \Phi (1 - e^{-\lambda_p t_{irr}}) e^{-\lambda_p (t - t_{EOI})}$$
$$= A_p(t_{EOI}) e^{-\lambda_p (t - t_{EOI})}. \quad (1)$$

After irradiation, a target is measured starting at time Begin Of Counting t_{BOC} to time End Of Counting t_{EOC}, the time difference being the counting time t_c. Then the net counts $NP_p(E_\gamma, t_c, t_{BOC})$ of a full energy peak of a γ-transition of the nuclide p with energy E_γ is given by

$$NP_p(E_\gamma, t_c, t_{BOC}) = \int_{t_{BOC}}^{t_{EOC}} A_p(t) \epsilon(E_\gamma) I_\gamma(E_\gamma) dt \quad (2)$$

with $\epsilon(E_\gamma)$ and $I_\gamma(E_\gamma)$ being the efficiency of the detector at energy E_γ and the absolute γ-branching for the energy E_γ, respectively. Combining Eqs. (1) and (2) one receives

$$NP_p(E_\gamma, t_c, t_{BOC})$$
$$= A_p(t_{EOI}) e^{-\lambda_p t_{BOC}} \epsilon(E_\gamma) I_\gamma(E_\gamma) (1 - e^{-\lambda_p t_c}). \quad (3)$$

The net-peaks NP_p are the results of the γ-spectrum-evaluation codes. From the NP_p the activity of the product at end of irradiation $A_p(t_{EOI})$ is calculated. Using this activity, the cross section is calculated using Eq. (1).

The nuclear data for the evaluation of the cross sections were taken from the following sources: half-lives from the chart of nuclides [100], energies and branching ratios of γ-rays from the compilation of Reus and Westmeier [101].

3.2. Corrections for radioactive progenitors

As a consequence of the experimental technique used, the cross sections are cumulative ones in most cases. Independent cross sections were only determined if either the product nuclide is naturally shielded from decay of radioactive progenitors or if the cross sections of the progenitor were determined, too. It is stated in the EXFOR compilation (see Section 4) if cross sections are independent. Since, however, the correction for radioactive progenitors can pose some problems if not done correctly we describe here shortly the calculational procedure how independent cross sections were calculated.

Eqs. (1)–(3) are correct if independent cross sections are determined or if the half-lives of all radioactive progenitors are very short compared to that of the nuclide in question. In the latter case in which all radioactive progenitors are completely decayed before measuring the target the cross sections σ is the cumulative one, i.e. the sum of all independent cross sections of nuclides decaying to the product p including that of this nuclide.

The assumption of very short-lived progenitors holds in many cases, but not in all. There are cases {e.g. ^{86}Zr (T = 16.5 h) and ^{86}Y (T = 14.74 h), ^{88}Zr (T = 83.4 d) and

^{88}Y (T = 106.6 d), ^{95}Zr (T = 64.0 d) and ^{95g}Nb (T = 34.97 d)} where a mother nuclide m decays to the product nuclide p with a decay constant λ_m comparable to λ_p. In this case use of Eq. (3) results in a wrong $A_p(t_{EOI})$ which here shall be denoted as $A_p^*(t_{EOI})$. The true $A_p(t_{EOI})$ is calculated from $A_p^*(t_{EOI})$ by

$$A_p(t_{EOI}) = A_p^*(t_{EOI}) + A_m(t_{EOI})\frac{\lambda_p}{(\lambda_p - \lambda_m)} \times [1 - e^{-(\lambda_m - \lambda_p)(t_{BOC} - t_{EOI})}]\frac{\lambda_p}{\lambda_m} \times \frac{[1 - e^{-\lambda_m t_c}]}{[1 - e^{-\lambda_p t_c}]}. \quad (4)$$

In this case the (cumulative) cross section of the mother nuclide can be measured and an independent cross section for the product p is determined using the correction of Eq. (4). Higher orders of grandparent progenitors can be neglected in all cases because of the strong decrease of half-lives with increasing distance from the valley of stability.

There are some particularly complicated cases with respect to the application in cosmochemistry. For stable rare gas nuclides, such as e.g. ^{3}He, ^{22}Ne, ^{36}Ar, sometimes the cumulative production has to be distinguished from the so-called direct production. This is done if there is a very long-lived progenitor, ^{3}H, ^{22}Na and ^{36}Cl in our examples. Then the cumulative yield means the production including also the long-lived progenitors, while the term *direct production* is used for the cumulative production excluding the particularly long-lived progenitor. As used in our ear-

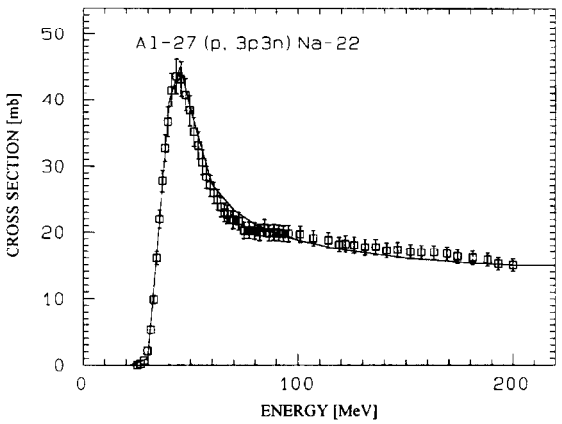

Fig. 2. Comparison of the excitation functions for the production of ^{22}Na from aluminum as recommended by the authors of Ref. [89] (full line) and as measured recently by [87] (open squares).

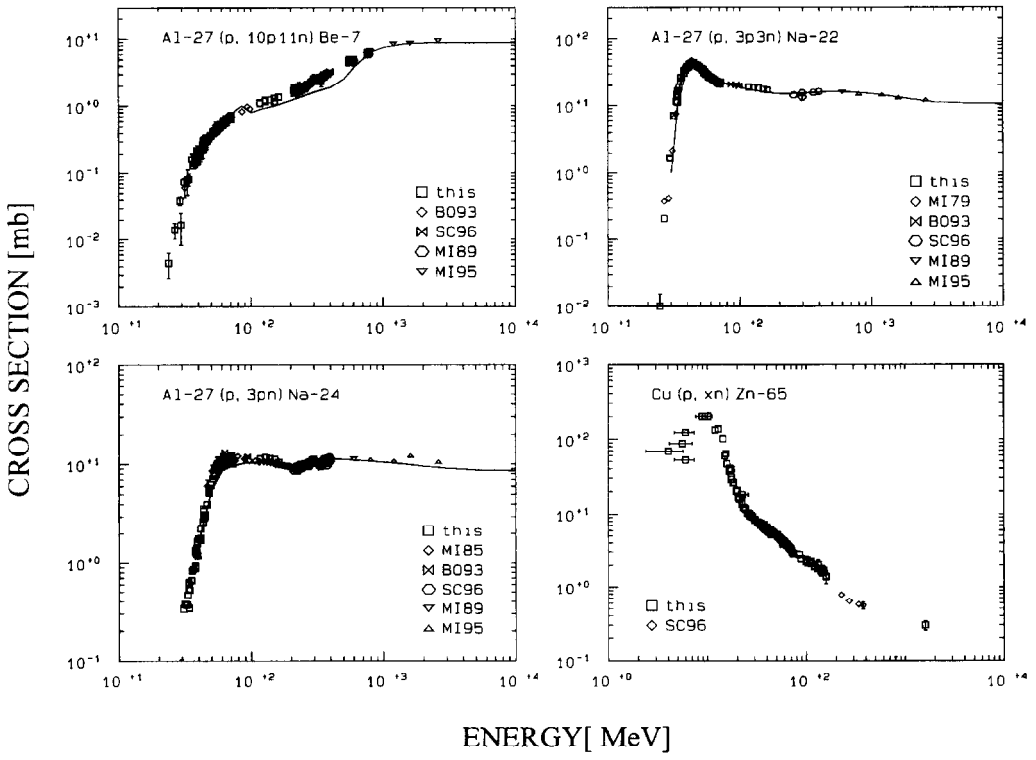

Fig. 3. Excitation functions for the production of ^{7}Be, ^{22}Na and ^{24}Na from aluminum and of ^{65}Zn from copper. The experimental data shown are exclusively from our work. The full lines are the *valeur adoptées* given by [89].

lier work [18,26] we distinguish such cross sections by *c* for *c*umulative and *d* for *d*irect, respectively. This was also done in Table 2.

3.3. Monitoring cross sections and absolute calibration

Absolute measurements of the fluxes of primary particles by Faraday cups were only performed in our experiments at Jülich, at both the JULIC and the CV28 cyclotrons [9–12]. Above 45 MeV, we adopted the recommended values of Tobailem and de Lassus St. Genies [88,89] in our earlier work at Louvain, IPN/Orsay and Uppsala [3,13,17]. Since the stacked-foil technique was used in these experiments, the fluxes in the stacks were determined from the ^{22}Na activities in the first Al-foils of each stack. Therefore, the experimental data reported in refs. [3,13,17] exclusively depend on the monitor cross sections given by Tobailem and de Lassus St. Genies [88,89] at proton energies of 72 MeV (Louvain), 100 MeV (Uppsala) and at 180 MeV (IPN/Orsay).

In 1990, Steyn et al. [87] published new absolute measurements of ^{27}Al(p,3p3n)^{22}Na which in some parts deviated from the recommendation of Tobailem and de Lassus St. Genies [88,89] (Fig. 2). Though the two excitation functions agree within the limits of the experimental errors given by Steyn et al. [87], there remain some systematic differences. The data are in excellent agreement from threshold up to 60 MeV. Above 60 MeV the data of Steyn et al. [87] are systematically lower than those recommended by Tobailem and de Lassus St. Genies [88,89]. Both data sets agree again at 90 MeV. Between 90 MeV and 200 MeV the data by Steyn et al. [87] are slightly higher than the other ones [88,89]. At 200 MeV both data sets again agree.

Our new experiments at PSI/Villigen (45 MeV and 72 MeV) and at TSL/Uppsala (130 MeV and 180 MeV), in which a large number of aluminum targets were included enabled us to investigate the consistency of the excitation functions of this monitor reaction. Our new data, [44] and this work, for the reaction ^{27}Al(p,3p3n)^{22}Na together with our earlier results [12] support the excitation function obtained by Steyn et al. [87], which will be used in this work and further for monitoring.

At the same time our investigations of targets irradiated at PSI/Villigen, TSL/Uppsala and LNS/Saclay enabled us to present new comprehensive data for the reactions ^{27}Al(p,X)^{7}Be and ^{27}Al(p,3pn)^{24}Na, for which the database was less complete and partially contradictory up to now. The new data [44] are presented in Fig. 3 for ^{27}Al(p,X)^{7}Be and ^{27}Al(p,3pn)^{24}Na. For the latter reaction, there exist additional measurements from our group in Ref. [13]. Thus, we now have a consistent set of excitation functions from thresholds up to 2.6 GeV for the three reactions ^{27}Al(p,X)^{7}Be, ^{27}Al(p,3p3n)^{22}Na, and ^{27}Al(p,3pn)^{24}Na (Fig. 3) which can serve as monitor reactions.

Above 200 MeV, only the evaluation by Tobailem and de Lassus St. Genies [88,89] exists as monitoring reactions. There are no other absolute measurements of the monitoring cross sections than those given by these authors. It has to be considered that the evaluation by Tobailem and de Lassus St. Genies [88,89] in the energy range from 600 MeV to 3 GeV is based on three absolute measurements by Friedlander et al. [102], Cumming et al. [103] and Heydegger et al. [104], only. The errors of the flux determinations in these investigations are 30% [102], 15% [103] and 10% [104]. The *valeurs adoptées* by Tobailem and de Lassus St. Genies [88,89] favor the results of Cummings et al. [103] and of Heydegger et al. [104].

A check of the consistency of the monitoring excitation function above 200 MeV is only possible for a few energy points between 200 MeV and 400 MeV for which we used a "semi-stacked-foil-technique" in our experiments at LNS/Saclay, Ref. [26] and this work. However, from the smoothness and consistency of the results which have been measured by us there is no indication of inconsistencies in the excitation function for the reaction ^{27}Al(p,3p3n)^{22}Na.

When performing the low-energy experiments at PSI, in particular with initial energies of 45 MeV, special care had to be taken for the flux monitoring. At low energies the reaction ^{27}Al(p,α pn)^{22}Na is not suitable for monitoring because of its high threshold of 23.35 MeV ($Q = -22.51$ MeV) and its strong gradient for energies below 40 MeV. However, in those experiments monitoring by the reaction ^{27}Al(p,α pn)^{22}Na was possible for the initial aluminum foils of each stack. This makes the data measured below 45 MeV at PSI consistent with those measured at higher energies. Moreover, the excellent agreement with our earlier absolute measurements at KFA Jülich couples them successfully to absolute calibrated cross sections. In addition, we used the reaction ^{65}Cu(p,n)^{65}Zn with a threshold of 2.17 MeV ($Q = -2.13$ MeV) for the incoming proton beam for monitoring at low energies deep inside the stacks irradiated with 45 MeV protons.

Generally, when going to proton-energies below 50 MeV, aluminum is not well suited as monitoring target element, because one has to measure near the threshold where the excitation functions have large gradients. Then, the uncertainty of the proton energy in a target becomes crucial. Here, copper offers an alternative solution. The reaction ^{65}Cu(p,n)^{65}Zn, which has a threshold of only 2.17 MeV ($Q = -2.13$) and a Coulomb wall of 7.14 MeV, is applicable down to energies of less than 10 MeV. For this reaction a large number of consistent measurements and also recent absolute measurements by Mills et al. [105] exist. We have determined the excitation function of this reaction relative to the aluminum monitoring reactions. The results of our investigation (Fig. 3) [44] are in excellent agreement with those reported by Mills et al. [105]. But, our measurements extend the range investigated by Mills et al. [105] up to 375 MeV. At higher energies, (p,n)-reactions are not suitable as monitor reactions because they become extremely sensitive to interferences by

low-energy secondary protons and secondary light complex particles [18].

The reaction $^{27}Al(p,3pn)^{24}Na$ ($Q = -31.43$ MeV) also has a similar threshold as $^{27}Al(p,\alpha pn)^{22}Na$ ($Q = -22.51$ MeV). In principle, it could also be used for consistency checks and monitoring purposes at lower energies. Our new results might be useful for this purpose. However, we did not use ^{24}Na from aluminum for monitoring purposes, because it is extremely sensitive to interferences by secondary neutrons via the reaction $^{27}Al(n,\alpha)^{24}Na$ which has a threshold of only 3.25 MeV ($Q = -3.13$ MeV).

Another problem came up when comparing the results obtained for the production of ^{7}Be from Al with the recommended cross sections by Tobailem and de Lassus St. Genies [88,89]. Our new results allow to resolve an inconsistency between two data sets by Furukawa et al. [106] and Miyano [107] which provided the basis for the recommendations by Tobailem and de Lassus St. Genies [88,89]. Our results, [45] and this work, are in agreement with the earlier measurements by Furukawa et al. [106] and decide together with a newer measurement by Grütter [108] against the *valeurs adoptées* of Tobailem and de Lassus St. Genies [88,89].

3.4. Corrections for interferences by secondary particles

Corrections for the interferences by secondary particles were performed for all experiments with initial proton energies above 200 MeV. The method of these corrections were described in detail elsewhere [18,26]. As discussed earlier for the high-energy case (800 MeV–2.6 GeV) these reactions which actually are $^{57}Fe(p,n)^{57}Co$, $^{58}Fe(p,2n)^{57}Co$, $^{58}Fe(p,n)^{58}Co$, and $^{26}Mg(p,n)^{26}Al$ can be interfered by reactions such as $^{56}Fe(\alpha,pxn)$ and $^{24}Mg(\alpha,pxn)$. The particular case for these reactions is that, due to the much higher abundance of ^{56}Fe in natural iron relative to ^{57}Fe and ^{58}Fe, even the low production of complex secondary particles can have significant effects. These effects cannot be corrected on the basis of our present knowledge. Generally, effects of secondary particles below 200 MeV have not been corrected for. There are some indications that interferences by secondary particles might be important also for energies between 100 MeV and 200 MeV for reactions such as $Fe(p,xn)^{57}Co$ and $Fe(p,xn)^{58}Co$ if too thick target stacks are used.

3.5. Errors of the experimental cross sections

The following sources of errors were considered and taken into account according to the laws of error propagation in the total errors quoted for the cross sections:

(1) Uncertainties in the determination of the number of target atoms and their homogeneity over the target area: 2%.

(2) Impurities in the target materials causing interfering nuclear reactions and errors resulting from the correction of contributions of other target constituents: Due to the high purity of the target materials used, the first source of error is negligible. For the determination of ^{7}Be and ^{10}Be from oxygen and nitrogen in quartz and Si_3N_4 targets, respectively, the latter source of error cannot be neglected; it is included in the errors quoted in Table 2. The same is true for all product nuclides from Mn which was applied as a Mn/Ni alloy.

(3) Fluctuation in beam intensity during irradiation: The beam intensities were continuously monitored and recorded. The fluctuations and interruptions of the irradiations were taken into account when calculating fluxes and cross sections. An analysis of the uncertainties of this procedure resulted in an overall error of 2%.

(4) Interference by reactions induced by secondary particles produced in the stacks: This turned out to be a problem in the experiments with initial proton energies above 200 MeV. A method was developed to describe quantitatively the influence of secondary particles produced in the target stacks and to correct the measured data for their interferences [18,26,49]. The additional uncertainty caused by the correction for each individual reaction is considered in the errors given for the cross sections. In those cases where the errors of the corrected cross sections became unacceptably high, no cross sections for the respective products are reported.

(5) Interference by reactions induced by secondary particles produced in the experiment halls: Such a general background of secondary particles was checked at LNS Saclay for the 1.6 GeV experiments by exposing Al, Fe, Co, and Ni foils at various places and by measuring the induced activities. It turned out that the interferences from this general background were below 1%, in the majority of cases about 0.1%, of the measured responses. Therefore, these interferences were neglected.

(6) Recoil loss and recoil contamination: By analyzing the foils in the inner part of each "target element unit" consisting of more than two identical foils these errors cancel out. If only one target of an element was irradiated as for Ca, Sr, and Ba these targets were so thick (1 mm to 3.25 mm) that the relative loss of activity by recoil was negligible since the mean ranges of recoil nuclei are much shorter than the thicknesses of the targets used. For target elements from vanadium to cobalt the mean ranges of recoil nuclei R can be approximately calculated by the empirical formula $R\ (mg/cm^2) \approx 0.045 \cdot \Delta A$ [53,109] with ΔA being the difference between target and product masses. The recoil contamination from the adjacent Al foils by ^{22}Na and ^{24}Na, however, had to be corrected for only for Ca and Sr targets near the thresholds. It was determined from Ca and Sr targets which were clearly below the respective thresholds.

(7) Error of the monitor cross section: No error was assigned to the monitor cross sections (compare discussion in Section 4.3).

(8) Uncertainty of the measurement of the monitoring

radionuclides (^{22}Na and ^{65}Zn): The relative precision of this determination was checked by multiple measurements and the error was estimated to be less than 1%.

(9) Error of the absolute efficiency calibration of γ-spectrometers: From the comparison of different calibrated radionuclide sets, the error of absolute efficiency calibration can be adopted to be below 5%. It is larger than the error of relative efficiency calibration. From comparisons of measurements performed on different detectors, the relative uncertainty of the efficiency calibrations can be considered to be 2%. Since the error in the absolute efficiency calibration affects the flux determination, it has also to be considered in the case of the cross sections measured by AMS or MS. It has to be omitted, however, when discussing cross section ratios of nuclides determined by these latter techniques.

(10) Reproducibility of photopeak integration: Up to 15 measurements were used for the determination of each nuclide, thus allowing to properly account for this source of error.

(11) Statistical counting error: This source of uncertainty is included by calculating the errors of individual photopeaks. The error of background subtraction was taken into account.

(12) Dead time and pile up losses in γ-spectrometry: By varying the distance between the sources and the detector, the dead time was always kept below 10%, where the internal life time correction of the ADC/MCA system was checked to be correct.

(13) Self-absorption of γ-rays in the sample: For γ-energies above 120 keV and for thin, light- and medium-weight target elements this source of error was negligible (corrections < 1%). For thicker targets, heavy target elements and low γ-energies corrections had to be partially applied which were calculated using attenuation coefficients calculated from the photon cross sections by Storm and Israel [110].

(14) Errors due to γ–γ-coincidences: Losses or gains in the net-peaks of γ-lines due to γ–γ-coincidences were usually negligible. Only for some nuclides decaying by β^+-decay the 511 keV γ-radiation caused some problems. Corrections for coincidence losses had to be done depending on the measuring geometry. However, the corrections were in general less than 1% if one carefully avoids γ-transitions with high coincidence probabilities. In particular, they were less than 1% and 3% for the 810 keV and 1274 keV γ-lines of ^{58}Co and ^{22}Na, respectively.

(15) Errors of the AMS measurements: The statistical

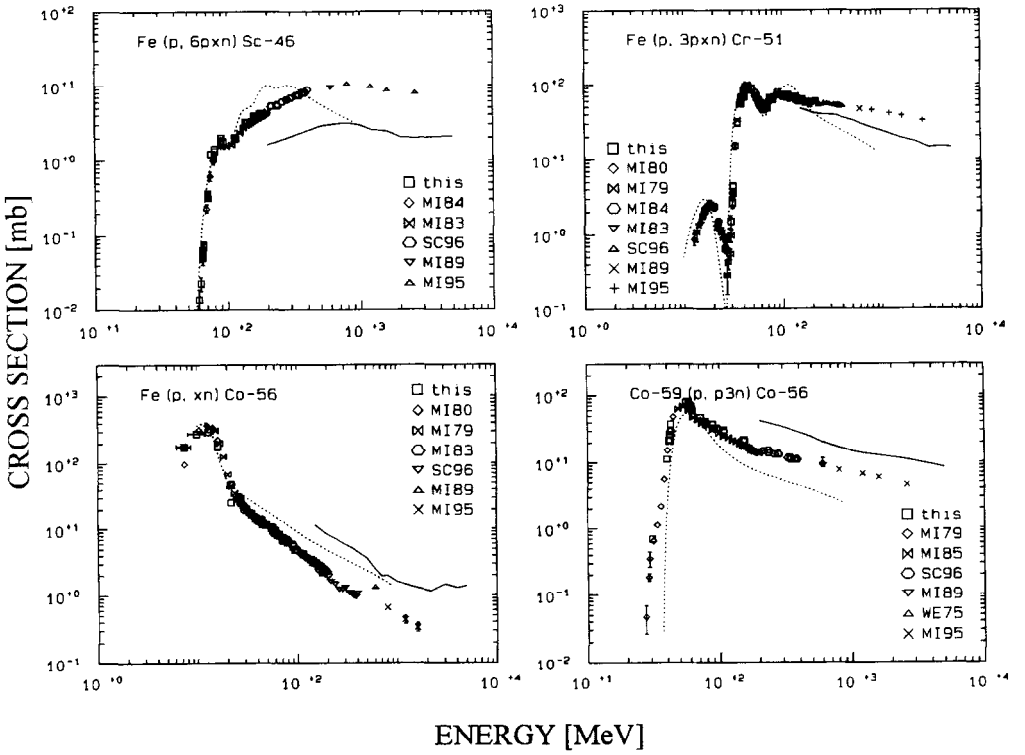

Fig. 4. Excitation functions for the production of ^{46}Sc, ^{51}Cr and ^{56}Co from iron and of ^{56}Co from cobalt as a demonstration of the typical consistency with earlier work of our group. Theoretical excitation functions were calculated by the HETC/KFA2 (full lines) and AREL (broken lines) codes.

counting errors for both samples and standards as well as the standard deviation of independent measurements of the same sample were taken into account.

(16) Nuclear decay data: The nuclear decay data used for the evaluation of the measurements may also be found in the EXFOR compilation (see Section 4). The error of the nuclear half-lives was not considered. Neither were those of absolute γ-intensities. However, it must be pointed out that the errors given for the cross sections also account for inconsistencies between the absolute γ-intensities of the γ-lines used.

All these errors were considered to be independent. Consequently, they were quadratically added according to the laws of error propagation to obtain *total errors* of the cross sections relative to the standard cross sections. However, some of the sources of errors are common to all data of our experiments in the same way, while others individually affect each reaction. The common errors sum up quadratically to about 6% and have to be quadratically subtracted when discussing ratios of cross sections from this work or the precision of the measured cross sections instead of their accuracy.

4. Experimental results

In this work, 9302 new cross sections were measured for a total of 428 target/product combinations. Table 2 gives a survey of the target/product coverage. Our entire up-to-now work covers 547 target/product combinations with nearly 15000 cross sections.

Since it is not feasible to publish all the new results in tabular form the data were converted to EXFOR format [111] by the NEA Data Bank of the OECD/Paris in cooperation with F.E. Chukreev/Nuclear Structure and Reaction Data Center/Moscow. They can be retrieved via INTERNET from the NEA Data Bank at Paris under the EXFOR number O0276. Also the earlier published results can be retrieved in this way via EXFOR numbers A0100 [3,36,112], A0145 [1,16], A0146 [11,16], A0151 [12], A0153 [34], A0344 [113], A0432 [37], A0435 [38], A0478, A0479, A0481 [39], A0516 [42], A0517 [41], B0083 [10], O0078 [15], O0088 [114], O0098 [22], B0100 [9], O0104 [20], O0277 [18], O0278 [27], O0279 [28], O0280 [76], O0281 [21], O0282 [17], O0284 [26].

The present data set will be considerably enlarged in

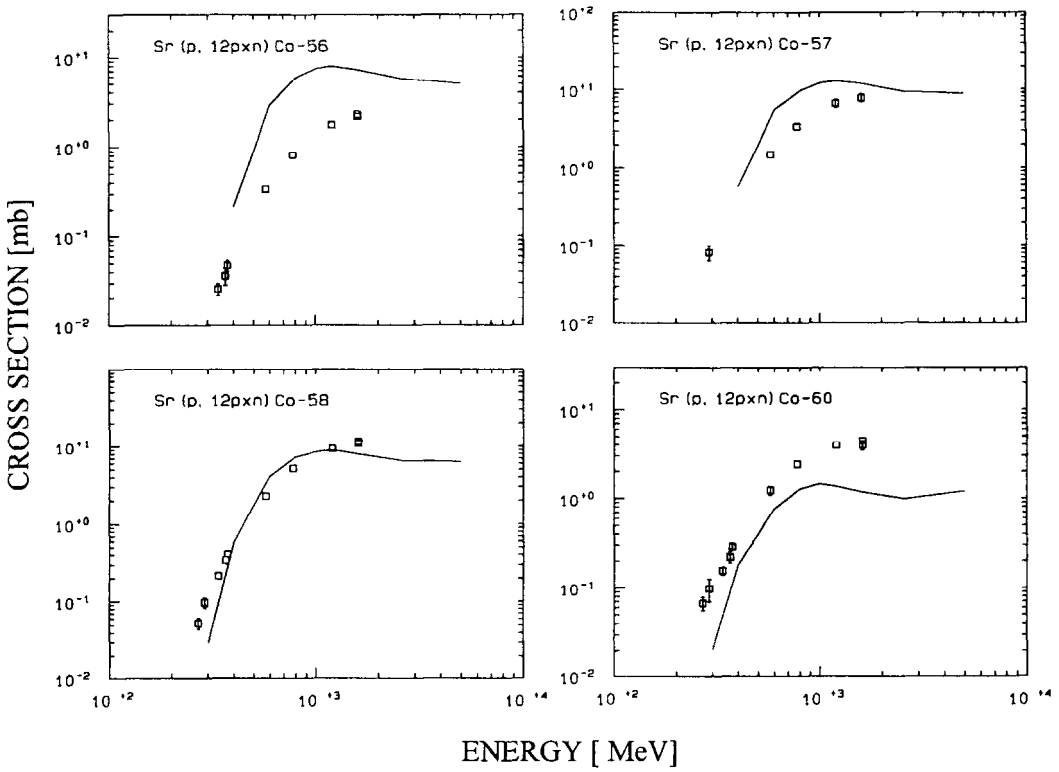

Fig. 5. Experimental and theoretical excitation functions for the production of ^{56}Co, ^{57}Co, ^{58}Co and ^{60}Co from strontium. The experimental data shown are exclusively from our work. Theoretical excitation functions were calculated by the HETC/KFA2 code (full lines).

the near future as soon as the final results of our experiments for target elements relevant for accelerator-driven waste transmutation and energy amplification become available [59–63].

4.1. Phenomenology of excitation functions

The new database allows an unprecedented survey on excitation functions of proton-induced reactions. For the target elements up to copper, such a survey was given earlier, both in tabular form and in figures [18,26]. Also for these target elements a large number of new data is now available. To demonstrate their consistency with the data published earlier, we show in Fig. 4 examples of the excitation functions for the production of ^{46}Sc, ^{51}Cr, and ^{56}Co from iron and of ^{56}Co from cobalt. The quality exhibited by these examples is typical for all the results obtained in this work. However, the number of data per excitation function is smaller for some of the newly investigated target elements.

For the heavier target elements which were not dealt with by us before, we give typical examples in form of figures for strontium, yttrium, zirconium, and niobium in Sections 4.1.1 and 4.1.3 for gold. All the figures of excitation functions contain besides experimental data results of theoretical calculations. These calculations will be described and discussed in Sections 5 and 6, respectively.

4.1.1. Excitation functions for targets elements strontium to niobium

The target elements from Sr (Figs. 5–7), Y (Figs. 8 and 9), Zr (Figs. 10–12) and Nb (Figs. 13 and 14) are heavy enough to exhibit a broad range of product nuclides and a variety of reaction types extending from compound nucleus and preequilibrium reactions to spallation and fragmentation without, however, the complication of intermediate energy fission.

The excitation functions of products far away from the target nuclides, i.e. typical spallation products, generally show few or no structure. For the target element strontium this is seen in Figs. 5 and 6 for reactions ranging from (p,14pxn) to (p,5pxn).

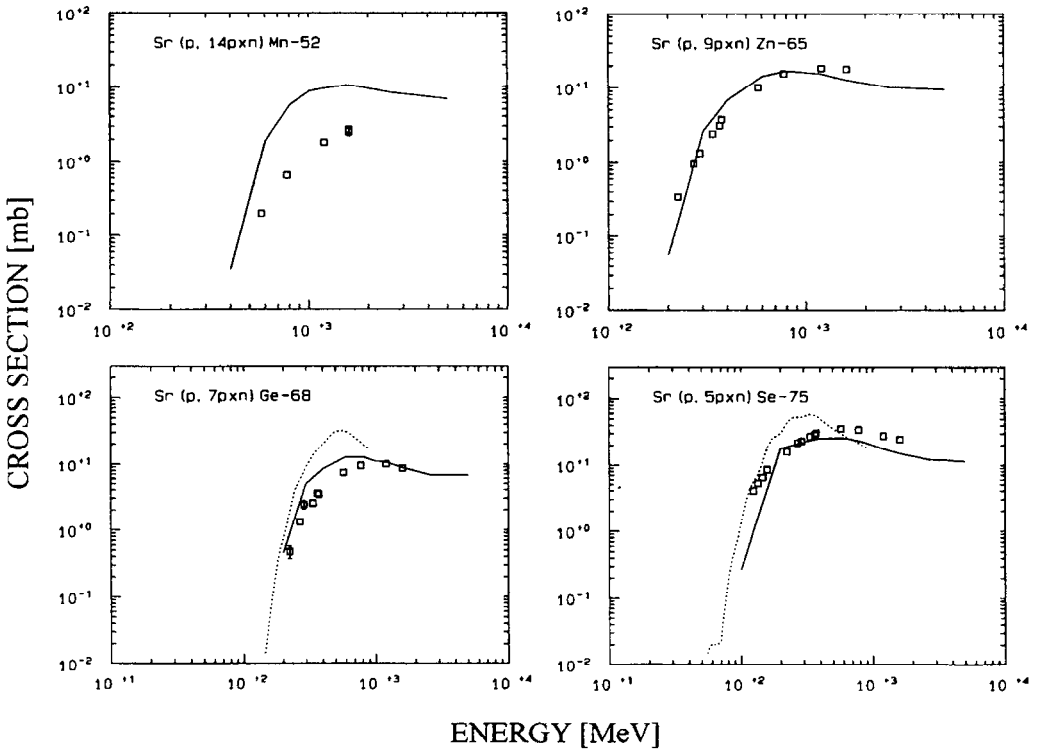

Fig. 6. Experimental and theoretical excitation functions for the production of ^{52}Mn, ^{65}Zn, ^{68}Ge and ^{75}Se from strontium. The experimental data shown are exclusively from our work. Theoretical excitation functions were calculated by the HETC/KFA2 (full lines) and AREL (broken lines) codes.

Note that the nomenclature (p,xpyn) does not necessarily imply that x protons and y neutrons are emitted successively as single particles in the reaction. Light complex particles may also contribute and fragmentation or fission may have occurred. It is generally not known by which reaction path the product nuclide was formed. This is the major complicating fact when modeling residual nuclide production. The nomenclature used here just counts the necessary balance of neutrons and protons to be lost during the reaction since one does not know to which extend complex particles are involved in the reaction.

As a consequence it is not possible to define energetically meaningful thresholds. One rather observes apparent thresholds defined by the lowest cross sections measurable under the given experimental conditions. In Figs. 5 and 6 the apparent thresholds of (p,7pxn)- to (p,14pxn)-reactions are well above 100 MeV with the general tendency of an increase with decreasing product masses. However, these apparent thresholds can energetically only be explained if the emission of complex particles or light nuclei is involved in the reactions.

As pointed out earlier [18], there are no constant plateaus in the excitation functions above a certain energy. Over the investigated energy range, i.e. up to 2.6 GeV, each excitation function has its characteristic shape. In the case of strontium, the (p,12xn)-reactions continuously increase with proton energy (Fig. 5). When the mass differences between target and product decrease a broad maximum appears at a few hundred MeV or 1 GeV (Fig. 6), the energy of the maximum being shifted to smaller energies with decreasing mass difference.

Pronounced structures are seen in the excitation functions for (p,2pxn)-reactions with α-particle emission. The excitation function for the production of ^{84}Rb from Sr (Fig. 7) which is dominated by the reactions ^{87}Sr(p,α)^{84}Rb and ^{88}Sr(p,αn)^{84}Rb shows two maxima from which the first one is attributed to evaporation of α-particles, the second one to emission of single nucleons. For a target element such as strontium with a number of stable isotopes such attributions are ambiguous. For mono-isotopic target elements such structures are more clearly defined as e.g. for ^{89}Y(p,2p3n)^{85}Sr (Fig. 9) or for ^{93}Nb(p,2p4n)^{88}Zr and ^{93}Nb(p,2p3n)^{89}Zr (Fig. 14). For the target elements yttrium and niobium, one can already see structures involving α-emission for (p,3pxn)-reactions (Figs. 9 and 14). Even for (p,5pxn)- and (p,4pxn)-reactions there are small

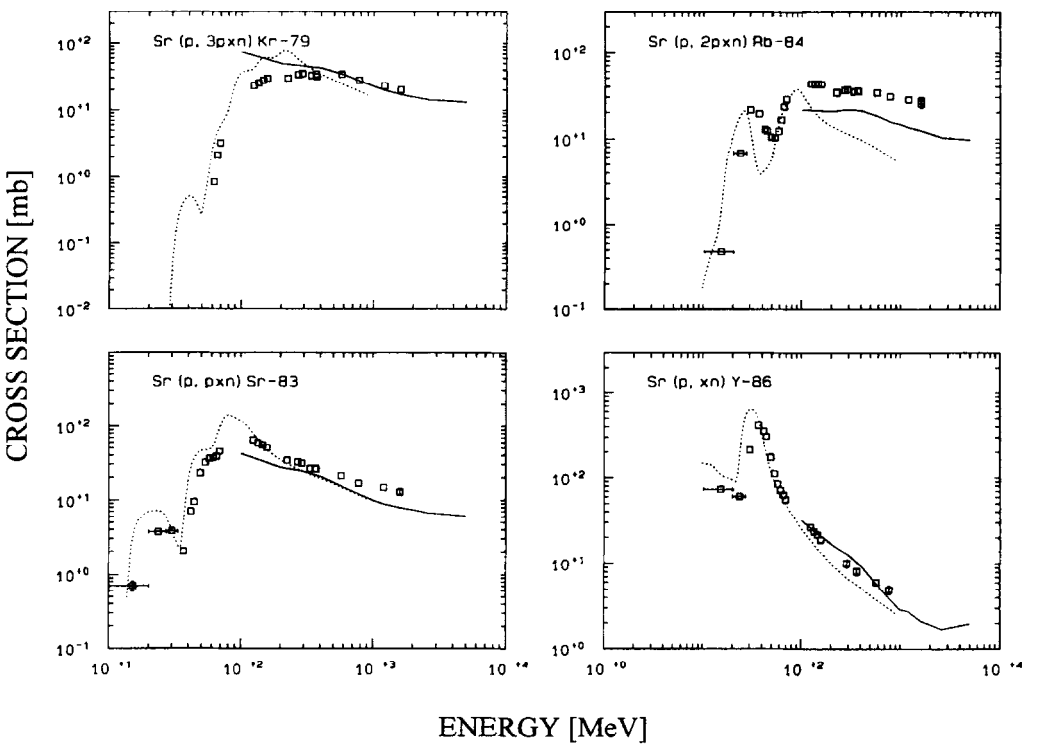

Fig. 7. Experimental and theoretical excitation functions for the production of ^{79}Kr, ^{84}Rb, ^{83}Sr and ^{86}Y from strontium. The experimental data shown are exclusively from our work. Theoretical excitation functions were calculated by the HETC/KFA2 (full lines) and AREL (broken lines) codes.

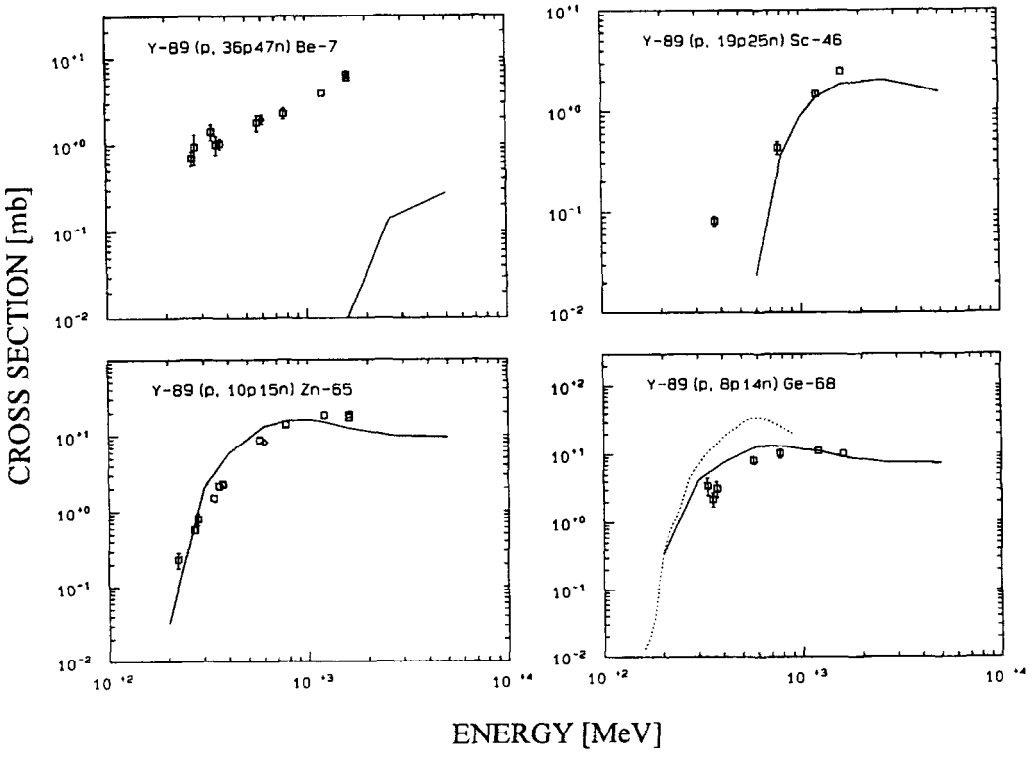

Fig. 8. Experimental and theoretical excitation functions for the production of ^{7}Be, ^{46}Sc, ^{65}Zn and ^{68}Ge from yttrium. The experimental data shown are exclusively from our work. Theoretical excitation functions were calculated by the HETC/KFA2 (full lines) and AREL (broken lines) codes.

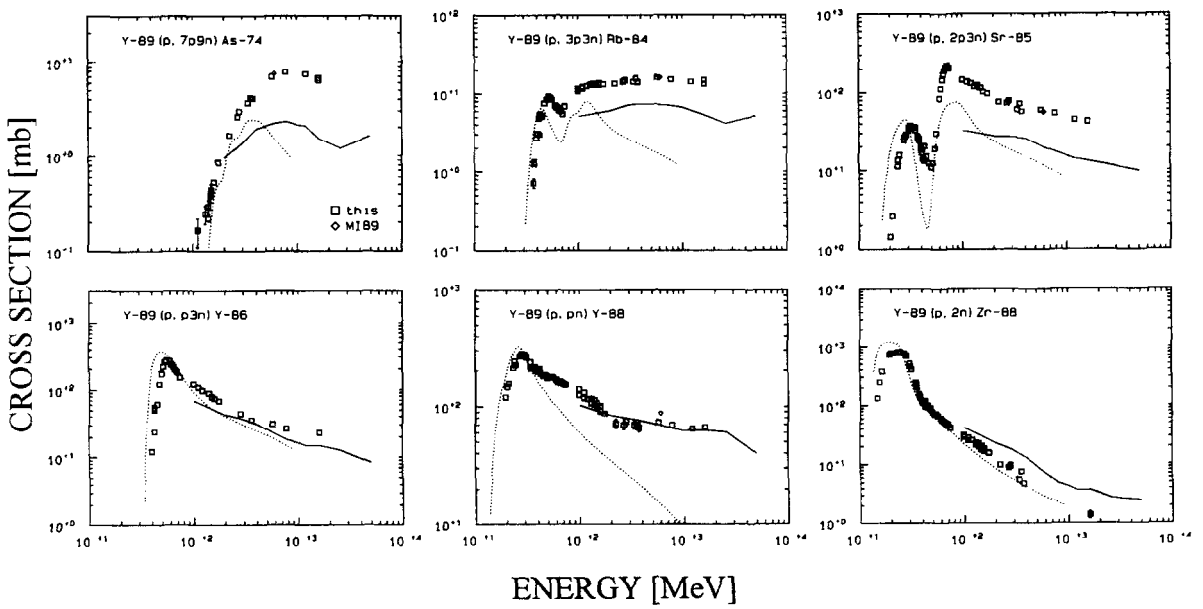

Fig. 9. Experimental and theoretical excitation functions for the production of ^{74}As, ^{84}Rb, ^{85}Sr, ^{86}Y, ^{88}Y and ^{88}Zr from yttrium. The experimental data shown are exclusively from our work. Theoretical excitation functions were calculated by the HETC/KFA2 (full lines) and AREL (broken lines) codes.

but significant structures at the low energy parts of the excitation functions which only can be explained by complex particle emission.

In contrast, the (p,pxn)- and (p,xn)-reactions on mono-isotopic target elements, such as yttrium (Fig. 9) and niobium (Fig. 14), exhibit simple shapes with a single maximum at low energies followed by a moderate or strong decrease with increasing p-energy, respectively (Figs. 9, 14 and 21). Influences of d- or t-emission can only rarely be seen in excitation functions because of the small binding energy of deuterons and tritons. The reaction ^{59}Co(p,p3n)^{56}Co is an example here (Fig. 4). The maxima are due to compound nucleus reactions at low energies, while the monotonically decreasing shapes for energies above 50 MeV have to be explained by preequilibrium reactions which evidently extend to the INC regime above 200 MeV.

Because of these simple shapes, the contributions from different isotopes can be nicely observed for (p,pxn)- and (p,xn)-reactions even if one looks for target elements with several stable isotopes. The production of ^{83}Sr and ^{86}Y from strontium (Fig. 7), and of ^{90}Nb from zirconium (Fig. 12) are good examples for such effects.

Excitation functions for the production of ^{7}Be (and ^{10}Be) are particular with respect to shape and absolute magnitude (e.g. Figs. 8 and 13). Their apparent thresholds do not follow the general trend of increase with increasing mass difference between target and product. Also the increase of the cross sections with proton energies is much smaller than for typical products of deep spallation. The reason for this peculiarity is that these nuclides are fragmentation products at medium energies and, moreover, that they can be produced by evaporation at lower energies [18,26].

The uniform systematics of shapes seen for the target elements strontium, yttrium, zirconium and niobium does not hold for the target element gold. Continuously and strongly increasing excitation functions are seen only for the lightest observed product nuclides, ^{54}Mn, ^{65}Zn, ^{74}As, and ^{75}Se (Section 4.1.3). However, already these products have apparent production thresholds which are much lower than seen for the medium mass target elements (Sr–Nb) at similar mass differences between target and products, thus pointing to other, new reaction modes. Since the most significant differences between the medium and heavy mass target elements show up best in the mass yields we will discuss them in some detail before we look for individual reactions on the target element gold.

4.1.2. Mass yields at medium energies

Important differences between medium energy reactions on medium and heavy mass target elements can be

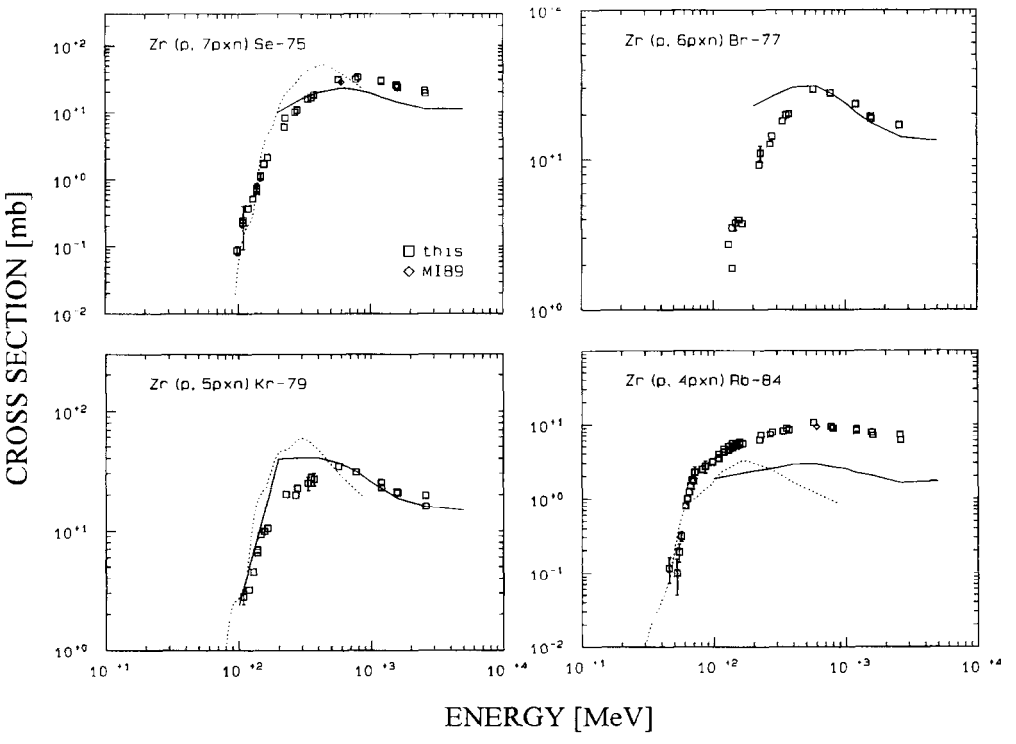

Fig. 10. Experimental and theoretical excitation functions for the production of ^{75}Se, ^{77}Br, ^{79}Kr and ^{84}Rb from zirconium. The experimental data shown are exclusively from our work. Theoretical excitation functions were calculated by the HETC/KFA2 (full lines) and AREL (broken lines) codes.

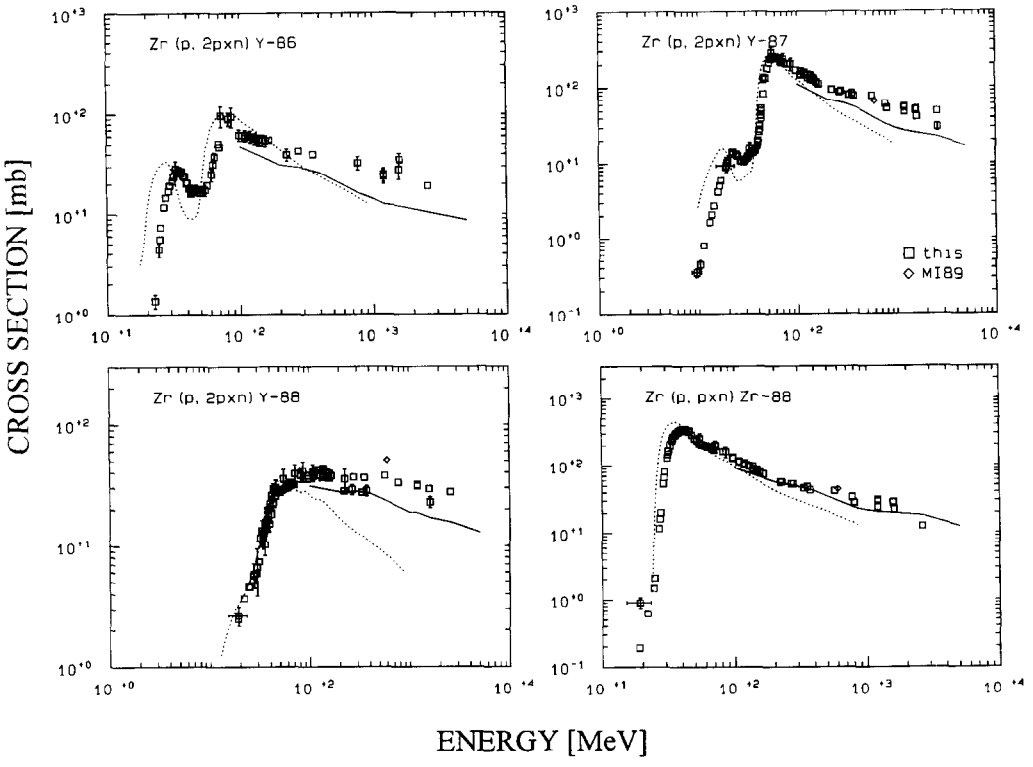

Fig. 11. Experimental and theoretical excitation functions for the production of ^{86}Y, ^{87}Y, ^{88}Y and ^{83}Sr from zirconium. The experimental data shown are exclusively from our work. Theoretical excitation functions were calculated by the HETC/KFA2 (full lines) and AREL (broken lines) codes.

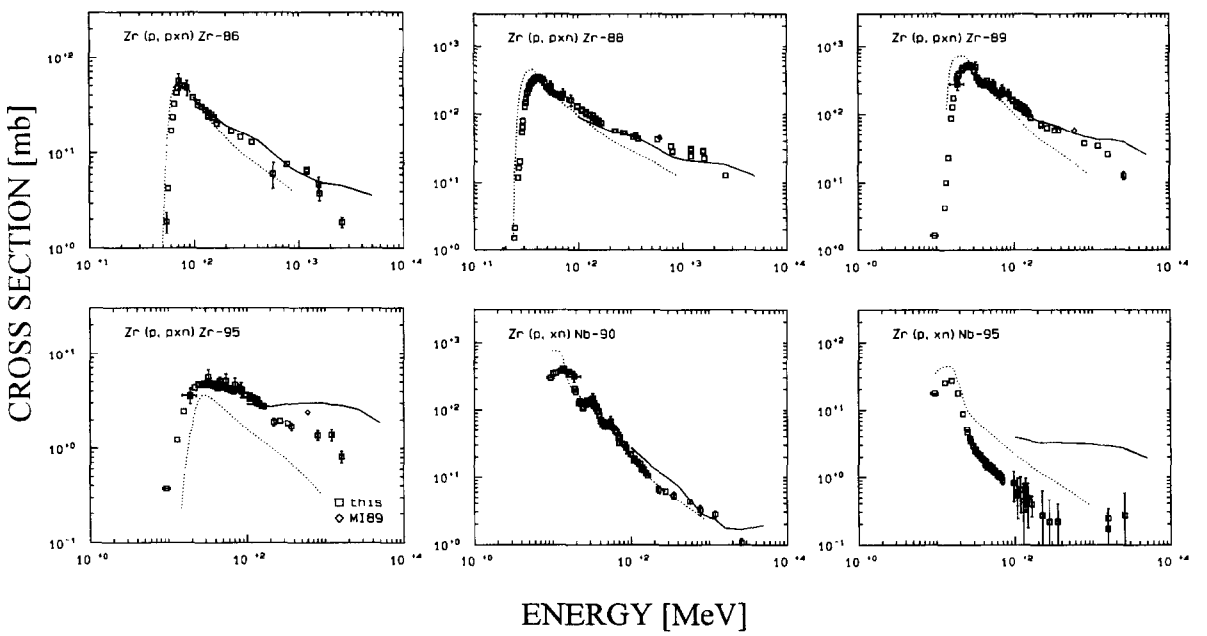

Fig. 12. Experimental and theoretical excitation functions for the production of ^{86}Zr, ^{88}Zr, ^{89}Zr, ^{95}Zr, ^{90}Nb and ^{95}Nb from zirconium. The experimental data shown are exclusively from our work. Theoretical excitation functions were calculated by the HETC/KFA2 (full lines) and AREL (broken lines) codes.

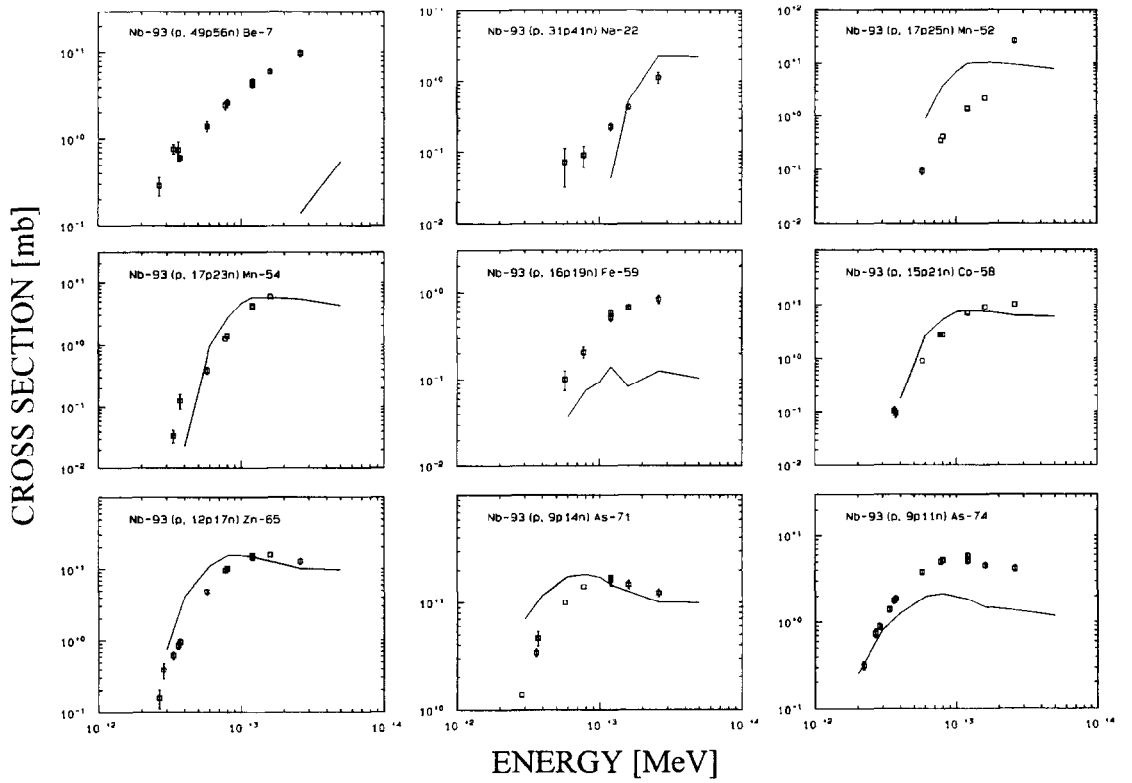

Fig. 13. Experimental and theoretical excitation functions for the production of ^{7}Be, ^{22}Na, ^{52}Mn, ^{54}Mn, ^{59}Fe, ^{58}Co, ^{65}Zn, ^{71}As and ^{74}As from niobium. The experimental data shown are exclusively from our work. Theoretical excitation functions were calculated by the HETC/KFA2 code (full lines).

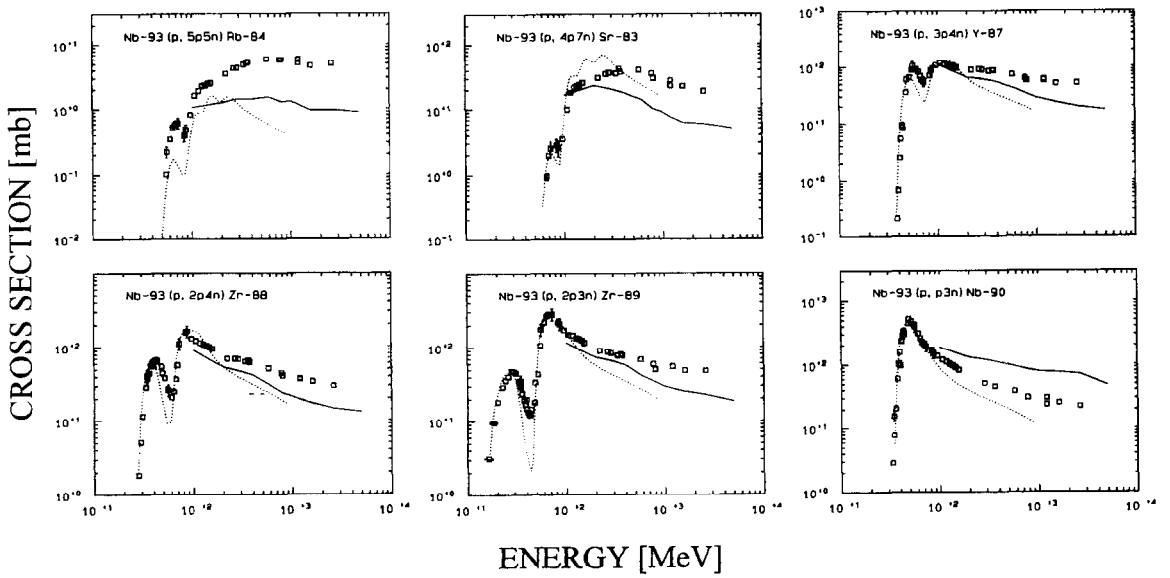

Fig. 14. Experimental and theoretical excitation functions for the production of ^{84}Rb, ^{83}Sr, ^{87}Y, ^{88}Zr, ^{89}Zr and ^{90}Nb from niobium. The experimental data shown are exclusively from our work. Theoretical excitation functions were calculated by the HETC/KFA2 (full lines) and AREL (broken lines) codes.

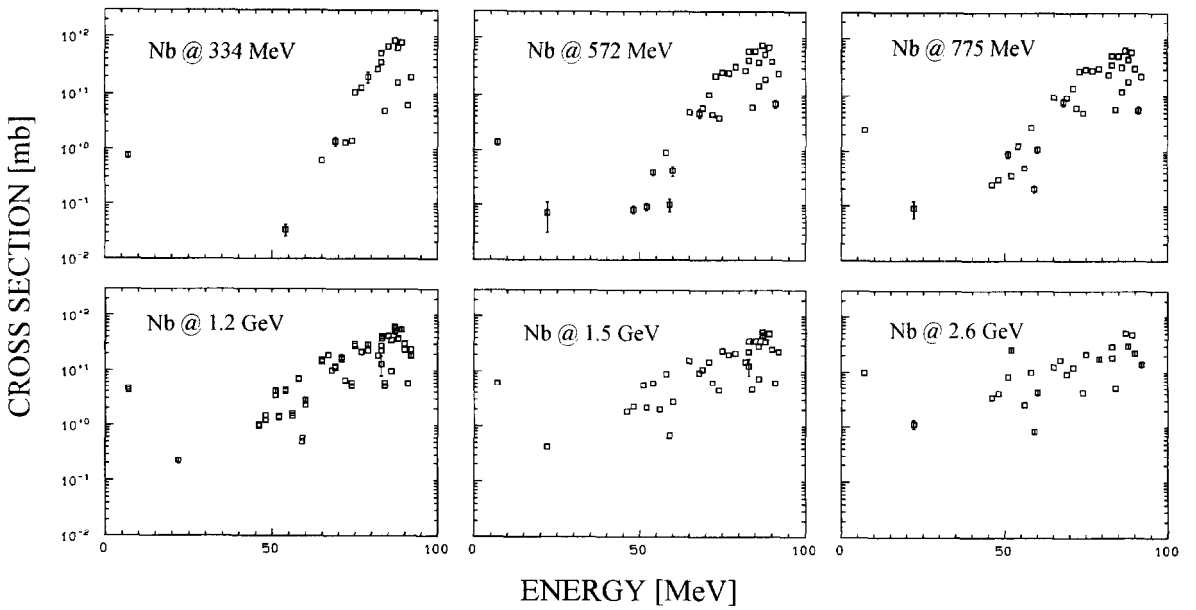

Fig. 15. Experimental cross sections from our work as a function of mass number of product nuclides for the target element niobium at proton-energies of 334, 572, 775, 1200, 1600 and 2600 MeV.

seen in detail when looking for the dependence of cross sections on mass differences between target and product nuclides for different energies. We have chosen the monoisotopic target element niobium (Fig. 15) and gold (Fig. 16) for such a comparison. For six energies between 330 MeV and 2.6 GeV we have plotted in Figs. 15 and 16 the measured cross sections against product masses. Since we did not measure the production of stable nuclides and since we did not sum up cross sections measured for isobaric products, these plots just give an impression of the isobaric yields. However, the upper envelopes of the cross sections give good approximations of the mass yield curves because the cumulative cross sections of nuclides close to the valley of stability sum up a lot of the total production.

For niobium (Fig. 15) one recognizes the typical patterns of spallation reactions. The mass yields decrease

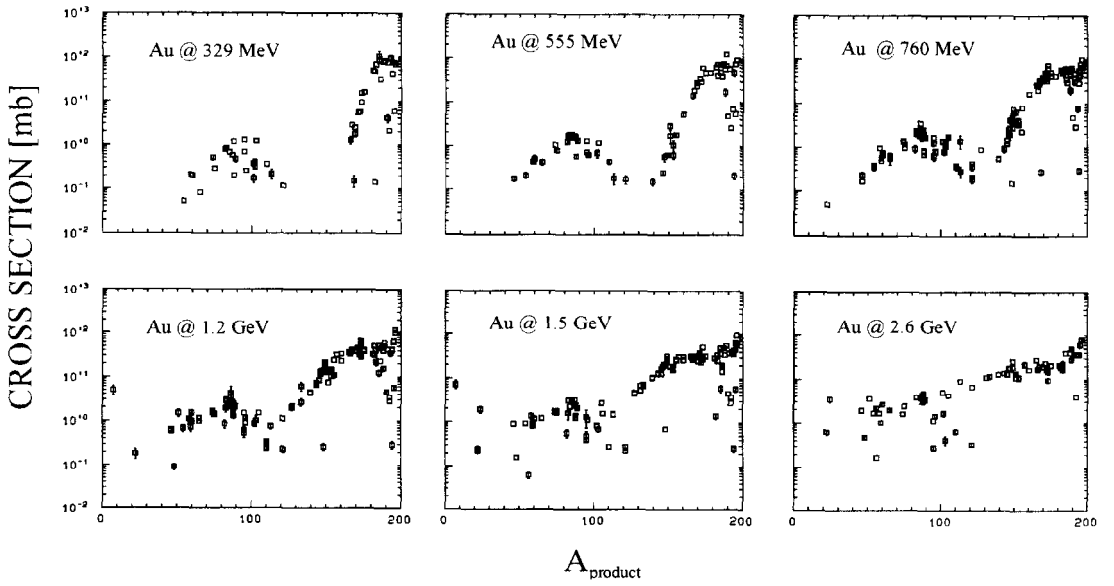

Fig. 16. Experimental cross sections from our work as a function of mass number of product nuclides for the target element gold at proton-energies of 329, 555, 760, 1200, 1600 and 2600 MeV.

exponentially with increasing mass differences, the slopes of the half-logarithmic linear envelopes becoming smaller with increasing proton energies. While at 334 MeV the observed cross sections and the seeming mass yield curve ranges over four orders of magnitude, at 2.6 GeV these data differ by less than two orders of magnitude.

The fragmentation product ^{7}Be falls out of the spallation systematics. The measured cross sections indicate that the mass yield curve raises again at small product masses due to the influence of fragmentation. For ^{7}Be also an alternative production mode, namely evaporation as well as preequilibrium emission have also been discussed [115,116]. In this context, however, it is a completely open question how the transition from evaporation and/or preequilibrium emission, on the one hand, to fragmentation, on the other, can be described. Indications of the possible energy ranges of the different production modes have been discussed earlier [26].

Generally, the lowest cross sections we were able to measure by γ-spectrometry are between 10 μb and 100 μb. For niobium, there is no evidence of any other than the two mentioned production modes, spallation and fragmentation, in the mass yield curves with cross sections significantly above 100 μb.

The mass yields of the target element gold look quite different (Fig. 16). At target-near masses the mass yield is nearly constant. Then, it decreases roughly exponentially indicating spallation reactions. But already at 329 MeV, there is a nearly symmetric peak in the mass yield curve at about half the target mass of gold which is attributed to fission. Though this peak is fairly broad with a half-width of more than 30 mass numbers at 329 MeV, its location indicates that the fissioning nuclides must be nuclides with masses close to that of gold. That means that the intranuclear cascade must have been very short and only few nucleons can have been emitted from the composite system before fission. Consequently, this fission mode must take place at relatively low excitation energies. A slight asymmetry of the peak to lower masses may point to wider range of nuclides undergoing fission. This may be also the reason for the nearly constant mass yields close to the target mass.

With increasing proton energies, the range of masses which exhibit small changes of production cross sections around the target nucleus extends to lower masses. At 1.5 GeV, the mass yields stay nearly constant for mass differences up to forty. The following part of the mass yield curves still shows spallation characteristics, i.e. exponential decrease of the mass yields with increasing mass differences and decrease of the slopes with increasing proton-energies. Also fragmentation shows up in the curves exhibited by high ^{7}Be cross sections. The distribution of fission products changes shape and location. With increasing proton energies, the location of the maximum is shifted to smaller target masses and the anisotropy of the peak at the lower mass side of the distribution increases. At 1.5 GeV, spallation and fission signatures begin to merge and at 2.6 GeV no clear-cut distinction between the two formation modes can be made anymore.

4.1.3. Excitation functions for the target element gold

The addition of a fission mode to those of spallation and fragmentation when going from medium mass (Nb) to

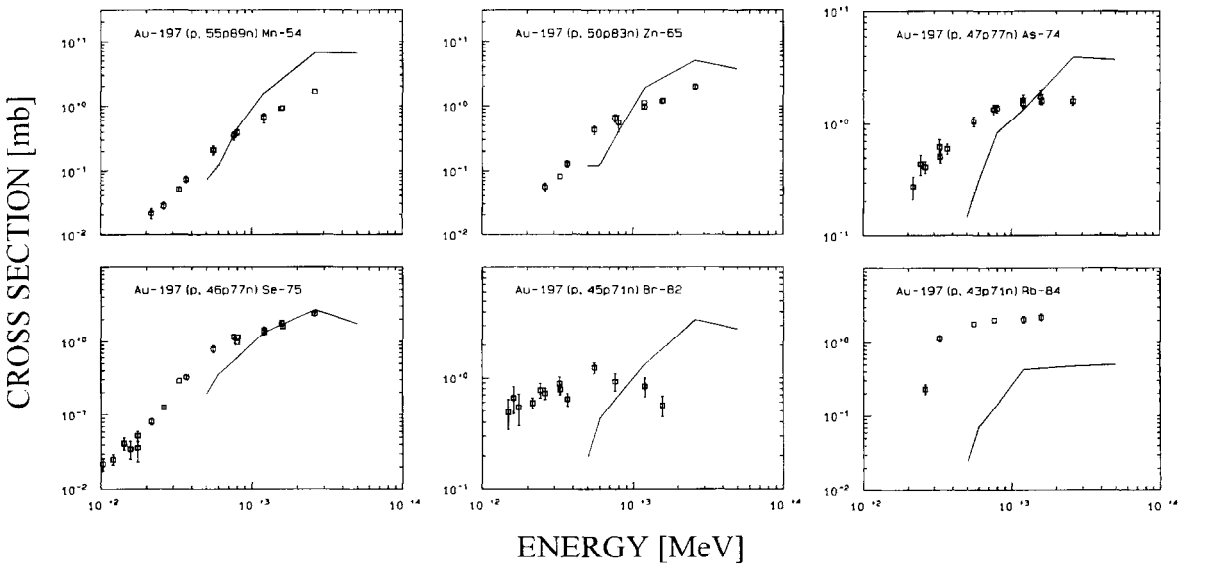

Fig. 17. Experimental and theoretical excitation functions for the production of ^{54}Mn, ^{65}Zn, ^{74}As, ^{75}Se, ^{82}Br and ^{84}Rb from gold. The experimental data shown are exclusively from our work. Theoretical excitation functions were calculated by the HETC/KFA2 code (full lines).

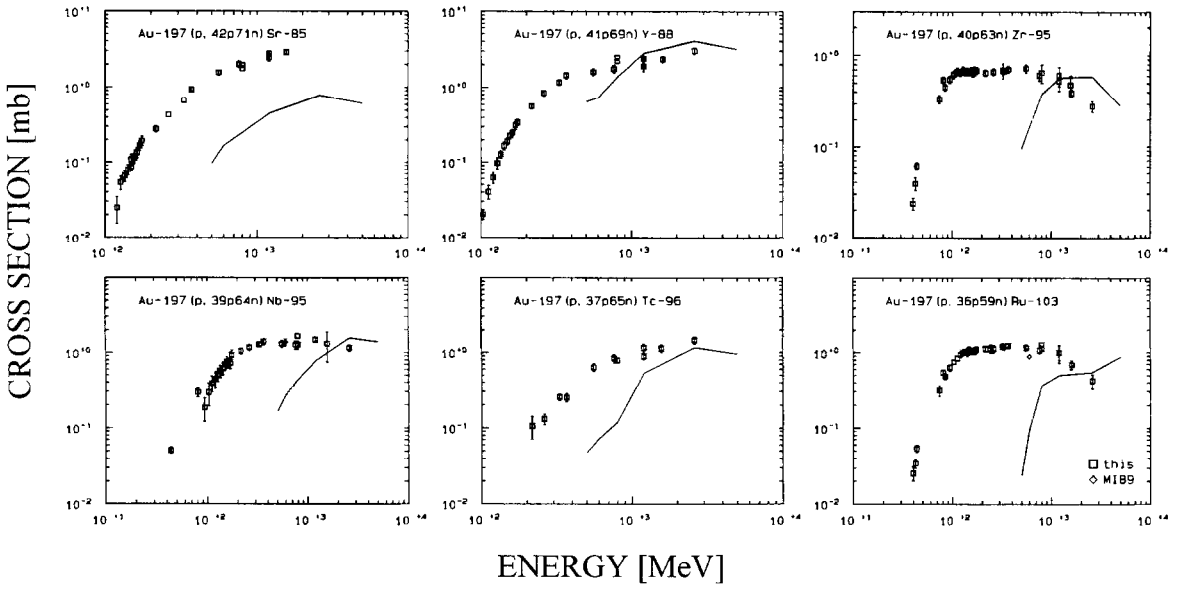

Fig. 18. Experimental and theoretical excitation functions for the production of ^{85}Sr, ^{88}Y, ^{95}Zr, ^{95}Nb, ^{96}Tc and ^{103}Ru from gold. The experimental data shown are exclusively from our work. Theoretical excitation functions were calculated by the HETC/KFA2 code (full lines).

high mass (Au) target elements, also strongly influences the shapes of the excitation functions. Looking for product masses between 54 and 103 (Figs. 17 and 18), the following distinctions can be made. On the one hand, the cross sections for the lightest product nuclides, ^{54}Mn, ^{65}Zn, ^{74}As, and ^{75}Se (Fig. 17) increase continuously with proton-energy. The apparent thresholds are 100 MeV and higher. The same is true for some fission products right from the

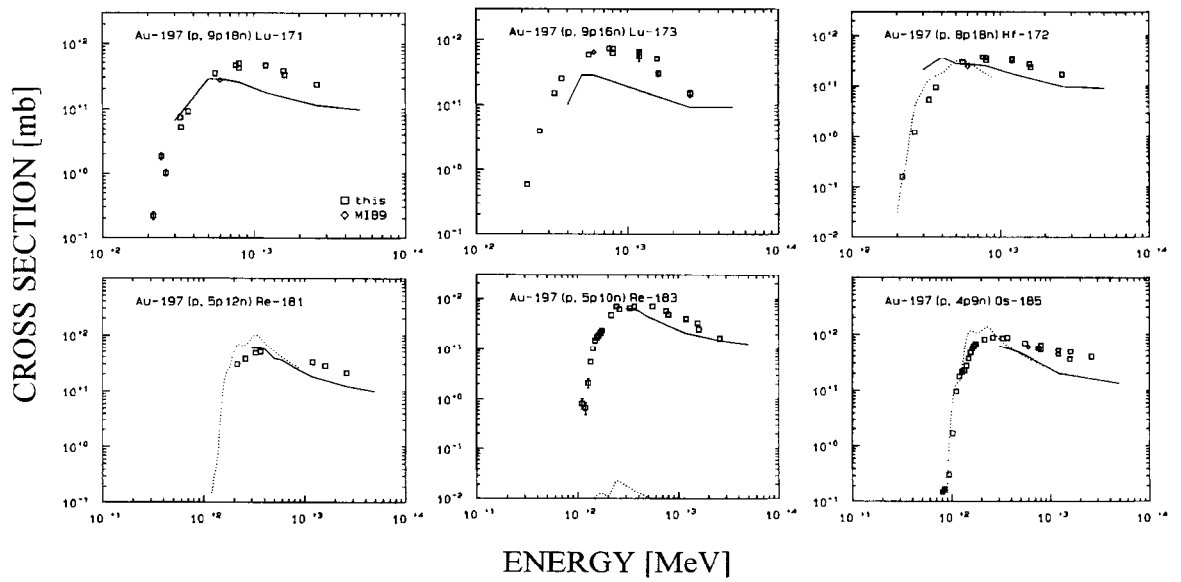

Fig. 19. Experimental and theoretical excitation functions for the production of ^{171}Lu, ^{173}Lu, ^{172}Hf, ^{181}Re, ^{183}Re and ^{185}Os from gold. The experimental data shown are exclusively from our work. Theoretical excitation functions were calculated by the HETC/KFA2 (full lines) and AREL (broken lines) codes.

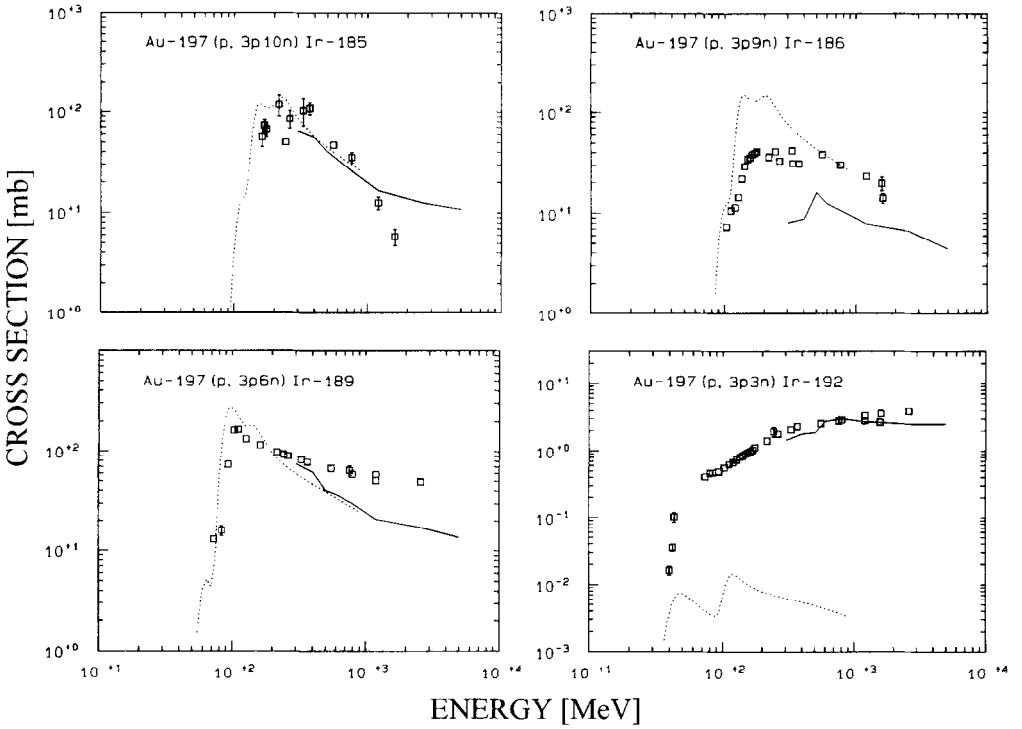

Fig. 20. Experimental and theoretical excitation functions for the production of ^{185}Ir, ^{186}Ir, ^{189}Ir and ^{192}Ir from gold. The experimental data shown are exclusively from our work. Theoretical excitation functions were calculated by the HETC/KFA2 (full lines) and AREL (broken lines) codes.

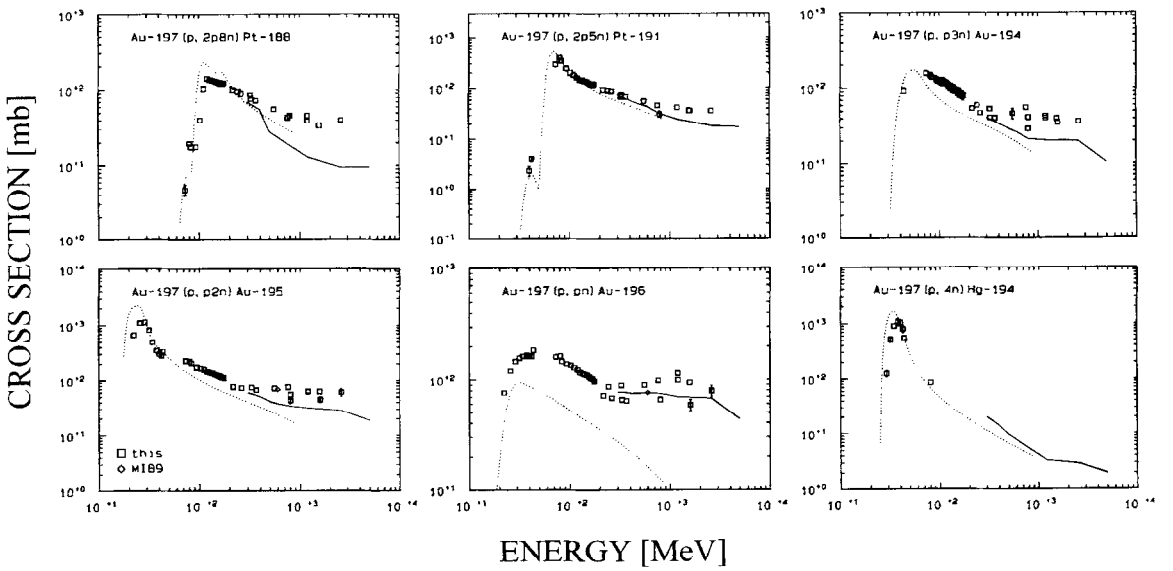

Fig. 21. Experimental and theoretical excitation functions for the production of ^{188}Pt, ^{191}Pt, ^{194}Au, ^{195}Au, ^{196}Au and ^{194}Hg from gold. The experimental data shown are exclusively from our work. Theoretical excitation functions were calculated by the HETC/KFA2 (full lines) and AREL (broken lines) codes.

Table 3
Survey on earlier work of other authors dealing with radionuclide production from Sr, Y, Zr, Nb and Au by proton-induced reactions

Energies or energy range [MeV]	Authors	Nuclides measured	Ref.
strontium			
1000	Alekseev et al. (1984)	As-74, Br-77, Kr-76,77,79, Rb-84	[118]
600	Felice et al. (1983)	As-74, Rb-82m, Y-86,87,88	[119]
730	Funk et al. (1967)	Kr-isotopes	[120]
400	Korteling and Caretto (1967)	Na-22,24	[121]
7.7–29.5	Levkovskii (1991)	(p,xn)-, (p,pxn)-, (p,2pxn)-reactions	[122]
7–85	Sachdev et al. (1967)	(p,xn)-, (p,pxn)-, (p,2pxn)-reactions	[123]
yttrium			
1000	Alekseev et al. (1984)	As-74, Br-77, Kr-76,77,79, Rb-84	[118]
60,100, 150, 180, 240	Caretto and Wiig (1959)	many radionuclides	[124]
540, 593	Grütter (1982)	many radionuclides	[125]
18200	Hagebo and Ravn (1969)	Sc-43-Sc-48	[126]
400	Korteling and Caretto (1967)	Na-22,24	[121]
800	Kolsky and Karol (1993)	Sc-44,46	[127]
600, 1050	Lagarde–Simonoff and Simonoff (1979)	Rb-83,84,86	[128]
7.7–29.5	Levkovskii (1991)	(p,xn)-, (p,pxn)-, (p,2pxn)-reactions	[122]
59, 75, 168, 200, 1010, 2500, 24000	Regnier et al. (1982)	radionuclides and stableKr-isotopes	[129]
5–85	Saha et al. (1966)	(p,xn)-, (p,pxn)-reactions	[130]
zirconium			
1000	Alekseev et al. (1984)	As-74, Br-77, Kr-76,77,79, Rb-84	[118]
660	Aleksandrov et al. (1994)	many radionuclides	[131]
600	Dropesky and O'Brien (1972)	many radionuclides	[132]
10–86	Kantelo and Hogan (1976)	Zr-90(p,2-4p1-6n)-reactions	[133]
15–68	Kondratyev et al. (1992)	many radionuclides	[134]
800	Kolsky and Karol (1993)	Sc-isotopes	[135]
7.7–29.5	Levkovskii (1991)	(p,xn)-, (p,pxn)-, (p,2pxn)-reactions	[122]
59, 75, 168, 200, 1010, 2500, 24000	Regnier et al. (1982)	radionuclides and stableKr-isotopes	[129]
250–440	Strohal and Caretto (1961)	(p,pn)-reactions	[136]
niobium			
1000	Alekseev et al. (1984)	As-74, Br-77, Kr-76,77,79, Rb-84	[118]
37–153	Albouy et al. (1963)	Y-88	[137]
240, 320, 500, 720	Korteling and Hyde (1964)	Na-, Ni, Cu-, Zr- and Nb-isotopes	[138]
400	Korteling and Caretto (1967)	Na-22,24	[121]
600, 1050	Lagarde–Simonoff and Simonoff (1979)	Rb-83,84,86	[128]
7.7–29.5	Levkovskii (1991)	(p,xn)-, (p,pxn)-, (p,2pxn)-reactions	[122]
12000	Noguchi et al. (1991)	H-3	[139]
38.8–95	Scholten et al. (1994)	Be-7	[140]
12000	Tominaka et al. (1984)	many radionuclides	[141]
800, 1200, 2600	Scholten et al. (1994)	Be-7	[140]
gold			
37–153	Albouy et al. (1963)	Ir-192	[137]
500	Asano et al. (1985)	many radionuclides	[142]
12000	Asano et al. (1988)	many radionuclides	[143]
1000, 2200, 3000	Baker et al. (1958)	Be-7	[144]
28000	Bächmann (1970)	lanthanoides	[145]
1000–6000	Caretto et al. (1958)	F-18, Na-24	[146]
320–880	Crespo et al. (1963)	F-18, Na-24	[147]
450, 2050	Currie et al. (1956)	H-3	[148]

Table 3 (continued)

Energies or energy range [MeV]	Authors	Nuclides measured	Ref.
gold			
600, 30000	Franz and Friedlander (1965)	Tb-149	[149]
32	Gonzalez-Vidal and Wade (1960)	H-3	[150]
< 20	Gritsyna et al. (1963)	Hg-197m,197g	[151]
24.8–27	Grimes et al. (1973)	(p,n)-reactions	[152]
750	Green et al. (1988)	He-3,4	[153]
40–155	Gusakow et al. (1960)	Au-195,196,Hg-195	[154]
20–155	Gusakow et al. (1961)	Au-196	[155]
4–13	Hansen et al. (1962)	Hg-197	[156]
18200	Hagebo and Ravn (1969)	Sc- and Sb-isotopes	[126]
3000, 10000, 30000	Hudis and Tanaka (1968)	Be-7, Na-22,24	[157]
1000, 2000, 3000	Hudis (1968)	Ne-24, Na-24	[158]
18–86	Kavanagh and Bell (1961)	Au-194,195,196	[159]
11.5-300000	Kaufmann et al. (1976)	many radionuclides	[133]
200–6000	Kaufmann and Steinberg (1980)	many radionuclides	[160]
400	Korteling and Caretto (1967)	Na-22,24	[121]
450	Kruger and Sugarmann (1955)	fission products	[161]
300, 450, 24000	Krämer et al. (1977)	many radionuclides	[162]
120–660	Lavrukhina et al. (1959)	Na-24, P-32	[163]
85	Lafleur et al. (1966)	Be-7	[115]
600, 10500, 21000	Lagarde-Simonoff and Simonoff (1979)	Rb-83,84,85	[128]
12000	Noguchi et al. (1991)	H-3	[139]
155	Poffé et al. (1959)	Hg-195,196	[164]
40–155	Poffé et al. (1961)	(p,*x*n)-reactions	[165]
198, 398, 547, 800	Porile et al. (1978)	Na-24	[166]
580	Ross and Bächmann (1974)	$46 \leq A \leq 110$	[167]
18000	Rudstam and Sorenden (1966)	I-118-I-124	[72]
25.8	Schery et al. (1974)	Hg-197	[168]
12000	Shibata et al. (1993)	Be-10, Al-26	[169]
2600	Sümmerer et al. (1990)	many radionuclides	[170]
8–60	Tilbury and Yaffe (1963)	Au-196, Hg-195,197	[171]
1200, 2600	Scholten et al. (1994)	Be-7	[140]
82–426	Yule and Turkevich (1960)	Au-196	[172]
11500, 300000	Yu and Porile (1975)	$A = 131$ and neighbouring nuclides	[173]

center of the fission mass yield curve, namely ^{85}Sr, ^{88}Y and ^{96}Tc (Fig. 18). On the other hand, the excitation functions for the production of ^{82}Br and — more pronounced — that of ^{95}Zr, ^{95}Nb and ^{103}Ru show broad maxima and a decrease above 1 GeV. For the latter three nuclides one even observes nearly constant production cross sections over wide ranges of energies. Their apparent thresholds are significantly below 100 MeV. For ^{95}Zr and ^{103}Ru the excitation functions are practically constant between 100 MeV and 1 GeV and the production of the two nuclides sets on at about 40 MeV.

The two types of shapes can be qualitatively interpreted in the following way: The production of nuclides such as ^{95}Zr and ^{103}Ru must be due to fission of intermediate products lying close to the target mass at relatively low excitation energies. An increase of proton energy does not increase the probability of producing these nuclides. Only at higher energies the enlargement of the variety of initial INC-outcomes decreases their production. The continuously increasing excitation functions, in contrast, point to a probability of production of fissioning nuclides increasing with proton energy. Since fission is a slow, collective process which has to be described in the framework of statistical models of the nucleus, the shapes are dominated by the production of fissioning nuclides, themselves, which with increasing proton energies are also more distant from the target nucleus. We will see later whether this simple picture holds in view of the theoretical calculations.

Looking for products closer to the target mass of gold (Figs. 19–21), there is a number of excitation functions which are typical for spallation reactions as observed for the medium mass target elements. Their production can be

understood to be due to a spallation mechanisms as proposed by Serber [117]. Differences relative to medium mass target elements are e.g. due to the fact that in the second slow phase of spallation reactions evaporation of neutrons is strongly favored compared to that of protons because of the higher Coulomb barrier. Mostly, the observed product nuclides have high excesses of neutrons in the exit channels. That such excesses result from evaporation can nicely be seen from reactions such as ^{197}Au(p,3p10n)^{185}Ir (Fig. 20) and ^{197}Au(p,2p8n)^{188}Pt (Fig. 21), the cross sections of which show each a strong maximum between 100 MeV and 200 MeV and a steep decrease to higher energies. Such decreases are not observed for medium mass target elements and can only be explained by the competition of evaporation with other reaction channels. It is also amazing to see that the excitation function of the reaction ^{197}Au(p,3p6n)^{189}Ir has maximum at about 100 MeV followed by a continuous decrease to higher energies, while ^{197}Au(p,3p3n)^{192}Ir rises continuously up to 2.6 GeV.

In summary, there are strong phenomenological differences between the medium mass target elements and the heavy target element gold. Thus, it will be of large interest to see whether these differences are also adequately treated by models of nuclear reactions.

4.2. Earlier work of other authors

With respect to the work of other authors detailed comparisons have been performed in the previously published work for target elements C–Cu [3,9–15,18,19,21–26] and Ba [16,27,28]. In this work, we shall continue this discussion only for the elements not dealt with in our earlier work, i.e. Sr, Y, Zr, Nb and Au.

A survey of the work of other authors for the target elements Sr, Y, Zr, Nb and Au is given in Table 3. Though this list is quite long, there are not many references with the entry "many radionuclides". Most earlier works were restricted to a few special nuclides and are not comprehensive. Moreover, the number of investigations covering a wider range of energies is very small. Thus, this is the first comprehensive work giving cross sections for a wide range of target/product combinations from thresholds up to 2.6 GeV.

Generally, the existing data from other authors do not show such large discrepancies as demonstrated in our earlier work [18] in case of iron and other light target elements. In spite of the generally better agreement, some detailed comments have to be made.

In the case of the target element strontium, the cross section at 400 MeV measured by Korteling and Caretto [121] for the production of ^{22}Na is a factor of two lower than ours. All other data agree fairly well with our new measurements.

The same is true for yttrium. However, there are a few discrepancies between our work and those of Caretto and Wiig [124] and Grütter [125]. The data by Caretto and Wiig [124] are higher for ^{84}Rb and ^{89}Y and lower for ^{82}Sr, ^{83}Sr and ^{86}Sr than our data, while they are in good agreement for all other products. The results by Grütter [125] are lower than ours in the case of ^{75}Se, ^{76}Br, ^{77}Br, ^{79}Kr and ^{87m}Sr, again the remaining being in very good agreement. The cross sections measured by Regnier et al. [129] for ^{85}Sr are too low and show a considerable scatter. This may be due to problems of resolving the 514 keV line of ^{85}Sr from the positron annihilation peak as these authors reported a resolution of their spectrometer of 4 keV only. The measurements of stable Kr isotopes from the same targets by Regnier et al. [129] are well in agreement with recent measurements from our collaboration [29,174]. The first cross section measurements of stable Kr-isotopes from our experiments for the target elements Rb, Sr, Y and Zr have recently been reported [29,174] and will soon be published in detail.

In the case of the target element zirconium several discrepancies between earlier works and ours are observed. The measurements by Dropesky and O'Brien [132] often are in significant disagreement with ours, even if one considers the relatively large errors quoted by these authors. Also, the results reported by Regnier et al. [129] show sometimes a considerable scatter and large errors. Their results for ^{85}Sr from Zr again are systematically lower than ours. Further, the measurements by Kondratyev et al. [134] partially deviate significantly from ours. In particular, there seems to be an "energy problem", e.g. for the production of ^{86}Y their results below 30 MeV being strongly shifted to lower energies compared to the results of this work and those of Levkovskii [122]. The latter two data sets are in excellent agreement. But also for some other product nuclides the results by Kondratyev et al. [134] deviate from ours.

For niobium, again most older work fits well and partially excellent to our new results if the measurements cover the same energies. It is just to mention that the data by Korteling and Hyde [138] are too low for ^{89}Zr while for other products they are well in agreement with ours.

By far most earlier work has been devoted to the target element gold. However, the scatter among the earlier data is relatively small in view of the spectroscopic problems to analyze heavy target elements. There is just one work by Krämer et al. [162] which is generally doubtful. Their results are mostly in contradiction with all other measurements and discrepancies by orders of magnitude are partially observed. Also some data by Asano et al. [142] at 500 MeV deviate significantly for quite a number of isotopes from our results. The recent comprehensive work by Sümmerer et al. [170] at a proton-energy of 2.6 GeV is in reasonable agreement with our work with the exception of a few data points which deviate from ours by a factor of two.

Some confusion exists in the literature with respect to cumulative and independent yields. Thus, for ^{195}Au there

are some discrepancies between our work and those of Kavanagh and Bell [159] and Gusakow et al. [154] which point to problems in reporting the proper quantities. Further there is one product, namely ^{196}Au, which shows an extreme scatter of reported data. At energies below 200 MeV the cross sections by Gusakow et al. [154] are too low, and also the results reported by Tilbury and Yaffe [171] and by Yu and Porile [172] are systematically lower than our data which are supported by the measurements by Kaufmann et al. [159]. Also for energies above 400 MeV there is some scatter in the data which may be caused by interferences from secondary neutrons in addition to spectroscopic problems.

5. Theoretical calculations

A systematic survey on the capabilities to predict cross sections for the production of residual nuclides by medium-energy protons can be obtained from a recent International Model and Code Intercomparison [74] for a large number of models and codes. In this intercomparison the target elements O, Al, Fe, Co, Zr and Au were systematically investigated. The experimental data presented in this work provided the experimental basis for this intercomparison. Covering 22 different models and codes, this intercomparison gives a broad survey on our present capabilities to predict cross sections for the production of residual nuclides. However, such an intercomparison cannot make an in-depth analysis of each individual model or code. It just provides the tools for such analyses which have to be performed elsewhere.

In this work, we compare in detail the new experimental data with theoretical ones calculated by two codes in order to discuss the predictive capabilities of two different models. These calculations exceed those of the mentioned model and code intercomparison. The hybrid model of preequilibrium reactions [64,79] was used in form of the AREL code which is a relativistic version of the ALICE LIVERMORE code [65] to calculate cross sections for energies up to 900 MeV. In addition, an intranuclear cascade evaporation (INC/E) model was used in form of the HETC/KFA2 code [68].

The AREL code [67] makes use of relativistic kinematics and includes preequilibrium emission of up to two precompound particles per interaction and allows calculations for proton energies up to 900 MeV. However, the code does not consider meson production, giant resonances, fragmentation or medium-energy fission. Due to internal limitations of array sizes the calculations are restricted to product nuclides with atomic and mass numbers differing not more than 9 and 22, respectively, from those of the target nucleus for p-induced reactions. From the large variety of options and parameters the following ones were chosen.

For preequilibrium reactions we used the Geometry Dependent Hybrid model (GDH) [64]. The total and partial reaction cross sections are calculated with AREL according to Pearlstein [175]. Energy-independent initial exciton numbers $n_0 = 3$ were used. In our former ALICE 900 calculations [18], we assumed that the ratio of free scattering cross sections of np- to pp- or nn-scattering is equal to three and does not depend on the energy of the incoming protons according to Blann and Vonach [65]. In the present work, as in [26], we adopt the energy dependence of these cross sections described by Kikuchi and Kawai [176]. The above cross section ratio is calculated explicitly for each energy of the incoming protons. A single particle level density parameter of A/9 was adopted for protons and neutrons. Excitation energies were treated in 0.5 MeV energy bins up to 900 MeV proton energy. Intranuclear transition rates were calculated using nucleon–nucleon scattering cross sections, since the built-in optical model parameters of AREL are valid only up to 55 MeV. The Pauli principle is taken into account when calculating intranuclear transition rates. For the equilibrium reactions standard Weisskopf and Ewing [177] evaporation calculations were performed with multiple particle emission of p, n, and α-particles.

It has been demonstrated by Bodemann et al. [17] that the choice of nuclide masses has an important influence on the results of the calculations. This effect was also investigated in detail for the target elements from Mg to Cu [26]. Also for the heavier target elements such analyses were routinely performed with at least two extreme mass options. In one option masses were calculated using the Myers and Swiatecki [178] mass formula without pairing and shell corrections. In the other calculations, experimental masses according to Wapstra and Audi [179] were used as far as available. Otherwise Myers and Swiatecki masses were calculated, considering pairing and shell effects.

Summarizing such analyses of the influences of mass options on the calculations, we can state: For light elements C, N, O for which the general applicability of a statistical approach is questionable only the simple option with the Myers and Swiatecki mass formula leads to the least unacceptable results. For elements from Mg to Cu the different mass options give strongly differing calculational results and no judgment about the preferable option can be made. The calculational option to use experimental masses as far as available and to consider pairing and shell effects is essential when calculating reactions close to magic proton or neutron configurations, e.g. ^{59}Co(p,4n)^{56}Ni.

For heavier elements the influences of the different mass options become less and less important and they cannot be made responsible for major discrepancies between theory and experiment. Therefore, we exclusively use the simple option of the Myers and Swiatecki mass formula in the present work as described above for the hybrid model calculations.

For the INC/E-calculations using the HETC/KFA2 code [68] exactly the same set up and calculational options

were used as described in our earlier work [18] and we reframe from repeating this here. It is, however, to be pointed out that medium-energy fission was taken into account for the calculations of the target element gold using the RAL-fission model [180] as implemented in HETC/KFA2.

6. Discussion

Modeling of residual nuclide production from thresholds up to several GeV has to include a wide range of reaction modes. In the low-energy range, reactions are dominated by formation and decay of a long-lived compound nucleus in statistical equilibrium (CN models). In the GeV range, reactions evolve via a fast intra-nuclear cascade of nucleon–nucleon interactions which ends in an evaporation phase of an intermediate nucleus in statistical equilibrium (Intra-Nuclear Cascade/Evaporation (INC/E) models). The basic ideas to describe these phenomena were developed by Bohr [181] and by Serber [117], respectively. The essential difference which allows such contradictory concepts to be successful rests upon the dependence of proton wave-length on energy. The de Broglie wavelength of the proton is comparable to the nuclear radii at low energies and small compared to nucleon–nucleon distances in the GeV range. Both concepts were extremely successful. Models of the compound nucleus in statistical equilibrium as formulated e.g. by Weisskopf and coworkers [177,182,183] describe nuclear reactions including residual nuclide production up to a few tens of MeV although preequilibrium effects are sometimes not negligible. Formulations of INC/E models based on the pioneering work of Bertini [184,185] use Monte Carlo techniques to follow the intra-nuclear cascades and finally end up with some CN-model to describe the final evaporation phase. The High Energy Transport Code (HETC) in its original form uses this concept [186].

However, these two approaches are simplifying extremes which only describe some aspects of all the reaction modes involved. It was found to be necessary to introduce a preequilibrium phase to extend the applicability of CN-models to higher energies. Among the various formulations of preequilibrium phenomena (see Ref. [187] for a review) the hybrid model of preequilibrium reactions [79] has been quite successful in calculations of residual nuclide production cross sections up to 200 MeV [3,13,18,26]. The present version of this model in the form of the code AREL [67] is a further attempt to extend its applicability to even higher energies. We here apply it up to 900 MeV. This is, however, problematic from the physical point of view since no medium-energy physics is considered in the model. Also limitations caused by the coding, i.e. limited coverage of product nuclides due to array sizes and, even more important, the neglect of multiple preequilibrium emission or pion production, are problematic. A way out of these problems is presently searched for by developing a Monte Carlo version of the hybrid model which even might incorporate medium-energy phenomena in the future [188] in order to extend its applicability into the medium-energy region in a physically adequate way.

Also in INC/E models preequilibrium phenomena have been considered, e.g. in the HETC-descendants LAHET [189] and HETC-3STEP [190] codes. HETC/KFA2 [68], the KFA Jülich version of HETC, has not yet incorporated a preequilibrium model.

In addition to the reaction modes mentioned, evaporation of light and medium-mass nuclei, production of residual nuclei by fragmentation and medium-energy fission have to be included. Here, the restrictions of the codes used are as follows: Both codes, AREL and HETC/KFA2, allow for calculation of evaporation of protons, neutrons and α-particles, but not of heavier nuclei. AREL does not consider preequilibrium emission of clusters like α-particles. Intermediate-energy phenomena such as fragmentation and medium-energy fission cannot be treated by AREL. Quite a number of changes and improvements have been made in HETC/KFA2 [68] compared to the classical HETC by Armstrong and Chandler [186]. Among other changes, the RAL-fission model [180] has been incorporated. However, Fermi break-up still has to be included to account for residual nuclide production by fragmentation. Since the HETC/KFA2 code describes the mere production by spallation, it allows to distinguish those reactions for which fragmentation is a significant production mode. Fragmentation shows up as a systematic underestimation of production cross sections.

At low energies, also direct reactions contribute to residual nuclide production, but they do not play an essential role for the vast majority of all reactions and energies dealt with in this work.

In this discussion we shall analyze in detail the capabilities of the AREL and HETC/KFA2 codes and work out the necessities of some improvements. This will be done by some global judgment based on a quantification of deviations between experiment and theories as well as by demonstration of the predictive capabilities and of shortcomings and problems on the basis of a systematic survey of individual reactions.

6.1. Quantification of the agreement between experiment and theory

In order to quantify the quality of model calculations when comparing calculated cross sections with experimental ones, mathematical measures were searched for. The agreement between experiment and theory can be described by deviation factors which are point-wise calculated for each reaction at each energy for which an experimental cross section exists. These point-wise deviation factors can then be averaged over certain energy ranges and also over all or a part of the different reactions.

For a given reaction (target/product combination) we have ($\sigma_{\mathrm{exp},i}$, $i = 1, \ldots, n_{\mathrm{exp}}$) experimental cross sections at energies (E_i, $i = 1, \ldots, n_{\mathrm{exp}}$). Then we define a *mean logarithmic deviation* by

$$\langle \log(\sigma_{\mathrm{exp}}) - \log(\sigma_{\mathrm{theo}}) \rangle = \frac{1}{n_s} \sum_{i=1}^{n_s} \left[\log(\sigma_{\mathrm{exp},i}) - \log(\sigma_{\mathrm{theo},i}) \right]. \quad (5)$$

The theoretical cross sections $\sigma_{\mathrm{theo},i}$ at the energies E_i were obtained from the calculated cross sections by double-logarithmic interpolation. No extrapolations were made. n_s is the number of energy points with experimental cross sections for which this procedure is possible in a given energy interval.

Then the *average deviation factor* $\bar{F}$ is defined by

$$\bar{F} = 10^{\frac{1}{n_s} \sum_{i=1}^{n_s} [\log(\sigma_{\mathrm{exp},i}) - \log(\sigma_{\mathrm{theo},i})]} \quad (6)$$

and the *average squared deviation factor* by

$$\langle F \rangle = 10^{\frac{1}{n_s} \sqrt{\sum_{i=1}^{n_s} [\log(\sigma_{\mathrm{exp},i}) - \log(\sigma_{\mathrm{theo},i})]^2}}. \quad (7)$$

Since the average deviation factors and the average squared deviation factors do not allow to distinguish underestimates and overestimates, we define in addition the *maximum and minimum deviation factors*, $F_{\max}$ and $F_{\min}$, respectively by:

$$F_{\max} = \max\left(\sigma_{\mathrm{exp},i} / \sigma_{\mathrm{theo},i},\ i = 1, \ldots, n_s \right), \quad (8)$$

$$F_{\min} = \min\left(\sigma_{\mathrm{exp},i} / \sigma_{\mathrm{theo},i},\ i = 1, \ldots, n_s \right). \quad (9)$$

It is to note that the number, n_s, of point-wise deviation factors may deviate from the number of experimental data, n_{exp}, depending on the energy coverage of the calculations. Therefore, it is meaningful to define the number of cross sections, $n_{s,i}$, of a given reaction i for which such a comparison was made. Since, moreover, the coverage of reactions is also differing with model calculation and energy regions one also has to know the number n_r of reactions for which a comparison was possible.

In order to obtain some global judgment about the quality of a given model calculation we define a *global mean squared deviation factor* $\langle\langle F \rangle\rangle$ by averaging for the model in question over all reactions j:

$$\langle\langle \left(\log(\sigma_{\mathrm{exp}}) - \log(\sigma_{\mathrm{theo}}) \right)^2 \rangle\rangle = \left(\sum_{j=1}^{n_r} n_{s,j} \right)^{-1} \sum_{j=1}^{n_r} \sum_{i=1}^{n_{s,j}} \left[\log(\sigma_{\mathrm{exp},i,j}) - \log(\sigma_{\mathrm{theo},i,j}) \right]^2. \quad (10)$$

$$\langle\langle F \rangle\rangle = 10^{\langle\langle [\log(\sigma_{\mathrm{exp}}) - \log(\sigma_{\mathrm{theo}})]^2 \rangle\rangle} \quad (11)$$

with its standard deviation $s(\langle\langle F \rangle\rangle)$

$$s(\langle\langle F \rangle\rangle) = 10^a \quad (12)$$

with

$$a = \left\{ \left(\sum_{j=1}^{n_r} n_{s,j} \right)^{-1} \times \sum_{j=1}^{n_r} \sum_{i=1}^{n_{s,j}} \left[\log(\sigma_{\mathrm{exp},i,j}) - \log(\sigma_{\mathrm{theo},i,j}) - \log(\langle\langle F \rangle\rangle) \right]^2 \right\}^{1/2}. \quad (13)$$

All the deviation factors defined above have the advantage of being intuitive. They were chosen instead of linear residuals since the variations observed for a given set of experimental cross sections are often large compared to the cross section values. Consequently, a linear normal distribution of deviations between theories and experiment is unlikely. A log-normal distribution of these deviations is the simplest assumption.

The global mean squared deviation factor $\langle\langle F \rangle\rangle$ describes the average of the factors by which a theory deviates from experiment. Together with its standard deviation $s(\langle\langle F \rangle\rangle)$ it defines an interval $[\langle\langle F \rangle\rangle / s(\langle\langle F \rangle\rangle), \langle\langle F \rangle\rangle * s(\langle\langle F \rangle\rangle)]$ which covers about two third of all the individual deviation factors.

The quantification of the agreement and deviation between experimental and calculated data as revealed by the mean deviation factors can be used globally as well as reaction- or target-element-wise. Apparently, small deviation factors can also be the result of a small energy coverage of a contribution, therefore one has to indicate the energy range, the numbers of reactions and individual cross sections which were used as basis to calculate deviation factors.

It is not meaningful to average deviation factors over the entire energy range covered in this work. Since the energy coverage of different models and codes varies too much and differing energy regions are dominated by different reaction modes, we distinguished three energy regions. From 0 MeV to 50 MeV, reactions are dominated by a compound nucleus in statistical equilibrium. In the preequilibrium region from 51 MeV to 200 MeV, precompound decay is the most characteristic feature and from 200 MeV to 5000 MeV an intranuclear cascade takes place as the initial phase of a reaction. Therefore, we quantify the agreement between theories and experiments independently for each of these three energy regions.

6.2. Predictive capabilities of the AREL and HETC / KFA2 codes

For the AREL code, such quantitative comparisons between calculations and experimental data were performed for all three energy ranges: 0–50 MeV, 50–200 MeV and 200–900 MeV. Since there is no preequilibrium model included in HETC/KFA2 we restricted our calculations of deviation factors to energies above 200 MeV where we can assume that the underlying model assump-

tions are justified. The target-element-wise global mean squared deviation factors, their standard deviations and the numbers n_r and n_s of reactions and cross sections considered in each case are given for the different energy regions in Table 4.

The global mean squared deviation factors $\langle\langle F\rangle\rangle$ demonstrate that neither AREL nor HETC/KFA2 are capable to predict excitation functions for residual nuclide production better than a factor of two on the average.

In case of the AREL calculations, the global mean squared deviation factors have to be interpreted in dependence of energy. The energy ranges 0–50 MeV and 51–200 MeV are those where the applicability of the model is well established. The element-wise mean squared deviation factors are between 1.77 and 3.93 for the elements Sr, Y, Zr and Nb in these energy ranges. For the target element gold they are much higher at low energies ($\langle\langle F\rangle\rangle = 17.7$) and moderately higher at the 51–200 MeV range ($\langle\langle F\rangle\rangle = 4.26$). For energies above 200 MeV where the applicability of the model is doubtful, the deviation factors for each element are slightly higher than in the 51–200 MeV region. This is mostly due to the neglect of multiple preequilibrium decay as will be seen in the reaction-wise discussion. Again, AREL behaves worse for the target element gold than for the others.

The case of Au for energies up to 50 MeV is particularly problematic. Generally, large deviation factors are likely to be found near the reactions thresholds. Codes occasionally calculate wrongly the threshold energies. This can be due to various reasons, e.g. problems with nuclear masses or optical model parameters as well as neglect of γ-competition in deexcitation. In spite of such problems, the codes calculate cross sections in the extreme proximity of the thresholds where absolute magnitudes of cross sections are in the nb-region.

Even if the global deviation factors are moderate, the individual, reaction-wise deviation factors can reach even orders of magnitude. The global deviation factors have considerable standard deviations. For the AREL calculations, we present in Fig. 22 exemplarily reaction-wise mean deviation factors, $\bar{F}$, and the minimal and maximal deviation factors, $F_{\min}$ and $F_{\max}$ for the target elements yttrium and gold for energy ranges from 50–200 MeV and for 200–900 MeV. For HETC/KFA2, yttrium, niobium and gold were selected to exemplify reaction-wise mean, minimal and maximal deviation factors for energies above 200 MeV (Fig. 23).

Deviation factors do not exhibit whether the shapes of the excitation functions have been correctly calculated. In this case all relevant reaction modes might have been properly accounted for and just some scaling problems could be the reason for deviations. Therefore, one has to look for the maximum and minimum deviation factors, too. Small deviations between maximum and minimum deviation factors point to the shape of the excitation functions being correctly reproduced, while large differences indicate that there are problems with the calculated energy dependence of the cross sections.

From Fig. 22, one distinguishes easily the difference in quality of the AREL calculations for the target element gold, on the one hand, and for yttrium as an example of the lighter target elements, on the other. There is no

Table 4
Global mean squared deviation factors $\langle\langle F\rangle\rangle$ and their standard deviations $s(\langle\langle F\rangle\rangle)$ according to Eqs. (10) and (11) between theoretical and experimental cross sections. In addition, the number of reactions n_r and the total number of cross sections n_s used for calculating theses deviation factors are given

Element	Energy range: Quantity	0–50 (MeV)	50–200 (MeV)	200–900 (MeV)	200–2600 (MeV) HETC/KFA2
		AREL			
strontium	$\langle\langle F\rangle\rangle$ * : $s(\langle\langle F\rangle\rangle)$	2.25 * : 1.31	1.77 * : 1.15	3.61 * : 2.04	2.47 * : 1.40
	n_r	6	11	17	32
	n_s	38	75	127	303
yttrium	$\langle\langle F\rangle\rangle$ * : $s(\langle\langle F\rangle\rangle)$	2.56 * : 1.44	2.15 * : 1.24	3.63 * : 2.00	2.61 * : 1.44
	n_r	10	16	20	32
	n_s	157	251	129	350
zirconium	$\langle\langle F\rangle\rangle$ * : $s(\langle\langle F\rangle\rangle)$	2.70 * : 1.40	3.93 * : 1.82	4.48 * : 1.91	2.55 * : 1.43
	n_r	8	22	23	49
	n_s	277	258	101	523
niobium	$\langle\langle F\rangle\rangle$ * : $s(\langle\langle F\rangle\rangle)$	3.29 * : 1.69	1.93 * : 1.18	2.60 * : 1.42	2.67 * : 1.48
	n_r	3	9	8	32
	n_s	59	109	61	334
gold	$\langle\langle F\rangle\rangle$ * : $s(\langle\langle F\rangle\rangle)$	17.7 * : 10.5	4.26 * : 2.25	6.05 * : 2.92	3.75 * : 1.85
	n_r	7	18	18	75
	n_s	77	184	163	615

systematic trend in the deviation factors for the target element yttrium in the region from 51 MeV to 200 MeV and the ranges of individual deviation factors are significantly smaller than one order of magnitude. For gold, the mean deviation factors also cluster around unity, but there are two nuclides (^{190}Ir and ^{192}Ir) which are systematically underestimated by more than one order of magnitude and, generally, the minimum deviation factors demonstrate a tendency of AREL to systematically underestimate the cross sections.

For energies above 200 MeV, the data calculated by AREL for yttrium are systematically too low for product masses between 80 and 88. In case of gold, such a systematic underestimation is not seen except for the two product nuclides mentioned. But, again the ranges of deviation factors are often much larger and can reach an order of magnitude.

We do not give deviation factors for energies below 50 MeV for the AREL calculations in Fig. 22. Because of the steep gradients of the excitation function near threshold a slight error in energy can be the cause of very large deviations. These cases will be discussed in detail in Section 6.3.1 on the basis of individual reactions.

For the HETC/KFA2 calculations, there is no significant difference in the performance for medium-mass and heavy target elements (Fig. 23). However, the reaction-wise mean deviation factors point to some systematic underestimation in the case of gold, which is not clearly observed for the lighter elements. Generally, the ranges of deviation factors are larger for the HETC/KFA2 calculations than for the AREL calculations thus pointing out that the shapes of the excitation functions are better described by the latter code. One has to keep in mind, however, that the product nuclide coverage of the Monte Carlo calculations by HET/KFA2 widely exceeds that accessible by AREL.

The effects of neglecting fragmentation is seen in case of the production of ^{7}Be from yttrium (Fig. 23) where the calculations are lower than the experimental data by nearly two orders of magnitude on the average. The same problem exists for gold, where the underestimate is more than two orders of magnitude: $\langle\langle F\rangle\rangle = 0.0032$ with $F_{min} = 0.0028$ and $F_{max} = 0.0035$. We shall discuss this in Section 6.4.2.

6.3. Cross section calculations by the AREL code

Extensive comparisons of theoretical excitation functions calculated by the AREL code can be made for individual reactions using the new database. Here, we present such a comparison for a wide range of target

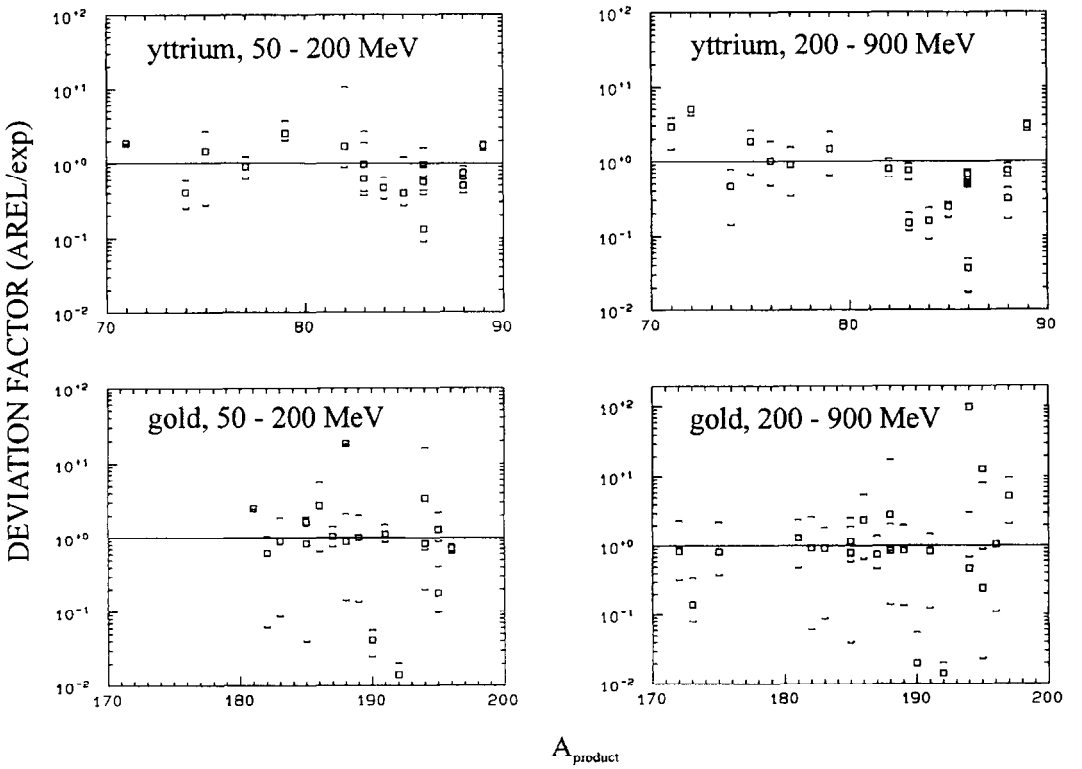

Fig. 22. Minimum, maximum and mean deviation factors (up-brackets, down-brackets and squares, respectively) between experimental and theoretical data calculated by the AREL code as a function of mass number of product nuclides for the target elements yttrium and gold for the energy ranges from 50 MeV to 200 MeV and from 200 MeV to 900 MeV.

elements. We start with some typical examples of the iron group elements (Section 6.3.1) in order to recall our earlier discussion [18,26]. Then for the new target elements we discuss the results for the elements Sr, Y, Zr, Nb (6.3.2), and for Au (6.3.3).

6.3.1. Target elements from titanium to copper

With respect to light and medium weight target elements we shall not repeat the discussion of the elements C, N, O, Mg, Al and Si [26,45] where, on the one hand, the

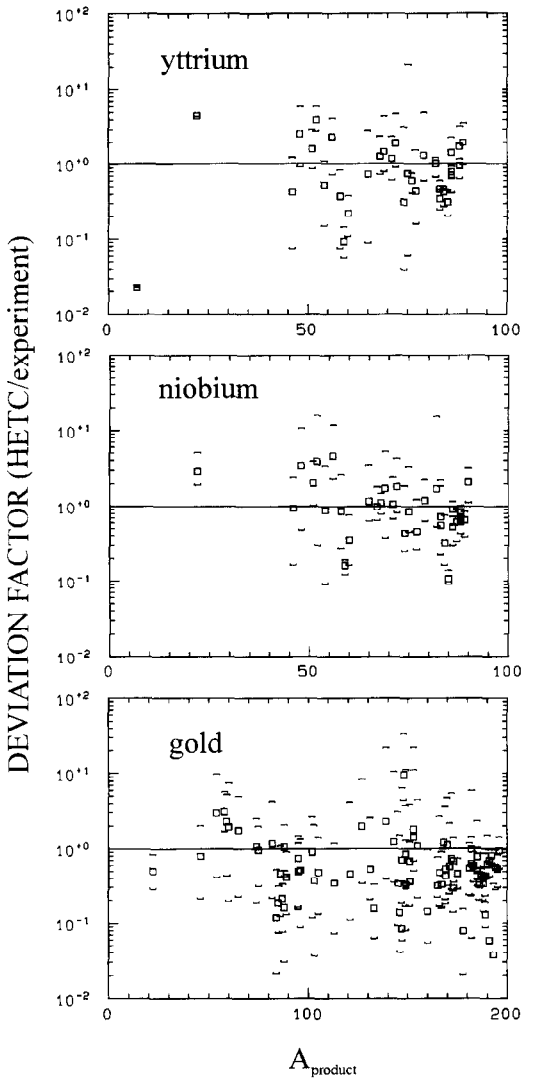

Fig. 23. Minimum, maximum and mean deviation factors (up-brackets, down-brackets and squares, respectively) between experimental and theoretical data calculated by the HETC/KFA2 code as a function of mass number of product nuclides for the target elements yttrium, niobium and gold for the energy range from 200 MeV to 2600 MeV.

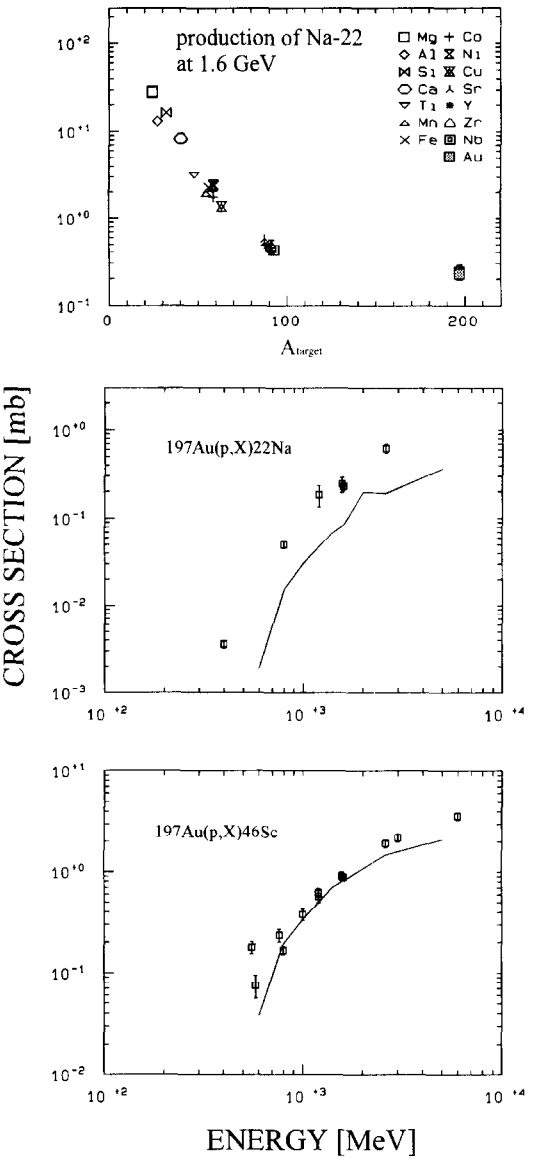

Fig. 24. Production cross sections of ^{22}Na as function of target masses at 1.6 GeV and excitation function of ^{22}Na and ^{46}Sc from Au. The solid lines are HETC/KFA2 calculations.

general applicability of any statistical model is doubtful and where, on the other hand, such models are only applied because of lack of any other model. But for elements from Ti to Cu there is no doubt on the applicability of the model and calculations with AREL and its predecessor codes ALICE and ALICE900 were rather successful [3,13,18,26]. This is also revealed by the examples given in Fig. 4. We note again that all AREL calculations of this work use the simplest form that is Myers and Swiatecki mass formula without taking into account shell

effects in the level densities. For the target elements around iron, no problems appear from Fig. 4 and, in general, the calculations describe the measurements fairly well. However, for some reactions, such as ^{59}Co(p,4n)^{56}Ni, shell corrections must be considered in order to get meaningful results [74].

There are some deviations between theory and experiment which are typical and will be seen later on for the heavier target elements, too. In the very low energy range there are occasionally problems with an energy shift between theory and experiment as seen here for Fe(p,3pxn)^{51}Cr below 30 MeV. In the case of the target element barium, such shifts were earlier observed to be quite important and were attributed to the neglect of γ-deexcitation competing with particle emission [27,28]. This problem should no longer be important, since γ-competition has been included into the ALICE versions since 1992. Alternatively, the use of the rather crude mass formula still can be the cause of such energy shifts. Also for the examples in Fig. 4 this is a likely explanation of the observed energy shifts. However, the discrepancy seen for the reaction ^{59}Co(p,p3n)^{56}Co for energies below 30 MeV can be explained in a different way. It is due to the neglect of evaporation of complex particles, here ^{2}H and ^{3}H, in the calculations.

Also the neglect of preequilibrium emission of complex particles can be seen in Fig. 4. The minimum in the excitation function of the reaction Fe(p,3pxn)^{51}Cr between 20 MeV and 30 MeV is strongly underestimated pointing to the importance of the reaction ^{56}Fe(p,α pn)^{51}Cr.

Compared to our earlier ALICE900 calculations [26] there is a considerable improvement in the AREL calculations. The underestimation of experimental cross sections for energies above 200 MeV has become much smaller than before, though it has not vanished. This still pertaining discrepancies are attributed by us to the neglect of multiple preequilibrium decay in the calculations. There are also some indications of problems regarding the balance of neutron and proton emission in the preequilibrium phase. The (p, xn)-reactions tend to be overestimated while the (p, ypxn)-reactions tend to be underestimated. These discrepancies are increasing with increasing ratios of protons to neutrons in the exit channel, see e.g. Figs. 4, 11, 12 and 21.

Finally, as seen for the reaction Fe(p,6pxn)^{46}Sc for energies between 100 MeV and 400 MeV, the AREL calculations exhibit structures or oscillations due to evaporation peaks of complex particles which are not seen in the experimental excitation functions. This again can be attributed to the neglected smoothening effect of multiple preequilibrium decay. The present calculations assume a much shorter initial phase of the intranuclear cascade than is indicated by the experiments. Also some general tendency of AREL calculations to overestimate evaporation peaks of reactions with just a few nucleons in the exit channels support this view.

6.3.2. Target elements from strontium to niobium

While all the experimental cross sections are for target elements with natural isotopic composition, the theoretical ones are composites of model calculations for individual isotopes. They thereby allow to distinguish the individual reaction modes for multi-isotope target elements. One can judge the plausibility of experimentally determined cross sections. Independently of the capability of model calculations to reproduce quantitatively the experimental data, this adds to the quality assurance of cross section measurements. This can be seen for instance in the case of the target element strontium (Fig. 7) and also later for zirconium (Figs. 11 and 12).

In Fig. 7, the reactions Sr(p,2pxn)^{84}Rb, Sr(p,pxn)^{83}Sr and Sr(p,xn)^{86}Sr show strong structures which can be attributed to reactions involving different target isotopes and reaction modes and which can be explained qualitatively by the calculations. For ^{84}Rb the importance of α-emission in the reactions ^{87}Sr(p,2p2n)^{84}Rb and ^{88}Sr(p,2p3n)^{84}Rb is clearly seen. The underestimate between 20 MeV and 60 MeV again can be explained by the neglect of preequilibrium α-emission in the calculations. For ^{83}Sr the first maximum in the excitation function can be unambiguously attributed to the reaction ^{86}Sr(p,α)^{83}Sr. For the production of ^{86}Y which is dominated by the reaction ^{88}Sr(p,3n)^{86}Y the still incompletely measured increase towards lower energies below 30 MeV can be explained by ^{87}Sr(p,2n)^{86}Y and ^{86}Sr(p,n)^{86}Y, the latter being the important one. In the case of ^{88}Sr(p,3n)^{86}Y and for the production of ^{83}Sr from Sr we observe significant energy shifts between theory and experiment, the calculations being shifted to lower energies. Possible reasons for such shifts have been discussed above.

For products far away from the target nuclei such as ^{68}Ge, ^{75}Se (both Fig. 6) and ^{79}Kr (Fig. 7), the AREL calculations overestimate the experimental data and show some structures which are smeared out in reality. Underestimates above 200 MeV also exist but rarely are important as e.g. for ^{84}Rb. The latter is close enough to the target nuclides to have preequilibrium emission as a major production mode, but far enough to need multiple preequilibrium decay to account for its production at higher energies.

Some of the problems are seen much clearer for the mono-isotopic target element yttrium (Figs. 8 and 9). While the reaction ^{89}Y(p,2n)^{88}Zr in the high energy part is excellently described, there is an important shift in energy between experiment and calculations for energies up to 30 MeV (Fig. 9). This energy shift is also seen for ^{89}Y(p,p3n)^{86}Y and ^{89}Y(p,2p3n)^{85}Sr (Fig. 9). As calculations with other mass and level density options showed, these shifts can be avoided by using experimental masses and considering shell corrections in the case of yttrium.

The underestimate of ^{89}Y(p,2p3n)^{85}Sr cross sections at 40 MeV cannot be explained by mass and level density options. It has to be attributed to the neglect of preequilibrium α-emission. Another, alternative explanation namely

that preequilibrium emission of protons is overestimated thereby leaving no configuration which allows α-emission by evaporation is unlikely, since there is a general tendency of the AREL calculations to underestimate proton-emission relative to that of neutrons. This effect is seen for yttrium in Figs. 8 and 9. The (p,pn)-reaction in contrast to the (p,2n)-one is underestimated, the discrepancy increasing with proton-energy and reaching one order of magnitude at 900 MeV (Fig. 9). The (p,p3n)-reaction leading to ^{86}Y is just slightly underestimated, but the excitation functions for the production of ^{74}As, ^{84}Rb and ^{85}Sr are severely underestimated for energies above 200 MeV. For ^{86}Ge, however, where much more neutrons are to be emitted than protons the calculations even overestimate the experimental data. In this context we had extreme problems when calculating the reaction ^{30}Si(p,3p)^{28}Mg [45] or the ^{138}Ba(p,3p)^{136}Xe [27,28].

In the case of the target element zirconium one rarely observes problems of this types. Because of the existence of many stable isotopes, several reactions usually contribute to the production of a residual nuclide. There are, however, three cases which show the problem of strong underestimates at higher energies: ^{84}Rb, ^{88}Y (both Fig. 11) and ^{95}Zr (Fig. 12). The latter nuclide is exclusively produced by ^{96}Zr(p,pn)^{95}Zr and the same argument hold as for the production of ^{88}Y from yttrium. Production of ^{88}Y and ^{84}Rb from zirconium are dominated by the (p,2pn)- and (p,4p3n)-reactions on ^{90}Zr, respectively. In these cases, one might presume the influence of the magic neutron number 50 and the neglect of shell effects to be responsible for the observed problems. However, use of experimental masses and shell corrections does not improve the calculations here. In case of ^{88}Y such calculations make the results even worse. The underestimate at high energies remains and an additional maximum in the excitation function is calculated which overestimates the cross sections for energies between 40 MeV and 70 MeV.

The (p,xn)-reactions of zirconium (Fig. 12) are relatively well described, but sometimes a little overestimated by theory. In case of ^{90}Nb from zirconium one can well distinguish the individual evaporation maxima of the reactions ^{92}Zr(p,3n)^{90}Nb and ^{94}Zr(p,5n)^{90}Nb at about 30 MeV and 55 MeV, respectively, while those of ^{90}Zr(p,n)^{90}Nb and ^{91}Zr(p,2n)^{90}Nb are not resolved in the broad first maximum of the excitation function. The calculations describe the individual reaction causing the small maxima in the excitation function excellently.

The production of ^{95}Nb is exclusively due to ^{96}Zr(p,2n)^{95}Nb (Fig. 12), since (p,γ)-reactions have cross sections in the μb region only. For this neutron-richest target nuclide of zirconium the cross sections are increasingly overestimated, again pointing to the problem of a wrong balance of proton and neutron emission.

The results and problems discussed so far are also seen for the target element niobium (Fig. 14) and have, in addition, been observed earlier for the target element barium [27,28]. Thus, except for the lightest target elements, C, N and O, the capabilities of the hybrid model of preequilibrium reactions are fairly uniform for target masses up to 140. It is therefore particularly interesting to look for the heaviest of our target elements, namely gold.

6.3.3. AREL calculations for the target element gold

Though the AREL calculations are restricted due to array size limitations to product nuclides having atomic and neutron numbers differing from that of the target nucleus by no more than 9 and 22, respectively, this fact does not in principle reduce the codes capabilities since the missing cross sections for Au due to spallation, fission and fragmentation are small compared to the cross sections of the near-target products for energies below 900 MeV (Fig. 16). This can even be seen for the calculated cross sections of one of the most distant product nuclides ^{172}Hf (Fig. 19). Also the production cross sections of ^{181}Re and ^{185}Os are well described though the calculated excitation functions show more structures than the experimental ones (Fig. 19).

There is, however, the case of ^{183}Re (Fig. 19) which is underestimated by three orders of magnitude, a discrepancy for which we have no explanation at all. In particular, it cannot be attributed to a neglect of radioactive precursors with higher atomic numbers, since the same effect should then also affect the production of ^{181}Re. This, however, is not the case.

There are some more similarly strange discrepancies for the target element gold which altogether cause the larger mean deviation factors for gold compared to the other target elements. One of these cases is the (p,3p3n)-reaction leading to ^{192}Ir. Fig. 20 gives a survey on the production of Ir-radioisotopes ranging from ^{185}Ir to ^{192} Ir. The excitation functions for the production of ^{185}Ir and of ^{189}Ir both are reasonably well reproduced by the calculations. For ^{192}Ir and for ^{186}Ir, however, there are discrepancies which point to a general misinterpretation of these reactions by the calculations.

The excitation function of the reaction ^{197}Au(p,3p9n)^{186}Ir (Fig. 20) has a threshold of nearly 100 MeV. A strong increase above 100 MeV is followed by a flat maximum which extends to 1.6 GeV declining between 200 MeV and 1.6 GeV only by about a factor of two. The AREL calculations show a slight energy shift to lower energies for the increasing part and they even reproduce a slight structure in this part of the excitation function. Between 150 MeV and 400 MeV, however, the calculations overestimate the experimental data by nearly an order of magnitude and wrongly predict a strongly structured excitation function with two maxima.

However, for this reaction a real comparison between calculations and experiment is not possible. There are two ^{186}Ir states in the table of isotopes: one with a half-life of 15.8 h which was measured in this work, and one with a half-life of 1.75 h. Both decay by β^+-decay to ^{186}Os and it is not clear which one is the isomeric state. The calcula-

tions do not distinguish production of ground states and isomers. Therefore, the overestimation by theory may be due to the production of the 1.75 h ^{186}Ir which is not included in the experimental data.

Generally, it is an important problem that there is no model available for the prediction of isomeric cross sections. This limits the use of model calculations for applications, in general, and makes, in particular, a comparisons between experimental and calculated cross sections difficult for a target element such as gold. In spite of this difficulty, some discrepancies between theory and experiment can be clearly identified.

So, for the reaction ^{197}Au(p,3p3n)^{192}Ir, which is a reaction type mostly well described for light and medium-weight target elements, the experimental data are generally underestimated by up to two orders of magnitude (Fig. 20). The same is true for the production of ^{190}Ir from gold (not shown in a figure). In both cases, the calculations predict a strong structure with two maxima. For ^{192}Ir, the first one is due to evaporation of an α-particle in combination with that of one proton and one neutron and a second one is caused by evaporation of 6 nucleons. Such structures have been observed in analogous reactions on light and medium-weight target elements. The problems due to neglect of preequilibrium α-emission and of p/n-emission balance discussed above are moderate compared to the complete failure in the cases of ^{192}Ir and ^{190}Ir production from gold. No argument of explanation can be made here from the fact that ^{192}Ir has two isomeric states and that our cross sections do not contain the production of ^{192m}Ir ($T = 241$ a).

For nuclides produced by (p,2pxn)-, (p,pxn)- and (p,xn)-reactions on gold (Fig. 21) the situation is not so bad in general. However, the reaction ^{197}Au(p,pn)^{196}Au is systematically underestimated by a factor of at least two, an effect which again is unusual for lighter target elements. If the problem of balancing p/n-emission is responsible here then it must be stated that it is much worse for the heavy target elements than for light and medium-weight ones.

Whatever the reasons are for the occasional substantial failure of the AREL calculations for gold the observed discrepancies significantly reduce the capability of the code to predict unknown excitation functions for heavy target elements and make experimental investigations indispensable.

6.4. Cross sections calculations by the HETC / KFA2 code

A comparisons of theoretical excitation functions calculated by HETC/KFA2 with experimental data for Sr, Y, Zr, Nb and Au extends quantitatively and qualitatively our earlier discussion of target elements up to copper [18]. Since HETC/KFA2 is not reduced in the coverage of product nuclides due to limitations of coding techniques, the calculations for the medium and heavy mass target elements give a much larger dataset for comparison. Moreover, intermediate energy fission is a significant mode of nuclide production for the target element gold and fragmentation becomes more important for heavy target elements.

In our earlier work on target elements up to copper [18] a similar quality of HETC/KFA2 calculations was observed as revealed by the deviation factors in Table 4 of this work for the heavier target elements. Looking for individual reactions, the situation for target elements up to copper is here exemplified in Fig. 4. The shapes of the excitation functions are fairly well described, but significant systematic deviations can be seen. Occasionally, experimental excitation functions are described by the calculations within the limits of experimental uncertainties [18], but this seems to be more accidental than merit of the model.

6.4.1. Spallation reactions on elements from strontium to niobium

The new data allow to get some insight into the problem of such deviations. One characteristic feature of spallation reactions is that the isobaric yields decrease exponentially with increasing mass difference between target and product masses. The distribution of zero time yields of isotopes, isotones or on an isobar should be roughly Gaussian distributions [72]. A comparison of the new experimental data for the production of Co-isotopes from the target element strontium with HETC/KFA2 calculations shows (Fig. 5) that the location of this Gaussian distribution is not properly described by the Monte Carlo calculations.

They underestimate the emission of protons relative to that of neutrons. As a consequence the excitation functions of neutron-poor isotopes (^{56}Co, ^{57}Co) are systematically overestimated, while the contrary is the case for neutron-rich isotopes (^{60}Co). ^{58}Co shows the highest experimental cross sections for the production of the Co-isotopes from strontium. This maximum is calculated wrongly by HETC/KFA2 to be expected for ^{57}Co. Thus, much better agreement would be obtained if the distribution of isotopic yields would be shifted by one to higher masses. This is a general observation [18] which can be demonstrated best by the data of Fig. 5. Also in Fig. 6 a strong overestimate of the production of neutron-poor ^{52}Mn from strontium is observed. The other three excitation functions for the production of ^{65}Zn, ^{68}Ge and ^{75}Se (Fig. 6) are fairly well described both with respect to absolute height and shapes.

Another typical problem of the Monte Carlo calculations is seen in case of the reaction Sr(p,3pxn)^{79}Kr (Fig. 7). For strontium the calculations were done down to 100 MeV and for this reaction they fail to reproduce the maximum of the excitation function. The calculations continue to increase with decreasing energy below 200 MeV in contrast to the experimental data. This effect at lower energies can frequently be observed and is attributed by us to the neglect of a preequilibrium transition between the INC and evaporation part of the calculations. The same

effect can be made responsible for the underestimate of ^{83}Sr production between 100 MeV and 200 MeV. The (overestimated) structures seen in the results of the preequilibrium model are not reproduced by HETC/KFA2.

In case of the mono-isotopic target element yttrium, again the far distant products ^{46}Sc, ^{65}Zn and ^{68}Ge are fairly well described by pure INC/E calculations (Fig. 8). However, the production of ^{7}Be is underestimated by more than an order of magnitude (Fig. 8). This is due to ^{7}Be being produced at higher energies mainly by fragmentation which is not considered in the Monte Carlo calculations. Another example of this type is seen in Fig. 13 for the production of ^{7}Be from niobium. Thus, one necessary improvement of the code is the inclusion of Fermi break-up in this model.

For the target element yttrium another problem exists for residual nuclides which are some mass units lighter than the target nucleus and which are produced by emission of about equal numbers of protons and neutrons, i.e. ^{74}As, ^{84}Rb and ^{85}Sr (Fig. 9). All three nuclides are systematically underestimated. Also this can be explained by a wrong book-keeping of p- and n-emission wrongly favoring the emission of neutrons. This effect gets smaller when looking to the reaction ^{89}Y(p,p3n)^{86}Y and vanishes for the (p,pn)-reaction leading to ^{88}Y. The excitation function of the reaction ^{89}Y(p,2n)^{88}Zr is even slightly overestimated.

The target element zirconium is less suited for theoretical analysis because of its many stable isotopes. Thus, systematic differences tend to be smeared out by contributions from different target isotopes and consequently the agreement between theory and experiment tends to become better (Figs. 10–12). Important discrepancies are seen for the production of ^{84}Rb (Fig. 10) and of ^{95}Zr and ^{95}Nb (Fig. 12). In case of the latter two nuclides, the production is unambiguously linked to the reactions ^{96}Zr(p,2n)^{95}Nb and ^{96}Zr(p,pn)^{95}Zr. Both excitation functions are much overestimated by the calculations for reasons which are not yet clear.

The results obtained for niobium fit into the general picture obtained so far (Figs. 12 and 13). It is worthwhile to mention that the increase from the threshold of the excitation function for the production of ^{22}Na is not reproduced by the calculations below 1 GeV. Though the experimental data have large uncertainties there is evidence for production below 1 GeV which cannot be explained by mere INC/E calculations. Whether this is due to an upcoming influence of fragmentation cannot be decided from the existing data. For niobium one observes again a strong systematic underestimate for the production of ^{84}Rb (Fig. 14) and another important discrepancy is seen for the production of the neutron-rich product ^{59}Fe (Fig. 13).

6.4.2. Intermediate energy fission of gold

For the target element gold, intermediate-energy fission is an additional, significant reaction mode. Excitation functions for nuclides which are produced by fission are shown in Figs. 17 and 16. As indicated by the excitation functions for the production of ^{95}Zr and ^{103}Ru from Au (Fig. 19) fission sets on at about 40 MeV. Both nuclides show exceptional shapes of their excitation functions: a steep increase above 40 MeV, a plateau between 100 MeV and 1 GeV followed by a decrease by about half an order of magnitude up to 2.6 GeV. ^{95}Nb shows a similar shape with, however, a less pronounced decrease above 1 GeV. Other fission products such as ^{85}Sr, ^{88}Y and ^{96}Tc have apparent thresholds above 100 MeV and increase continuously with proton energy (Fig. 18). As seen in Fig. 16 the isobaric fission yields at low energies are centered about symmetrically around half the mass of gold pointing to symmetrical fission of nuclides close to the target. This is also in accordance with the observation of low thresholds for nuclei as ^{95}Nb, ^{95}Zr and ^{103}Ru. The peak of fission products at 329 MeV in Fig. 16, however, is fairly broad and ranges from mass 54 to mass 121. This indicates a rather broad mass range of the fissioning nuclides if fission is the right term at all and not multi-fragmentation or Fermi break-up. The two different types of excitation functions mentioned above, point clearly to at least two different fission-like production modes. One is that of a moderately excited nuclide close to the target, while the other is a consequence of a larger energy transfer to the composite system which then implies fission or break-up of the outcome of a relatively long intranuclear cascade which decreased significantly the mass of the fissioning system. The observed increase of asymmetry of the fission peak in the isobaric yields with a preference of lighter products supports this view (Fig. 16).

None of the excitation functions in Figs. 17 and 18 is adequately described by the HETC/KFA2 calculations. Shapes and magnitudes mostly are poorly reproduced. Complete failure of the fission model is observed for the low-threshold fission leading to nuclides as ^{95}Nb, ^{95}Zr and ^{103}Ru (Fig. 18). But also for ^{74}As (Fig. 17), ^{82}Br (Fig. 17) and ^{88}Y (Fig. 18) the shapes are in contrast to the observed ones. In other cases, such as ^{84}Rb (Fig. 17) and ^{85}Sr (Fig. 18), the shapes are met, but the cross sections are off by nearly an order of magnitude. Consequently, the fission model used does not adequately describe the observed phenomena. Its applicability for calculations of fission products has to be generally questioned and better models have to be searched for. To this end, exclusive measurements of the intermediate-energy fission process are urgently needed.

Typical spallation products from gold are seen for product masses larger than 140. Some selected excitation functions are shown in Figs. 19 to 21. The degree of agreement between experimental cross sections and HETC/KFA2 calculations for such products is similar to that observed for medium-mass target elements. Since the highest cross sections of nuclides produced by fission from gold are of the order of 1 mb, a significant influence on the

products shown in Figs. 19 to 21 cannot be expected and is not observed.

6.4.3. Production of residual nuclides by fragmentation

Fragmentation should be more important for heavy target elements than for lighter ones. As mentioned above, this is also revealed for the target element gold by the discrepancy between HETC/KFA2 calculations and the experimental production cross sections of ^{7}Be which is underestimated by the calculations by more than two orders of magnitude. The general question is up to which product masses fragmentation is a significant production mode. In a recent paper Shibata et al. [169] discussed this problem for 12 GeV protons reacting with Al, Fe, Co, Ni, Cu, Zn, Ag and Au. They concluded that at this energy fragmentation is a dominant process for the production of ^{10}Be from iron to gold targets, and of ^{24}Na from silver to gold. Moreover, they suggested that the production of ^{7}Be, ^{22}Na and ^{26}Al by fragmentation from Ag to Au is suppressed relative to that of ^{10}Be and ^{24}Na. The different behavior was attributed to a negative or zero neutron excess of the former product nuclides in contrast to positive one of the latter nuclides.

Though the energies dealt with here are much lower and there is no indication that an energy-independent cross section formula can be used for analysis in our energy range as these authors did at 12 GeV, it is possible to draw some conclusions from our comparison of the experimental cross sections with those calculated by an INC/E model without Fermi break-up.

As pointed out above for ^{7}Be and as discussed earlier for ^{7}Be and ^{10}Be [18,26], the extreme underestimation of the production of these nuclides by the INC/E model points to them being predominantly produced by fragmentation by all target elements from Al to Au. Calculations performed by Lange [191] using the ISABEL code [70] coupled to a fragmentation model in form of the SMM code [71] support this interpretation. Results of these calculations may be found elsewhere [74]. Also recent measurements of production cross sections of ^{14}C from iron and nickel [32] show that they are much larger than those calculated by HETC/KFA2 demonstrating that ^{14}C is mainly produced by fragmentation. A further argument for fragmentation being the predominant production mode of ^{7}Be and ^{10}Be (and ^{14}C) is the dependence of their production cross sections at a given energy on the target mass. While spallation products show an exponential decrease of the cross sections with increasing mass difference between target and product, ^{7}Be and ^{10}Be show much less dependence on this mass difference and are roughly constant over wide ranges of target masses. For ^{7}Be they are about 10 mb at 2 GeV for all target elements from carbon to gold; see also Refs. [18,26].

For the cross sections describing the production of ^{22}Na and ^{26}Al from elements up to the iron group, however, the exponential dependence of cross sections from mass difference between target and product holds for energies up to 2.6 GeV and no systematic deviations from INC/E calculations were observed which would point to production by fragmentation. To decide this question for heavier target elements we have plotted our experimental cross sections for the production of ^{22}Na at 1.6 GeV as function of target mass in Fig. 24. The exponential decrease of the cross sections up to target mass 100 clearly demonstrates spallation to be the important mode. The cross sections for the production of ^{22}Na from Au do not fit into this systematics. For Au, they are just slightly lower than those of mass 100 targets indicating a change in production mode. However, a comparison of the experimental excitation function for the reaction ^{197}Au(p,X)^{22}Na with the results of the HETC/KFA2 calculations in Fig. 24 shows that about half the production of ^{22}Na from Au can be explained by a pure INC/E model. It is to point out that calculations of ^{24}Na production from Au is underestimated by the Monte Carlo calculations by nearly a factor of ten which would be in accordance with the results of Shibata et al. [169]. Also the apparent threshold of ^{24}Na production is more than 100 MeV lower for ^{24}Na than for ^{22}Na production from gold. Heavier products ($46 \leq A_{\text{product}} \leq 65$) can completely be explained by the HETC/KFA2 calculations. Thus, for the target element gold one has to take into account fragmentation as a production mode for product masses up to at least 24.

Summarizing the HETC/KFA2 analysis it can be stated, on the one hand, that there are problems with book-keeping of neutron- and proton-emission, that there are indications of preequilibrium effects not described by the model, that the neglect of fragmentation leads to severe problems for some light nuclides with increasing importance for heavy target elements and that the modeling of intermediate-energy fission is obsolete. On the other hand, for true spallation products the shapes of the excitation functions mostly are well reproduced and in many cases even the absolute cross sections are well described.

For applications of integral excitation functions in technology and other fields of science, however, the present predictive capabilities of both models dealt with in this work are not sufficient. The existing models have to be essentially improved until they can dispense further high quality measurements of cross sections for residual nuclide production. Presently, the experimental data can be used to distinguish the shortcomings of the models and codes and to point out the areas where such improvements are most urgently needed.

7. Conclusions

A comprehensive and consistent database of cross sections for the proton-induced production of residual nu-

clides from target elements C, N, O, Mg, Al, Si, Ca, Ti, V, Mn, Fe, Co, Ni, Cu, Sr, Y, Zr, Nb, Ba and Au for energies from thresholds up to 2.6 GeV has been established.

The database satisfies to a large part the data needs from a wide range of applications of medium-energy proton-induced reactions.

Upcoming new applications such as accelerator-driven nuclear waste transmutation and energy amplification call for an extension of this work with respect to the target element coverage. Such work is under way.

By comparing the experimental data with the results of model calculations using the AREL and HETC/KFA2 codes it is demonstrated by examples that reliable data for applications can at present only be obtained by experiments.

But the new experimental database provides a tool to distinguish the shortcomings of nuclear models and codes. It gives thereby an opportunity to improve the models of nuclear reactions in wide energy and mass regions.

Acknowledgements

The authors are grateful to the authorities and staffs of the accelerators at the Laboratoire National Saturne/Saclay/France, the Los Alamos National Laboratory/USA, the Paul Scherrer Institute/Villigen/Switzerland, and the The Svedberg Laboratory/University of Uppsala/Sweden for making available the beam time and for excellent cooperation. This work was partially supported by the Deutsche Forschungsgemeinschaft/Bonn and by the CEC in the framework of the Human Capital and Mobility Program. The silicon wafers used as target materials were courtesy of Wacker Chemitronic/Burghausen. The authors are particularly grateful to F.E. Chukreev who transformed the data to the EXFOR format thereby carefully looking for inconsistencies and errors and to P. Nagel and the NEA Data Bank for supporting this work.

References

[1] R. Michel, G. Brinkmann, J. Radioanal. Chem. 59 (1980) 467.
[2] R. Michel, G. Brinkmann and R. Stück, Earth Planet. Sci. Lett. 59 (1982) 33; Erratum, ibid 64 (1983) 174.
[3] R. Michel and R. Stück, J. Geophys. Res. 89 B, Suppl. (1984) 673.
[4] R. Michel, in: Intermediate Energy Nuclear Data for Applications, ed. N.P. Kocherov, INDC(NDS)-245 (IAEA, Wien, 1991) pp. 17–36.
[5] R. Michel, P. Dragovitsch, G. Dagge, P. Cloth, D. Filges, Meteoritics 26 (1991) 221.
[6] R. Michel, M. Lüpke, U. Herpers, R. Rösel, M. Suter, B. Dittrich-Hannen, P.W. Kubik, D. Filges, P. Cloth, Planet. Space Sci. 43 (1995) 557.
[7] R. Michel, in: Proc. Int. Conf. Nuclear Data for Science and Technology, May 9–13, 1994, Gatlinburg, TN, USA, ed. J.K. Dickens (American Nuclear Society, Inc., La Grange Park, IL, 1994) pp. 337–343.
[8] R. Michel, I. Leya and L. Borges, Nucl. Instr. and Meth. B 113 (1996) 434.
[9] R. Michel, G. Brinkmann, H. Weigel, W. Herr, J. Inorg. Nucl. Chem. 40 (1978) 1845.
[10] R. Michel, H. Weigel, W. Herr, Z. Physik A 286 (1978) 393.
[11] R. Michel, G. Brinkmann, H. Weigel, W. Herr, Nucl. Phys. A 322 (1979) 40.
[12] R. Michel, G. Brinkmann and W. Herr, NEANDC(E)-202U Vol. V, INDC(Ger)-21/L + Special (1979) 68.
[13] R. Michel, F. Peiffer, R. Stück, Nucl. Phys. A 441 (1985) 617.
[14] R. Michel, P. Dragovitsch, P. Englert, F. Peiffer, R. Stück, S. Theis, F. Begemann, H. Weber, P. Signer, R. Wieler, D. Filges, P. Cloth, Nucl. Instr. and Meth. B 16 (1986) 61.
[15] R. Michel, B. Dittrich, U. Herpers, T. Schiffmann, P. Cloth, P. Dragovitsch, D. Filges, Analyst 114 (1989) 287.
[16] K. Prescher, G. Brinkmann and W. Herr, in: Progr. Rep. on Nuclear Data Research in the Federal Republic of Germany for the Period April 1 1979 to March 31 1980, NEANDC(E)-212 U Vol. V, INDC(Ger)-22/L+Special (1980) pp. 50–54.
[17] R. Bodemann, H.J. Lange, I. Leya, R. Michel, T. Schiekel, R. Rösel, U. Herpers, H.J. Hofmann, B. Dittrich, M. Suter, W. Wölfli, B. Holmqvist, H. Condé, P. Malmborg, Nucl. Instr. and Meth. B 52 (1993) 9.
[18] R. Michel, M. Gloris, I. Leya, H.J. Lange, M. Lüpke, U. Herpers, B. Dittrich-Hannen, R. Rösel, D. Filges, P. Dragovitsch, M. Suter, H.J. Hofmann, P.W. Kubik, W. Wölfli, H. Baur and R. Wieler, Nucl. Instr. and Meth. B 103 (1995) 183.
[19] Th. Schiekel, U. Herpers, M. Gloris, I. Leya, R. Michel, B. Dittrich-Hannen, H.A. Synal, M. Suter, P.W. Kubik, Nucl. Instr. and Meth. B 113 (1996) 484.
[20] D. Fink, M. Paul, G. Hollos, S. Theis, P. Englert, S. Vogt, R. Stück, R. Michel, Nucl. Instr. and Meth. B 29 (1987) 275.
[21] B. Dittrich, U. Herpers, H.J. Hofmann, W. Wölfli, R. Bodemann, M. Lüpke, R. Michel, P. Dragovitsch, D. Filges, Nucl. Instr. and Meth. B 52 (1990) 588.
[22] B. Dittrich, U. Herpers, M. Lüpke, R. Michel, H.J. Hofmann, W. Wölfli, Radiochim. Acta 50 (1990) 11.
[23] Th. Schiekel, R. Rösel, U. Herpers, I. Leya, M. Gloris, R. Michel, B. Dittrich-Hannen, P.W. Kubik, H.-A. Synal and M. Suter, in: Proc. Int. Conf. Nuclear Data for Science and Technology, May 9-13, 1994, Gatlinburg, TN, USA, ed. J.K. Dickens (American Nuclear Society, Inc., La Grange Park, IL, 1994) pp. 344–346.
[24] Th. Schiekel, M. Gloris, U. Herpers, I. Leya, R. Michel, F. Sudbrock, M. Suter and H.A. Synal, PSI Progress Report 1993, Annex IIIA (1994) p. 50.
[25] Th. Schiekel, F. Sudbrock, U. Herpers, I. Leya, R. Michel, H.A. Synal, M. Suter, in: Progr. Rep. on Nuclear Data Research in the Federal Republic of Germany for the Period April 1st, 1994 to March, 31th (1995), NEA/NSC/DOC(95)10, INDC(Ger)-040, Jul-3086 (1995) 31.
[26] Th. Schiekel, U. Herpers, I. Leya, R. Michel, B. Dittrich-

Hannen, H.-A. Synal, M. Suter, P.W. Kubik, Nucl. Instr. and Meth. 114 (1996) 91.
[27] K. Prescher, F. Peiffer, R. Stück, R. Michel, R. Bodemann, M.N. Rao, K.J. Mathew, Nucl. Instr. and Meth. B 53 (1991) 105.
[28] K.J. Mathews, M.N. Rao, H. Weber, P. Dragovitsch, F. Peiffer, R. Michel, Nucl. Instr. and Meth. B 94 (1994) 449.
[29] E. Gilabert, B. Lavielle, Th. Schiekel, U. Herpers, S. Neumann, R. Michel, Meteoritics 30 (1995) 510.
[30] Ch. Schnabel, H.-A. Synal, M. Suter, R. Michel, M. Gloris, I. Leya, U. Herpers, Radiocarbon 38 (1996) 107.
[31] B. Dittrich-Hannen, F. Ames, M. Suter, Ch. Schnabel, R. Michel, U. Herpers, E. Günther, Nucl. Instr. and Meth. B 113 (1996) 453.
[32] U. Neupert, Thesis, Universität Hannover (1996).
[33] R. Michel, G. Brinkmann, H. Weigel and W. Herr, in: Progr. Rep. on Nuclear Data Research in the Federal Republic of Germany for the Period April 1, 1977 to March 31, 1978. NEANDC(E)-192 U Vol. V INDC(Ger)-2012 + Special (1978).
[34] R. Michel, G. Brinkmann and W. Herr, in: Progr. Rep. on Nuclear Data Research in the Federal Republic of Germany for the Period April 1, 1979 to March 31, 1980, NEANDC(E)-212 U Vol. V INDC (Ger)-22/L + Special (1980) p. 45.
[35] R. Michel, G. Brinkmann, M. Galas, R. Stück, in: Progr. Rep. on Nuclear Data Research in the Federal Republic of Germany for the Period April 1, 1981 to March 31, 1982, NEANDC(E)-232 U Vol. V INDC(Ger)-24/L + special,FIZ-KA 4 (1982) 36.
[36] R. Michel, F. Peiffer and R. Stück, in: Progr. Rep. on Nuclear Data Research In the Federal Republic of Germany for the Period April 1, 1983 to March 31, 1984, NEANDC(E)-252 U Vol.V, INDC(Ger)-27/L + Special (1984) p. 32.
[37] R. Michel, P. Dragovitsch, K. Prescher, M.N. Rao and J. Mathew, in: Progr. Rep. on Nuclear Data Research in the Federal Republic of Germany for the Period April 1, 1987 to March 31, 1988, NEANDC(E)-292 U Vol. V INDC(Ger)-32/LN + Special (1988) p. 25.
[38] B. Dittrich, U. Herpers, M. Lüpke and R. Michel, in: Progr. Rep. on Nuclear Data Research in the Federal Republic of Germany for the Period April 1, 1988 to March 31, 1989, NEANDC(E)-302 U Vol. V INDC(Ger)-34/LN + Special (1989) p. 31.
[39] B. Dittrich, U. Herpers, R. Bodemann, M. Lüpke, R. Michel, P. Signer, R. Wieler, H.J. Hofmann and W. Wölfli, in: Progr. Rep. on Nuclear Data Research in the Federal Republic of Germany for the Period April 1, 1989 to March 31, 1990, NEANDC(E)-312-U Vol. V INDC(Ger)-35/LN + Special (1990) p. 45.
[40] B. Dittrich, U. Herpers, R. Bodemann, R. Michel, H. Condé, B. Holmqvist and P. Malmborg, in: Progr. Rep. on Nuclear Data Research in the Federal Republic of Germany for the Period April 1, 1989 to March 31, 1990, NEANDC(E)-312-U Vol. V INDC(Ger)- 35/LN + Special (1990) p. 57.
[41] B. Dittrich, U. Herpers, R. Rösel, H.J. Lange, T. Hahn, R. Michel, H.J. Hofmann and W. Wölfli, in: Progr. Rep. on Nuclear Data Research in the Federal Republic of Germany for the Period April 1, 1990 to March 31, 1991, NEANDC(E)-322-U Vol. V INDC(Ger)-36/LN + Special (1991) p. 55.
[42] M. Lüpke, H.-J. Lange, M. Schnatz-Büttgen, R. Michel, R. Rösel, U. Herpers, P. Cloth, D. Filges, in: Progr. Rep. on Nuclear Data Research in the Federal Republic of Germany for the Period April 1, 1991 to March 31, 1992, NEA/NSC/DOC(92)5, INDC(Ger)-036/L, KFK 5079 (1992) 51.
[43] R. Bodemann, H.-J. Lange, I. Leya, R. Michel, T. Schiekel, R. Rösel, U. Herpers, H.J. Hofmann, B. Dittrich, M. Suter, W. Wölfli, B. Holmqvist, H. Condé, P. Malmborg, in: Progr. Rep. on Nuclear Data Research in the Federal Republic of Germany for the Period April 1, 1992 to March 31, 1993, NEA/NSC/DOC (93) 17, INDC(Ger)-037/LN, Jul-2803 (1993) 49.
[44] R. Bodemann, H. Busemann, M. Gloris, I. Leya, R. Michel, T. Schiekel, U. Herpers, H. Condé, B. Holmqvist, P. Malmborg, in: Progr. Rep. on Nuclear Data Research in the Federal Republic of Germany for the Period April 1, 1994 to March 31, 1995, NEA/NSC/DOC(95)10, INDC(Ger)-040 Jul-3086 (1995) 29.
[45] R. Bodemann, Thesis, University of Hannover (1993).
[46] G. Brinkmann, Thesis, University of Cologne (1979).
[47] B. Dittrich, Thesis, University of Cologne (1990).
[48] P. Dragovitsch, Thesis, University of Cologne (1987).
[49] M. Lüpke, Thesis, University of Hannover (1993).
[50] F. Peiffer, Thesis, University of Cologne (1986).
[51] R. Rösel, Thesis, University of Cologne (1995).
[52] Th. Schiekel, Thesis, University of Cologne (1995).
[53] R. Stück, Thesis, University of Cologne (1983).
[54] C.D. Bowman, E.D. Arthur, P.W. Lisowski, G.P. Lawrence, R.J. Jensen, J.L. Anderson, B. Blind, M. Cappiello, J.W. Davidson, T.R. England, L.N. Engel, R.C. Haight, H.G. Highes, J.R. Ireland, R.A. Krakowski, R.J. LaBauve, B.C. Letellier, R.T. Perry, G.J. Russell, K.P. Staudhammer, G. Versamis, W.B. Wilson, Nucl. Instr. and Meth. A 320 (1992) 336.
[55] Y. Nakahara, in: Nuclear Data for Science and Technology, ed. S.M. Qaim (Springer, Berlin, 1992) p. 23.
[56] F. Carminati, R. Klapisch, J.P. Revol, Ch. Roche, J.A. Rubio and C. Rubbia, CERN/ AT/93-47(ET) (1993).
[57] A.J. Koning, Reports ECN-C-93-05 (1993) and ECN-C-93-041 (1993).
[58] A.J. Koning, NEA/NSC Subgroup 13 of the WPEC, SG13 document: Doc. S13.21.
[59] M. Gloris, I. Leya, R. Michel, T. Schiekel, U. Herpers, B. Dittrich-Hannen, H.-A. Synal, M. Suter, P.W. Kubik, in: Progr. Rep. on Nuclear Data Research in the Federal Republic of Germany for the Period April 1, 1993 to March 31, 1994, NEA/NSC/DOC(94) 21, INDC(Ger)-039/LN, Jul-2950 (1994) 33.
[60] M. Gloris, R. Michel, U. Herpers, F. Sudbrock, Nucl. Instr. and Meth. B 113 (1996) 429.
[61] M. Gloris, R. Michel, U. Herpers, F. Sudbrock, B. Holmqvist, H. Condé and P. Malmborg, TSL Progress Report 1994–1995 (1996) p. 31.
[62] M. Gloris, R. Michel, U. Herpers, F. Sudbrock, D. Filges, B. Holmqvist, H. Condé, P. Malmborg, P.-W. Kubik, H.-A. Synal and M. Suter, Proc. 2nd Int. Conf. on Accelerator-Driven Technologies and Applications, 3–7 June 1996, Kalmar, Sweden, in press.

[63] M. Gloris, R. Michel, U. Herpers, F. Sudbrock, in: Progr. Rep. on Nuclear Data Research in the Federal Republic of Germany for the Period April 1, 1995 to March 31, 1996, NEA/NSC/DOC(96) 24, INDC(Ger)-042/LN, Jul-3246 (1996) 31.
[64] M. Blann, Phys. Rev. Lett. 28 (1972) 757.
[65] M. Blann, H.K. Vonach, Phys. Rev. C 28 (1983) 1475.
[66] M. Blann, CODE ALICE LIVERMORE 900, private communication (1990).
[67] M. Blann, CODE AREL, private communication (1994).
[68] P. Cloth, D. Filges, R.D. Neef, G. Sterzenbach, Ch. Reul, T.W. Armstrong, B.L. Colborn, B. Anders and H. Brueckmann, Juel-2203 (1988).
[69] P.G. Young and E.D. Arthur, LANL-Report LA-6947.
[70] Y. Yariv, Z. Fraenkel, Phys. Rev. C 24 (1981) 488.
[71] A.S. Botvina, I.N. Mishustin, Phys. Lett. B 294 (1992) 23.
[72] G. Rudstam, G. Sorenden, J. Inorg. Nucl. Chem. 28 (1966) 771.
[73] R. Silberberg and C.H. Tsao, Astrophys. J. 220 (1973) 315; ibid 335; R. Silberberg, C.H. Tsao and M.M. Shapiro, in: Spallation Nuclear Reactions and their Applications, eds. B.S.P. Shen and M. Merker (Reidel, Dordrecht, 1976) p. 49; C.H. Tsao and R. Silberberg, Proc. 16th Int. Cosmic Ray Conf., Kyoto, Vol. 2 (1979) p. 202; R. Silberberg, C.H. Tsao and J.R. Letaw, Appl. J. Suppl. Ser. 58 (1985) 873; R. Silberberg, C.H. Tsao and J.R. Letaw, 20th Int. Cosmic Ray Conf., Moscow, Vol. 2 (1987) p. 133; R. Silberberg, C.H. Tsao, J.H. Adams and J.R. Letaw, AIP Conf. Proc. 186, High Energy Radiation Background in Space, Sanibel Island, FL, 1987 (American Institute of Physics, New York, 1989) and references therein.
[74] R. Michel and P. Nagel, International Codes and Model Intercomparison for Intermediate Energy Activation Yields, NEA/OECD, Paris, 1997, NSC/DOC(97)-1.
[75] B. Dittrich, U. Herpers, T. Schiffmann, R. Michel, P. Cloth, P. Dragovitsch, D. Filges, J. Beer, W. Wölfli, Analyst 114 (1989) 295.
[76] R. Michel, F. Peiffer, S. Theis, F. Begemann, H. Weber, P. Signer, R. Wieler, P. Cloth, P. Dragovitsch, D. Filges, P. Englert, Nucl. Instr. and Meth. B 42 (1989) 76.
[77] R. Michel, M. Lüpke, U. Herpers, D. Filges, P. Dragovitsch, W. Wölfli, B. Dittrich, H.J. Hofmann, J. Radioanal. Nucl. Chem. 169 (1993) 13.
[78] R. Michel, H.-J. Lange, M. Lüpke, U. Herpers, R. Rösel, D. Filges, P. Cloth and P. Dragovitsch, in: Proc. Int. Conf. Nuclear Data for Science and Technology, May 9–13, 1994, Gatlinburg, TN, USA, ed. J.K. Dickens (American Nuclear Society, Inc., La Grange Park, IL, 1994) pp. 377–379.
[79] M. Blann, Phys. Rev. Lett. 27 (1971) 337.
[80] H.H. Andersen and J.F. Ziegler, Hydrogen Stopping Powers and Ranges in All Elements (Pergamon, New York, 1977).
[81] C.F. Williamson, J.P. Boyot and J. Picard, CEA-R-3042 (1966).
[82] J.F. Janni, At. Data Nucl. Data Tabl. 27 (1982) 147.
[83] R.B. Firestone and V.S. Shirley, eds., in: Table of Isotopes, 8th Ed. (Wiley, New York, 1996).
[84] J.F. Ziegler, J.P. Biersack and U. Littmark, The Stopping and Range of Ions in Solids, Vol. 1 (Pergamon Press, New York, 1985).
[85] N. Bohr, Philos. Mag. 30 (1915) 581.
[86] P. Marmier and E. Sheldon, Physics of Nuclei and Particles (Academic Press, New York, 1969) pp. 156–170.
[87] G.F. Steyn, S.J. Mills, F.M. Nortier, B.R.S. Simpson, B.R. Meyer, Appl. Radiat. Isot. 41 (1990) 315.
[88] J. Tobailem and C.H. de Lassus St. Genies, Additif No. 2 a la CEA-N-1466(1) (1975) and CEA-N-1466(4) (1977).
[89] J. Tobailem and C.H. de Lassus St. Genies, Rapport CEA-N-1466(5) (1981).
[90] R. Michel, M. Gloris, I. Leya, H.-J. Lange, M. Lüpke, U. Herpers, B. Dittrich-Hannen, R. Rösel, D. Filges, P. Dragovitsch, M. Suter, H.J. Hofmann, P.W. Kubik, W. Wölfli, H. Baur, R. Wieler, Nucl. Instr. and Meth. B 103 (1995) 183.
[91] W. Westmeier, commercially available code GAMMA-W Ver. 15.03 (1994).
[92] W. Westmeier, Nucl. Instr. and Meth. 180 (1981) 205.
[93] W. Westmeier, Nucl. Instr. and Meth. A 242 (1986) 437.
[94] M. Suter, R. Balzer, G. Bonani, H.J. Hofmann, M. Morenzoni, M. Nessi, W. Wölfli, M. Andree, J. Beer, H. Oeschger, Nucl. Instr. and Meth. B 5 (1984) 117.
[95] H.J. Hofmann, J. Beer, G. Bonani, H.R. von Gunten, S. Raman, M. Suter, R.L. Walker, W. Wölfli, D. Zimmermann, Nucl. Instr. and Meth. B 29 (1987) 32.
[96] H.-A. Synal, G. Bonani, R.C. Finkel, Th. Niklaus, M. Suter, W. Wölfli, Nucl. Instr. and Meth. B 56 (1991) 864.
[97] H.-A. Synal, J. Beer, G. Bonani, Ch. Lukasczyk, M. Suter, Nucl. Instr. and Meth. B 92 (1994) 79.
[98] H.-A. Synal, G. Bonani, M. Döbeli, R.M. Ender, P. Gartenmann, P.W. Kubik, Ch. Schnabel and M. Suter, Nucl. Instr. and Meth. B 123 (1997) 62.
[99] P. Sharma, P.W. Kubik, U. Fehn, H.E. Gove, K. Nishizumi, D. Elmore, Nucl. Instr. and Meth. B 52 (1990) 410.
[100] W. Seelmann-Eggebert, G. Pfennig, H. Münzel and H. Klewe-Nebenius, Chart of the Nuclides 5. Aufl. (Kommunalschriften-Verlag Jehle, München, 1981).
[101] U. Reus and W. Westmeier, At. Data Nucl. Data Tabl. 29 (1983) 1 and 193.
[102] G. Friedlander, J. Hudis, R.L. Wolfgang, Phys. Rev. 99 (1955) 263.
[103] J.B. Cumming, J. Hudis, A.M. Poskanzer, S. Kaufmann, Phys. Rev. 128 (1962) 2392.
[104] H.R. Heydegger, A.L. Turkevich, A. van Ginneken, P.H. Walpole, Phys. Rev. C 14 (1976) 1506.
[105] S.J. Mills, G.F. Steyn, F.M. Nortier, Appl. Radiat. Isot. 43 (1992) 1019.
[106] M. Furukawa, S. Kume, M. Ogawa, Nucl. Phys. 69 (1965) 362.
[107] K. Miyano, J. Phys. Soc. Japan 34 (1973) 853.
[108] A. Grütter, Nucl. Phys. A 383 (1982) 98.
[109] J. Jastrzebski, H.J. Karkowski, M. Sadler, P.P. Singh, Phys. Rev. C 22 (1980) 1443.
[110] E. Storm, H. Israel, Nucl. Data Tabl. 29 (1970) 565.
[111] V. McLane, ed., in: EXFOR Sytems Manual: Nuclear Reaction Data Exchange Manual, BNL-NCS-6330 (1996).
[112] R. Michel, F. Peiffer, R. Stück, Nucl. Phys. A 441 (1985) 617.
[113] R. Michel, P. Dragovitsch, P. Englert, F. Peiffer, R. Stück, S. Theis, F. Begemann, H. Weber, P. Signer, R. Wieler, D. Filges, P. Cloth, Nucl. Instr. and Meth. B 16 (1986) 61.
[114] H. Weigel, R. Michel, U. Herpers, W. Herr, Radiochem. Radioanal. Lett. 21 (1975) 293.

[115] M.S. Lafleur, N.T. Porile, L. Yaffe, Can. J. Chem. 44 (1966) 2749.
[116] A.Y. Konobeyev, Y.A. Korovin, Kerntechnik 60 (1995) 147.
[117] R. Serber, Phys. Rev. 72 (1947) 1114.
[118] E.G. Alekseev, V.S. Guselnikov, V.M. Saytsehev, T.V. Koneva, Radiochimia 5 (1984) 667.
[119] P.D. Felice, R. Ocone, A. Rindi, J. Tuyn, R. Deltenre, G. Roubaud, Nucl. Instr. and Meth. 212 (1983) 359.
[120] H. Funk, F. Podosek, M.W. Rowe, Earth Plan. Sci. Lett. 13 (1967) 193.
[121] R.G. Korteling, A.A. Caretto, J. Inorg. Nucl. Chem. 29 (1967) 2863.
[122] V.N. Levkovskii, Middle Mass Nuclides Activation Cross Sections by Medium Energy Protons and α-particles (Inter-Vesi, Moscow, 1991).
[123] D.R. Sachdev, N.T. Porile, L. Yaffe, Can. J. Chem. 45 (1967) 1149.
[124] A.A. Caretto, E.O. Wug, Phys. Rev. 115 (1959) 1238.
[125] A. Grütter, Int. J. Appl. Radiat. Isot. 33 (1982) 725.
[126] E. Hagebo, H. Ravn, J. Inorg. Nucl. Chem. 31 (1969) 897.
[127] K. Kolsky, P.J. Karol, Phys. Rev C 1 (1993) 236.
[128] M. Lagarde-Simonoff and G.N. Simonoff, Phys. Rev. C 20 (1979) 1498.
[129] S. Regnier, B. Lavielle, M. Simonoff and G.N. Simonoff, Phys. Rev. C 26 (1982) 931.
[130] G.B. Saha, N.T. Porile, L. Yaffe, Phys. Rev. 144 (1966) 962.
[131] Yu.V. Alexandrov, V.P. Eismont, R.B. Ivanov, L.M. Krizhansky, M.A. Mikhailova, T.I. Popova, V.P. Prikhodtzeva and S.K. Vasilijev, in: Nuclear Data for Science and Technology, ed. J.K. Dickens (The American Nuclear Society, La Grange Park, IL, USA, 1994) pp. 371–373.
[132] B.J. Dropesky and H.A. O'Brien, Los Alamos Scientific Lab. Report. La-5120-Pr (1972).
[133] S.B. Kaufmann, M.W. Weisfield, E.P. Steinberg, B.D. Wilkins, D. Henderson, Phys. Rev. C 14 (1976) 1121.
[134] V.A. Kondratyev, Y.N. Kuz'menko, V.S. Lobach, V. Propopenko, D. Skylarenko and V.V. Tokarevskii, Sov. At. Energy 71 (1992) 832.
[135] K. Kolsky, P.J. Karol, Phys. Rev. C 1 (1993) 236.
[136] P.P. Strohal, A.A. Caretto, Phys. Rev. 121 (1961) 1815.
[137] G. Albouy, J.P. Cohen, M. Gusakow, N. Poffé, H. Sergolle and L. Valentin, J. Phys. Radium 24 (1963) 67.
[138] R.G. Korteling and E.K. Hyde, Phys. Rev. 136 (1964) B 425.
[139] M. Noguchi, T. Miura, K. Kondo, T. Suzuki, Y. Oki, M. Takasaki, K.H. Tanaka, M. Ieiri, Appl. Radiat. Isot. 42 (1991) 577.
[140] B. Scholten, S.M. Qaim, G. Stöcklin, Radiochim. Acta 65 (1994) 81.
[141] T. Tominaka, S. Ban, H. Ikeda, K. Katoh, K. Kondo, M. Takasaki, A. Yamamoto, H. Hirabayashi, Y. Narahara, Nucl. Phys. A 414 (1984) 385.
[142] Y. Asano, S. Mori, M. Noguchi, M. Sakano, K. Katoh, K. Kondo, J. Phys. Soc. Japan 54 (1985) 3734.
[143] Y. Asano, H. Kariya, S. Mori, M. Okano, M. Sakano, J. Phys. Soc. Japan 57 (1988) 2995.
[144] E. Baker, G. Friedlander, J. Hudis, Phys. Rev. 112 (1958) 1319.
[145] K. Bächmann, J. Inorg. Nucl. Chem. 32 (1970) 1.
[146] A.A. Caretto, J. Hudis, G. Friedlander, Phys. Rev. 110 (1958) 1130.
[147] V.P. Crespo, J.M. Alexander, E.K. Hyde, Phys. Rev. 131 (1963) 1765.
[148] L.A. Currie, W.F. Libby, R.L. Wolfgang, Phys. Rev. 101 (1956) 1557.
[149] E.M. Franz, G. Friedlander, Nucl. Phys. 76 (1966) 123.
[150] J. Gonzalez-Vidal, W.H. Wade, Phys. Rev. 120 (1960) 1354.
[151] V.T. Gritsyna, A.P. Klyucharev, V.V. Remaev, L.N. Reshetoua, Sov. Phys.JETP 17 (1963) 1186.
[152] S.M. Grimes, J.D. Anderson, J.C. Davis, W.H. Dunlop, C. Wong, Phys. Rev. C 8 (1973) 1770.
[153] S.L. Green, W.V. Green, F.H. Hegedus, M. Victoria, W.F. Summer and B.M. Oliver, J. Nucl. Mat. 155–157 (1988) 1350.
[154] M. Gusakow, Y. Legoux, H. Sergolle, Compt. Rend. 251 (1960) 70.
[155] M. Gusakow, G. Albouy, N. Poffe, C. Riehl, J. Phys. Radium 22 (1961) 636.
[156] F. Hansen, R.C. Jopson, H. Mark, C.D. Swift, Nucl. Phys. 30 (1962) 389.
[157] J. Hudis, S. Tanaka, Phys. Rev. 171 (1968) 1297.
[158] J. Hudis, Phys. Rev. 171 (1968) 1301.
[159] T.M. Kavanagh, R.E. Bell, Can. J. Phys. 39 (1961) 1172.
[160] S.B. Kaufmann, E.P. Steinberg, Phys. Rev. C 22 (1980) 167.
[161] P. Kruger, N. Sugarman, Phys. Rev. 99 (1955) 1459.
[162] S. Krämer, B. Neidhard, K. Bächmann, Inorg. Nucl. Chem. 13 (1977) 205.
[163] A.K. Lavrukhina, L.P. Moskaleva, L.D. Krasavina, I.M. Grechishcheva, J. Nucl. Energy 8 (1959) 231.
[164] N. Poffé, M. Riou, J. Teillac, Compt. Rend. 248 (1959) 3552.
[165] N. Poffe, G. Albouy, M. Gusakow, J.L. Sarrouy, J. Phys. Radium 22 (1961) 639.
[166] N.T. Porile, B.J. Dropesky, R.A. Williams, Phys. Rev. C 18 (1978) 2231.
[167] E. Ross, K. Bächmann, Radiochim. Acta 21 (1974) 13.
[168] S.D. Schery, D.A. Lind, H.W. Fielding, C.D. Zafiratos, Nucl. Phys. A 234 (1974) 109.
[169] S. Shibata, M. Imamura, H. Nagai, K. Kobayashi, K. Sakamoto, M. Furukawa, I. Fujiwara, Phys. Rev C 48 (1993) 2617.
[170] K. Sümmerer, W. Brüchle, D.J. Morissey, M. Schädel, B. Szweryn and Yang Weifan, Phys. Rev. C 42 (1990) 2546.
[171] R.S. Tilbury and L. Yaffe, Can. J. Chem. 41 (1963) 2634.
[172] H.P. Yule, A. Turkevich, Phys. Rev. 118 (1960) 1591.
[173] Y.W. Yu, N.T. Porile, Phys. Rev. C 12 (1975) 938.
[174] E. Gilabert, B. Lavielle, Th. Schiekel, U. Herpers, S. Neumann, R. Michel, Meteoritics 80 (1996) A31.
[175] S. Pearlstein, Astrophys. J. 346 (1989) 1049.
[176] K. Kikuchi and M. Kawai, Nuclear Matter and Nuclear Reactions (North-Holland, Amsterdam, 1968).
[177] V.F. Weisskopf, D.H. Ewing, Phys. Rev. 57 (1940) 472.
[178] W.D. Myers, W.J. Swiatecky, Nucl. Phys. 81 (1966) 1.
[179] A.H. Wapstra, G. Audi, Nucl. Phys. A 383 (1985) 1.
[180] F. Atchison, Meeting on Targets for Neutron Beam Spallation Sources, KFA Jülich, Report Jül-Conf-34 (1980) p. 17.
[181] N. Bohr, Nature 137 (1936) 344.

[182] V.F. Weisskopf, Phys. Rev. 52 (1937) 295;
V.F. Weisskopf and H.D. Ewing, Phys. Rev. 50 (1940) 475.
[183] V.F. Weisskopf, Phys. Rev. 57 (1940) 295.
[184] H.W. Bertini, Phys. Rev. 131 (1963) 1801.
[185] H.W. Bertini, Phys. Rev. 188 (1967) 1711.
[186] T.W. Armstrong, K.C. Chandler, Nucl. Sci. Eng. 49 (1972) 110.
[187] M. Blann, Ann. Rev. Nucl. Sci. 25 (1975) 123.
[188] M. Blann, UCRL-JC-123495, Febr. (1996) and UCRL-JC-109052, Lawrence Livermore National Laboratory, Nov. (1991).
[189] R.E. Prael and H. Lichtenstein, LA-UR-89-3014 (1989).
[190] Y. Nakahara and T. Nishida, Monte Carlo Algorithms for Simulating Particle Emissions from Pre-equilibrium States during Nuclear Spallation Reactions 1, JAERI-M86-074 (1986).
[191] H.-J. Lange, Thesis, University of Hannover (1994).